12-18-2015

Cooperative, Cognitive and Coordinated Communications for Underwater Acoustic Networks

Yu Luo
Computer Sciences, yu.luo@engr.uconn.edu

Cooperative, Cognitive and Coordinated Communications for Underwater Acoustic Networks

Yu Luo, Ph.D.

University of Connecticut, 2015

Due to the wide range of applications, underwater acoustic networks (UANs) have attracted significant attention from both academia and industry in the past decade. However, UANs face grand challenges on the narrow communication bandwidth. To tackle this challenging issue, in this dissertation, I explore three critical techniques: cooperative communications (COP-COM), cognitive communications (COG-COM) and coordinated communications (COD-COM), to improve the acoustic spectrum usage.

In the first research thread, I propose a new relay selection criterion, called cooperative best relay assessment (COBRA), for underwater COP-COM. COBRA takes into account not only the spectral efficiency but also the long propagation delays of acoustic signals. In addition to COBRA, I develop a new cooperative scheme, called mirror node assisted communication (MNAC). MNAC harnesses the destructive interference of acoustic waves, and makes multiple data streams sent in parallel without causing any collisions.

COG-COM essentially allows nodes to smartly change frequencies and power based on their communication context. In this research thread, I propose a receiver-initiated spectrum management (RISM) system for underwater cognitive acoustic networks (UCANs). Control packets in RISM are shared amongst collaborative spectrum sensing, collision avoidance and spectrum decision. Therefore, the overhead of RISM is

significantly reduced. In addition to RISM system, I design a dynamic control channel MAC (DCC-MAC), to mitigate congestion on common control channel (CCC) of UCANs. In DCC-MAC, nodes could flexibly extend the bandwidth of their control channel whenever CCC is congested, or return excessive frequency bands back when the control channel becomes idle.

In the third research thread, I propose a competitive transmission media access control (MAC), called CT-MAC, for COD-COM. CT-MAC aims to coordinate the channel sharing in underwater multi-user uplink networks. In this protocol, control packets produced by each user only need to reach the immediate neighbors with a low transmission power. Meanwhile, the data generated in different time slots can join the competition in parallel to improve the channel utilization. Compared with conventional underwater MAC protocols, CT-MAC significantly improves the channel utilization and delivery delay, while maintaining comparable energy efficiency.

Cooperative, Cognitive and Coordinated Communications for Underwater Acoustic Networks

Yu Luo

B.E., Northwestern Polytechnical University, 2009

M.E., Northwestern Polytechnical University, 2012

A Dissertation

Submitted in Partial Fulfillment of the

Requirements for the Degree of

Doctor of Philosophy

at the

University of Connecticut

2015

APPROVAL PAGE

Doctor of Philosophy Dissertation

Cooperative, Cognitive and Coordinated Communications for Underwater Acoustic Networks

Presented by

Yu Luo, B.E., M.E.

Major Advisor _____
Jun-Hong Cui

Associate Advisor _____
Mohammad Khan

Associate Advisor _____
Song Han

Associate Advisor _____
Zheng Peng

University of Connecticut

2015

ACKNOWLEDGEMENTS

My sincere gratitude goes to my major advisor, Professor Jun-Hong Cui, for her excellent guidance and constant support in the past four years. Her abundant knowledge, sharp insights, extraordinary vision and outstanding passion have always been and will always be the source from which I seek inspiration, courage, wisdom and progress.

I also would like to thank Professor Mohammad Khan, Professor Song Han and Dr. Zheng Peng for their guidance. Their excellence in research and perfection in academia have always been my strongest motivation to complete my Ph.D. study.

My thanks go to my lab mates in the Underwater Sensor Networks Lab at University of Connecticut: Fei Dou, Jun Liu, Lei Wan, Li Wei, Michael Zuba, Robert Martin, Son Le, Xia Xiao, Xiaoka Xu, Xiaoyan Lu, Yibo Zhu and Zigeng Wang. Working with them is one of the most enjoyable things in the last four years.

I am truly grateful to my wife, Lina Pu, who has always been there cheering me up and standing by me through the good times and bad. With her company, my life is filled with excitement and happiness.

Finally, I want to give my deepest gratitude to my parents. Without them, none of the achievements I have made is possible. It is their education and encouragement that has made me realize how to enjoy the fantastic view along the journey everyday.

PUBLICATIONS

Yu Luo, Lina Pu, Zheng Peng, and Jun-Hong Cui, "Dynamic control channel MAC for underwater cognitive acoustic networks," In *Proceedings of the International Conference on Computer Communications (INFOCOM)*, IEEE, 2016 (Accepted).

Yu Luo, Lina Pu, Zheng Peng, and Zhijie Shi, "RSS-based secret key generation in underwater acoustic networks: advantages, challenges and performance improvements," *IEEE Communications Magazine*, 2016 (Accepted).

Yu Luo, Lina Pu, Zheng Peng, Zhong Zhou, and Jun-Hong Cui, "An efficient MAC protocol for underwater multi-user uplink communication networks," *Ad Hoc Networks*, 2015, vol. 34, pp. 75–91, 2015.

Yu Luo, Lina Pu, Michael Zuba, Zheng Peng, and Jun-Hong Cui, "Cognitive acoustics: making underwater communications environment-friendly," In *Proceedings of the International Conference on Underwater Networks & Systems (WUWNet)*, pp. 48. ACM, 2014

Yu Luo, Lina Pu, Michael Zuba, Zheng Peng, and Jun-Hong Cui, "Challenges and opportunities of underwater cognitive acoustic networks," *IEEE Transactions on Emerging Topics in Computing*, vol. 2, no. 2, pp. 198211, 2014.

Yu Luo, Lina Pu, Zheng Peng, Yibo Zhu, and Jun-Hong. Cui, "RISM: an efficient spectrum management system for underwater cognitive acoustic networks," In *Proceedings of International Conference on Sensing, Communication, and Networking (SECON)*, pp. 414–422, IEEE, 2014.

Yu Luo, Lina Pu, Zheng Peng, Zhong Zhou, and Jun-Hong Cui, "Effective relay selection for underwater cooperative acoustic networks," In *Proceedings of the International Conference on Mobile Ad-Hoc and Sensor Systems (MASS)*, pp. 104–112. IEEE, 2013.

Yu Luo, Lina Pu, Zheng Peng, Zhong Zhou, and Jun-Hong Cui, "CT-MAC: a MAC protocol for underwater MIMO based network uplink communications," In *Proceedings of the ACM International Conference on Underwater Networks and Systems (WUWNet)*, pp. 1–6, ACM, 2012.

Lina Pu, **Yu Luo**, Haining Mo, Son Le, Zheng Peng, Jun-Hong Cui, and Zaihan Jiang, "Comparing underwater MAC protocols in real sea experiments," *Computer Communications*, vol. 56, pp. 47–59, 2015.

Cheng Wei, **Yu Luo**, Zheng Peng, and Mardi C. Hastings. "A framework of acoustic channel availability prediction for avoiding interfering marine mammals," In *Proceedings of the International Conference on Underwater Networks & Systems (WUWNet)*, pp. 34. ACM, 2014.

Lina Pu, **Yu Luo**, Haining Mo, Zheng Peng, Jun-Hong Cui, and Zaihan Jiang, "Comparing underwater MAC protocols in real sea experiment," In *Proceedings of the IFIP Networking Conference*, 2013, pp. 1–9. IEEE, 2013. (**Best Paper Award**)

Lina Pu, **Yu Luo**, Zheng Peng, Haining Mo, and Jun-Hong Cui, "Traffic estimation based receiver initiated MAC for underwater acoustic networks," In *Proceedings of the ACM International Conference on Underwater Networks and Systems (WUWNet)*, pp. 1–6, ACM, 2013.

Lina Pu, **Yu Luo**, Yibo Zhu, Zheng Peng, Jun-Hong Cui, Shruti Khare, Lei Wang, and Benyuan Liu, "Impact of real modem characteristics on practical underwater MAC design," In *Proceedings of the OCEANS*, 2012, pp. 1–6, IEEE, 2012.

Zhao, Yanxiao, Jems Pradhan, Jun Huang, **Yu Luo**, and Lina Pu, "Joint energy-and-bandwidth spectrum sensing with GNU radio and USRP," *ACM SIGAPP Applied Computing Review*, vol. 2, no. 4, pp. 40–49, 2015.

Le Son, Jun Liu, Zheng Peng, Jiaxing Che, **Yu Luo**, and Jun-Hong Cui. "Seamark-assisted inertial navigation for autonomous underwater vehicles," In *Proceedings of the International Conference on Underwater Networks & Systems (WUWNet)*, pp. 24. ACM, 2014.

TABLE OF CONTENTS

LIST OF FIGURES

LIST OF TABLES

LIST OF ABBREVIATIONS

ACK	acknowledgement
AF	amplify-and-forward
AGC	automatic gain control
ASTS	assist-to-send
ATIM	ad hoc traffic indication message
ATS	available-to-send
AUV	autonomous underwater vehicle
BP	beaconing period
C-MAC	cognitive MAC
CA	cognitive acoustic
CCC	common control channel
CF	compress-and-forward
COBRA	cooperative best relay assessment
COD-COM	coordinated communications
COG-COM	cognitive communications
COP-COM	cooperative communications
CP	competition packet
CPCN	control-packet-collision-notification
CR	cognitive radio
CSI	channel state information

CT-MAC	competitive transmission MAC
CTS	clear-to-send
CW	continuous wave
DCC-MAC	dynamic control channel MAC
DF	decode-and-forward
DFHC	dynamic frequency hopping communication
DTP	data transfer period
FSK	frequency-shift keying
ID	identification
MAC	media access control
MBWA	mobile broadband wireless access
MIMO	multiple-input and multiple-output
MMAC-CR	multi-channel MAC for cognitive radio
MNA-MAC	mirror node assisted MAC
MNAC	mirror node assisted communication
OFDM	orthogonal frequency-division multiplexing
OPT	one-way packet transmission
PCC	preassigned control channel
PDC	preassigned data channel
PL	priority level
PN	pseudo-random noise
PSK	phase-shift keying
PTH	prepare-to-help

PU	primary user
QoS	quality of service
RC	rendezvous channel
RCBC	receive capability broadcast
RCTS	repeat-clear-to-send
RISM	receiver-initiated spectrum management
RISS	receiver-initiated spectrum sharing
RTR	request-to-receive
RTS	request-to-send
SINR	signal-to-interference-plus-noise ratio
SISO	single-input and single-output
SNR	signal-to-noise ratio
SRAC	single-radio adaptive channel
SYN-MAC	synchronized MAC
UAN	underwater acoustic network
UCAN	underwater cognitive acoustic network
WRAN	wireless regional area network

Chapter 1

Introduction

Oceans, as source of life, have created innumerable natural wonders in the last hundreds and thousands of years. We depend on the oceans, love them and desire to know them. Today, our aerospace technology could bring us to space, however more than 95% of the underwater world remains unexplored [1]. With dwindling resources on land, we are turning our attention to the "blue" [2–5].

To meet the growing demands on the ocean exploration, we devote our effort to developing advanced techniques for more efficient and intelligent acoustic communications. One of the key enabling technologies lies in the underwater acoustic network (UAN).

In past decade, UANs have received significant interest from both academia and industry due to its wide range of applications, such as offshore facility management, underwater target detection and environmental monitoring [6–8]. However, underwater acoustic channels have some unique features, that in turn, lead to significant challenges on UAN:

- *Narrow communication bandwidth*: Due to the frequency-dependent attenuation, the bandwidth of acoustic communications is very narrow, usually from tens of kilohertz to hundreds of kilohertz.

- *Low propagation speed*: The propagation speed of acoustic signals in water is very slow, around 1.5×10^3 m/sec, which is five orders of magnitude lower than that of electric magnetic waves (3×10^8 m/sec).
- *Complex underwater environment*: The sea is a highly dynamic environment in both the time domain and the space domain. In addition, the long multi-path effect in oceans makes the underwater channel more complicated. Moreover, the activities, e.g., echolocation, communication and prey, of marine animals also affect the performance of a UAN.

In order to make UANs work effectively, one direction is of improving the utilization of underwater channel, the scarce resource for acoustic communications. Therefore, in this dissertation I explore three critical techniques: cooperative communications (COP-COM), cognitive communications (COG-COM) and coordinated communications (COD-COM) for UANs, aiming to exploit the precious channel resource more efficiently.

1.1 Overview

In this section, I give an overview of underwater COP-COM, COG-COM and COD-COM that will be learned in this dissertation.

1.1.1 COP-COM

COP-COM exploits the spatial diversity inherent in the wireless network by allowing nodes with diverse channel qualities to cooperate and relay each other's messages to the destination. Each transmitted message passes through multiple independent relay paths and thus, the probability that the message fails to reach the destination is reduced significantly [9].

Many cooperative schemes have been proposed in the last ten years, including decode-and-forward (DF), amplify-and-forward (AF) [10], code cooperation [11], and compress-and-forward (CF) [12]. The critical problem of relay selection for an efficient cooperative data transmission is also well addressed in the terrestrial radio network. However, existing cooperative approaches need an overhaul before applying in UANs due to the unique features of underwater communications. To solve this problem, I split my work in COP-COM into two segments. First, I improve the performance of existing cooperative scheme in underwater environment with a new relay selection criterion, called cooperative best relay assessment (COBRA) [13]. Second, I develop a new cooperative scheme, called mirror node assisted communication (MNAC), to match the features of acoustic communications. Next, I give brief introductions on COBRA and MNAC.

1) ***COBRA***: In most of cooperative network, people select the best relay based on the quality of source – relay channel and relay – destination channel to maximize the transmission rate of the source node. Compared with the direct path between the source and the destination, the additional time an acoustic signal takes to travel along source – relay – destination is usually assumed negligible. This is reasonable in radio networks due to the fast propagation speed of electromagnetic waves. In underwater environments, however, the sound speed is much lower than the radio speed. In this situation, a relay with a good channel quality to both the source and the destination may not be the best one anymore if it is far from the sender and the receiver, since the receiver has to wait a long time for the arrival of the relayed signal.

To tackle the above problem, in COBRA I take into account not only the channel quality of each potentially relay to increase the transmission rate, but also the length of a relay path to reduce the propagation delay. The simulation results show that the throughput of a UAN with COBRA could increase by 20% and 40% when

compared with the channel quality based relay selection approach and non-cooperative communications, respectively.

2) ***MNAC***: It is a new cooperative scheme that I designed for static UANs. MNAC improves the channel efficiency by harnessing the destructive interference of acoustic waves. More specifically, in MNAC I select a proper mirror node for each specific source node, and then make the signals from the source and the mirror node add destructively at the certain receiver that want to protect. In this way, the protected node could receive data from its intended sender, while not be interfered by other mirror-assisted nodes, even if they transmit simultaneously. With the proposed technique, multiple data streams in a network could be sent in parallel without causing any collisions.

Although MNAC could significantly increase the channel efficiency of USNs, its implementation has to grapple with several unique challenges:

a) How to guarantee that the source node and the mirror node have the same data to send. The performance of destructive interference is susceptible to the difference between two destructive signals, the source and mirror nodes are required to have highly identical data for applying the MNAC in real applications.

b) Due to the hardware constraints and dynamics of acoustic channel, the amplitude and phase of a mirror signal may not be able to perfectly match that of the source signal at the protected receiver for interference cancellation. How this mismatch could affect the performance of MNAC should be evaluated carefully.

c) If there are multiple potential mirror nodes, which one is the best? In this dissertation, I will show that if the mirror node is not properly selected, signals from the source and the mirror node may cancel out each other on the intended receiver, instead of adding up to a stronger signal. This may hurt the reliability and the throughput of a network. Therefore, how to choose the best mirror node should be studied carefully in MNAC.

1.1.2 COG-COM

COG-COM improves the channel utilization by allowing nodes in a network to sense their surrounding spectrum usage and then switch to the vacant channel smartly based on the sensing results. When using the cognitive technique in UANs, acoustic nodes have opportunity to effectively and friendly share the underwater channel with other natural and man-made acoustic users, like marine mammals and sonars [14, 15].

However, when applying the cognitive technique in acoustic networks, we will face grand challenges due to the unique features of the underwater environment and real systems, such as the large overhead traffic, unknown signal pattern of marine animals and high dynamics of acoustic channel.

In this dissertation, I focus on reducing the overhead problem caused by the long propagation delay of underwater channel and the large preamble signals of acoustic modem. More specifically, a cognitive network relies more on the control packets than that in a conventional single channel network. Nodes use these control packets for handshaking to avoid collisions, negotiating to decide the communication channel (multi-channel rendezvous), or collaborating to improve the sensing accuracy. In cognitive radio (CR), the overhead traffic generated by the transmissions of control packets is usually overlooked. In UANs, when taking into account the features of long preamble and the propagation delay [16], the overhead would be much heavier in an underwater cognitive acoustic network (UCAN) than that in a CR network.

To address the above problem, in this dissertation, I propose a new spectrum management system, called receiver-initiated spectrum management (RISM) [17] system, and introduce a new MAC protocol, called dynamic control channel MAC (DCC-MAC), for UCAN:

1) ***RISM***: In RISM, a handshake process is initiated at the receiver side to negotiate for a sharing of vacant spectrum. Compared with sender-initiated schemes, which

are commonly applied in CR networks [18, 19], the receiver in RISM could work as a "small center" to collect local sensing results from its neighbors and to coordinate data transmission among surrounding senders. In addition, control packets, being used for negotiation among cognitive acoustic (CA) nodes to avoid data collisions on the media access control (MAC) layer, could be effectively shared by the collaborative spectrum sensing mechanism and the dynamic spectrum decision scheme on the physical layer, both of which thus do not generate extra traffic loads. In this way, the total overhead in RISM is reduced dramatically.

Simulation results show that RISM outperforms the multi-channel MAC for cognitive radio (MMAC-CR) [20], a typical sender-initiated protocol designed for CR network, in terms of throughput and end-to-end delay.

2) ***DCC-MAC***: DCC-MAC could mitigate the congestions of common control channel (CCC) in a UCAN. In DCC-MAC, the control channel is split into two parts: an out-of-band[1] CCC and one or more in-band data channels. According to the information of real-time network traffic, each node could flexibly select proper data channels to extend the bandwidth of their control channel, and return excessive frequency bands back when the control channel becomes idle.

Several key challenges are tackled in DCC-MAC, which include: (a) how to realize the situation (congested or idle) of the control channel distributively; (b) how to adjust the bandwidth of the control channel without generating too much traffic overheads; (c) how to design a good channel selection strategy to improve the channel efficiency, and (d) how to handle the multi-channel hidden terminal problem in the protocol.

[1]The frequency band physically separated from the in-band channel where data transmission occurs.

1.1.3 COD-COM

Underwater COD-COM is proposed for acoustic uplink transmissions. In an underwater multi-node uplink network, a group of nodes communicate to a common receiver, such as a sink node or a surface buoy. By equipping with multiple hydrophones, the receiver could decode multiple packets from different nodes simultaneously without any collisions. In the past decades, there have been significant research efforts on the physical layer of multi-node uplink communications [21–23]. To make this technique practical in UANs, however, we need an efficient MAC protocol to coordinate the activities (sending and receiving) of each node for the purpose of improving the channel utilization and energy efficiency of a network.

In this dissertation, I develop a new MAC protocol, called competitive transmission MAC (CT-MAC) [24], for underwater multi-node uplink networks. In CT-MAC, I aim to improve the channel utilization and energy efficiency of a network by using a parallel competition mechanism. With this mechanism, control messages produced by each node only need to reach its direct neighbors with a low transmission power to save energy. Meanwhile, the data generated by nodes in different time slots could join the competition transmission in parallel to improve the channel utilization. In addition, I propose two competition schemes for CT-MAC to achieve both the short-term and the long-term fairness in different network conditions. Theoretical analysis and simulation results illustrate that compared with the conventional multi-node uplink MAC protocols, such as channel aware Aloha [25] and multi-antenna reception MAC [26], CT-MAC could achieve higher channel utilization and much lower end-to-end delay, while maintaining comparable energy efficiency.

1.2 Author's contributions

To summarize, this dissertation makes six main contributions:

- I explore several unique features, such as the long preamble signal of acoustic modem, heavily shared underwater channel and narrowband response of acoustic transducer, from real acoustic systems. The impacts of these features on the performance of UANs are well discuss in this dissertation.
- In COP-COM, I propose a new criterion, COBRA, for the best relay selection. COBRA takes into account not only the spectral efficiency but also the long propagation delays of acoustic signals. The network performance in terms of throughput, packet delivery ratio could be significantly enhanced by COBRA when compared with conventional channel quality based relay selection approaches.
- I design a new cooperative scheme, called MNAC, for underwater COP-COM. MNAC is completely different from existing cooperative schemes. It aims to support the parallel data transmissions by harnessing the destructive interference of acoustic waves. With MNAC, the channel efficiency of UANs could be improved significantly.
- In COG-COM, I explore the challenges and opportunities of UCAN for channel efficient and environment-friendly communications. At the same time, a new spectrum management system, RISM, is proposed. Control packets in RISM are efficiently shared amongst different components, and thus the overhead of a network could be reduced dramatically.
- I design a new MAC protocol, DCC-MAC, for underwater COG-COM. Different from most of existing cognitive MAC protocols, I allow nodes in DCC-MAC to flexibly borrow the data channel for their control message transmissions, and to return excessive frequency bands back when the current control channel becomes idle. This strategy could mitigate the congestion problem of CCC in COG-COM, thereby improving the network performance in terms of throughput, energy efficiency and end-to-end delay.

- In COD-COM, I propose a new MAC protocol, CT-MAC, for underwater multiuser uplink communications. In this protocol, control packets generated by underwater nodes only need to reach the immediate neighbors instead of the surface buoy. Therefore, the competition for channel access is less power and time consuming. Meanwhile, the data generated by nodes in different time slots could join the competition in parallel to improve the channel utilization.

1.3 Outline

This dissertation is divided into seven chapters. Chapter 2 starts with the necessary background on UANs. In this chapter, I introduce what is a UAN and the features of UANs. I discuss the challenges of UANs in Chapter 3, which promote us to study the techniques of cooperative, cognitive and coordinated communications for the performance improvement of existing UANs. In Chapter 4, I introduce my first research thread, underwater COP-COM. Two pieces of work, COBRA and MNAC, are discussed. After that I introduce my second research thread, underwater COG-COM in Chapter 5. In this chapter, RISM and DCC-MAC are proposed to efficiently use the acoustic channel in UCANs. In Chapter 6, I introduce my third research thread, CT-MAC, a coordinated MAC protocol for underwater uplink networks. Chapter 7 concludes the dissertation.

Chapter 2

Background

UANs have a lot of potential applications, such as underwater target detection, off-shore infrastructure health monitoring and coastline protection. Compared with terrestrial radio network, UANs have some unique features, like long propagation delay, narrow communication bandwidth, long preamble of acoustic modem, heavily shared acoustic channel and curvilinear propagation of acoustic ray. In this chapter, I first define a UAN, and then give an insight into those unique features.

2.1 What is a UAN

A UAN is spatially distributed autonomous sensors to monitor underwater environment, for example ocean current, salinity and water temperature, and to cooperatively pass their data through the network to the destination through acoustic communications. An acoustic node may be static that attached to anchored buoys or to the seafloor; it could also be mobile that equipped on a ship or an autonomous underwater vehicle (AUV).

In Fig. 2.1, I show a typical UAN for underwater target detection. In this network, several bottom nodes are mounted on the seafloor. Each of them equips with specific

sensors to detect the presence of interesting target, e.g., marine mammals and ships. AUVs can bring the collected data back by cruise between mothership and bottom nodes periodically. For the real-time monitoring, surface nodes could communicate with bottom nodes directly, and forward the data to a data center through their RF antennas.

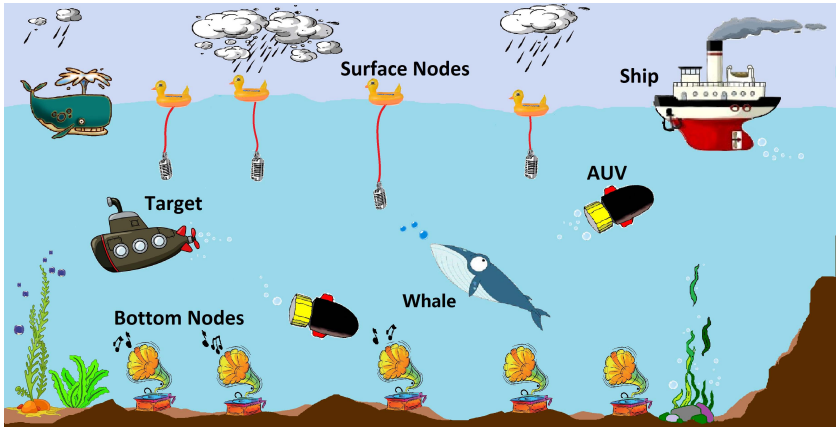

Figure 2.1: UAN for target detection, where bottom nodes and surface nodes as well as AUVs send sensing results via an ad hoc network whenever the presence of a target is detected, then keep quiet for the rest of time [27][2].

2.2 Features of UANs

Compared with terrestrial wireless networks, UANs have many unique features. Some of them, like the long propagation delay and frequency-dependent attenuation, have been well studied by pioneers; others, such as the narrowband response of acoustic transducers and the long preamble sequence of acoustic modems are still overlooked in the implementation of a real UAN. In this section, I give an insight into these unique features.

[2] © 2016 IEEE. Reprinted with permission from Yu Luo, Dynamic control channel MAC for underwater cognitive acoustic networks, IEEE INFOCOM, Apr. 2016 (Accepted)

2.2.1 Long propagation delay

In water, electromagnetic waves are heavily attenuated, while the optical waves suffer from sever scattering; as a result, acoustic waves have became a preferred carrier of information for wireless communications in underwater environments. However, the propagation speed of acoustic signals in water is only about 1.5×10^3 m/sec, five orders of magnitude lower than that of radio signals (3×10^3 m/sec). Moreover, the distance of neighboring nodes in a UAN is long, usually from hundreds of meters to several kilometers.

Due to the low speed of sound in water and the long distance of communications, an acoustic signal from the source may travel a long time, more than hundreds of milliseconds, to its destination. Hence, the propagation delay of data in UANs is much larger than that in terrestrial radio networks.

2.2.2 Narrow communication bandwidth

In a radio network, the frequency band for communications could achieve dozens of megahertz, e.g. 20 MHz for 4G [28] and 40 MHz for IEEE 802.11n [29], or even wider. In UANs, however, the available frequency band is much narrower than that in terrestrial wireless communications. Generally, the bandwidth in a mid-range acoustic communication is less than 40 kHz due to the frequency-dependent attenuation and the narrowband response of acoustic transducer:

1) ***Frequency-dependent attenuation***: Water is a dissipative propagation medium, in which the energy of acoustic wave is absorbed by the viscosity or chemical reactions [30]. The attenuation of acoustic wave, the most limiting factor in acoustic propagation, is proportional to the signal frequency.

To present the absorbtion of acoustic energy with the frequency, Francois and Garrison developed a precise model in 1982 [31, 32]. Here, I skip the detail of the

model but directly show the final results of absorbtion coefficient as the function of frequency in Fig. 2.2.

Fig. 2.2 demonstrates that the sound absorption increases rapidly with the frequency. More specifically, when the frequency of sound wave is lower than 1 kHz, there is only less than 0.1 dB/km absorption of acoustic signals, which has a small effect on long range of acoustic communications (> 10 km). At 10 kHz, the absorption reaches 1 dB/km, starting to challenge the mid-range ($1 - 10$ km) communications. When the frequency rises to 100 kHz, the absorption of acoustic signal could reach 40 dB/km, which may limit even short range communications (< 1 km).

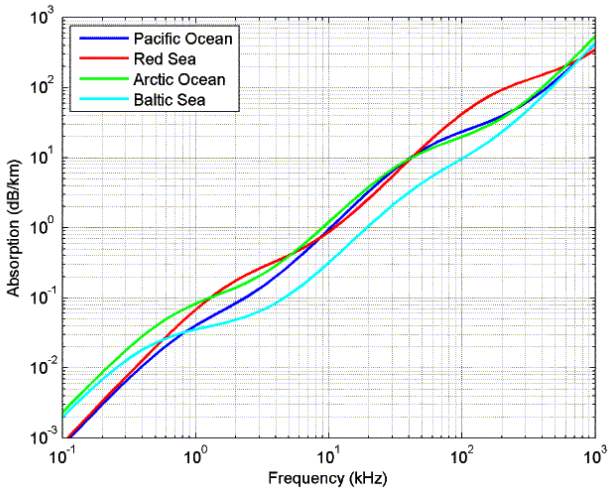

Figure 2.2: Sound absorption in sea water with respect to the frequency (from Ainslie and MAcColm, 1998).

2) ***Narrowband response of acoustic transducer***: Narrowband response of acoustic transducers is another essential reason resulting in a narrow frequency band of UANs. Particularly, acoustic transducers are usually designed to operate around their *resonant frequency* for maximizing the piezoelectric transfer efficiency. The frequency response of a transducer drops quickly once the frequency of transmission signal moves away from the resonant frequency.

We can use the *quality factor*, Q, to present the relative bandwidth of a transducer. Here, Q is defined as the ratio of the resonant frequency to the 3 dB bandwidth of the transducer. A typical value of Q ranges between 2 and 10 in underwater transducers [30]. In other words, the 3 dB bandwidth of an acoustic transducer is only 1/10 to 1/2 of its resonant frequency.

In UANs, the resonant frequency of a transducer usually stays at the middle frequency ($1 - 40$ kHz) to avoid severe frequency-dependent attenuation. However, a low resonant frequency leads to a narrowband response of acoustic transducers. For instance, assume the resonant frequency of an acoustic modem is 20 kHz, then its 3 dB bandwidth is only 2 kHz for $Q = 10$ or 10 kHz for $Q = 2$. For this reason, the transmission bandwidth of most acoustic modems within the range of $5 - 20$ kHz [33–35].

2.2.3 Long preamble sequence

For incoming signal detection, automatic gain control (AGC) and channel estimation purposes, a modem needs to add a sequence of specific signals, called the preamble, before each packet.

In a radio network, the duration of a preamble signal is very short, usually less than several hundreds of microseconds. For example, the preamble in IEEE 802.20 for mobile broadband wireless access (MBWA) consists of 8 symbols, and 104 μs for each one, i.e. total 832 μs preamble sequence [36]. In IEEE 802.22 for cognitive wireless regional area networks (WRANs) , the preamble segment includes three components: a superfame preamble, a frame preamble and a coexistence beacon protocol preamble, and the total length of them is less than 1 ms [37]. By contrast, the preamble signal in acoustic communications could reach one second or even longer, three orders of magnitude larger than that in radio networks. In Table 2.1, I list the length of preamble sequence in three different acoustic modems.

Table 2.1: Transmission rate and preamble length of different acoustic modems [15][3]

Modem	Data Rate	Preamble Length
Benthos ATM-88X Modem	140 - 2400 bps (MFSK)	1.2 s
	2.56 - 15.4 kbps (PSK)	
AquaSent OFDM Modem	3 kbps (1/2 coding rate, 4QAM)	0.5 s
	9 kbps (3/4 coding rate, 16QAM)	
WHOI Micro Modem	80 bps (Standard)	0.87 s
	300 - 5000 bps (High PSK mode)	

Two folds result in the long preamble of acoustic modems: the low data rate of acoustic modem and the long multipath of underwater channel. Next, I analyze them separately:

1) ***Low data rate of acoustic modems***: It is the primary reason of the long preamble in acoustic modems. Specifically, one major task of a preamble signal is to work as a mark, indicating the accurate time to receive oncoming data segments. We call it as point–to–point synchronization. To achieve a good synchronization performance, a sequence with hundreds of known bits, such as a pseudo-random noise (PN) sequence, is usually attached in a preamble. In radio networks, this PN sequence could be sent out in a very short time. In underwater environment, however, the low data rate of acoustic modems (Table. 2.1), extends the transmission time significantly. Taking 512-bit PN signal as an example, a node in IEEE 802.22 with 22.69 Mbps transmission rate takes only 22.6 μs to send it out, but the transmission time is extended to 0.64 secs for an acoustic modem with 800 bps data rate.

2) ***Long multipath of the underwater channel***: This is another factor that contributes to a long preamble in UANs. Specifically, a preamble signal is usually comprised of several blocks, and each block serves for different functionalities. To overcome the inter-block interference in multipath environments, a guard time for phase-shift keying (PSK) and frequency-shift keying (FSK) based modulation scheme, or a cyclic

[3] © 2014 IEEE. Reprinted with permission from Yu Luo, Challenges and opportunities of underwater cognitive acoustic networks, IEEE Transactions on Emerging Topics in Computing, Jul. 2014

prefix for OFDM based modem needs to be inserted between these blocks. The length of a guard time or a cyclic prefix depends on the length of multipath. The radio channel has very short multipath owning to the high propagation speed of electromagnetic signals. In this circumstance, the guard time or the cyclic prefix could be as short as tens of microseconds (e.g. 4.7/16.7/53.3 μs in 3GPP LTE standard on different channel conditions). By contrast, the multipath could reach tens of millisecond or even longer in underwater communications, depending on the network deployment and channel conditions. The length of the guard time or cyclic prefix signal in this case is considerably increased by almost 1000 times longer than that in radio networks.

2.2.4 Heavily shared acoustic channel

In terrestrial wireless network, the transmission of a radio signal does not affect the communication of humans, birds and other animals, since the voice signal and the radio signal use totally different waves to carry the information, which do not interfere with each other. Different from that in land, marine animals, UANs and sonars had to share the precious acoustic spectrum with each other, since they all use sound signals for communications. Fig. 2.3 shows the overall bandwidth associated with different acoustic systems.

Taking a closer look at Fig. 2.3 we observe that from the spectrum point of view, the underwater mid-frequency band is heavily shared. Marine mammals use this frequency band for orientation, communication and foraging [38], while sonars transmitting on this frequency band for navigation and bathymetry.

To name a few, toothed whales communicate on frequencies around 10 kHz; the echolocation signal produced by killer whales is $12 - 25$ kHz; the whistle signal (for communication) and click signal (for echolocation) sent by bottlenose dolphin are 200

Hz – 24 kHz and 200 Hz – 150 kHz, respectively. The sea lions could hear the sound frequency up to 70 kHz, and vocalize from 100 Hz to 10 kHz.

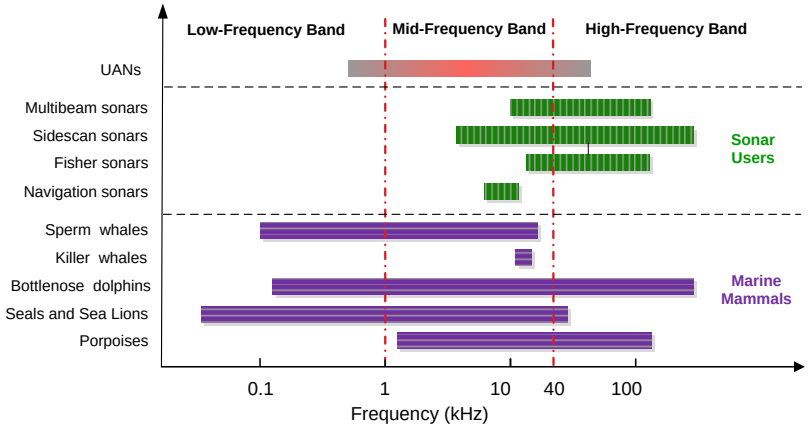

Figure 2.3: Spectrum usage of different acoustic systems [15][4].

Moreover, the operating frequency of sonar systems varies from hundreds of hertz to hundreds of kilohertz depending on the requirement of applications. Specifically, the frequency of continuous wave (CW) signal is usually $8-16$ kHz for navigation and ranges from 10 kHz to hundreds of kilohertz for bathymetry, e.g. 12 kHz in Simrad EM120 and 32 kHz in Simrad EM300. The fishery sonar, which is widely employed to find and harvest fish, works on frequencies 20 – 200 kHz. These sonars usually have a high source level from 185 to 200 dB re 1 μPa, thereby causing strong interference on surrounding acoustic systems.

2.2.5 Curvilinear propagation

Unlike radio signals, the ray tracing is generally considered as a straight line, the path of underwater acoustic signal is a curve, especially in long range communications ($>$ 10 km).

[4] © 2014 IEEE. Reprinted with permission from Yu Luo, Challenges and opportunities of underwater cognitive acoustic networks, IEEE Transactions on Emerging Topics in Computing, Jul. 2014

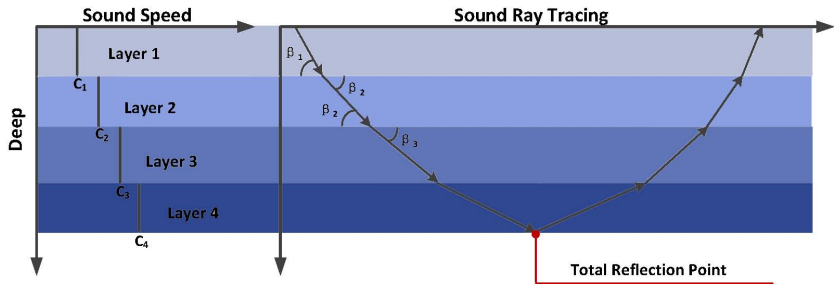

(a) Discontinuous change of sound velocity

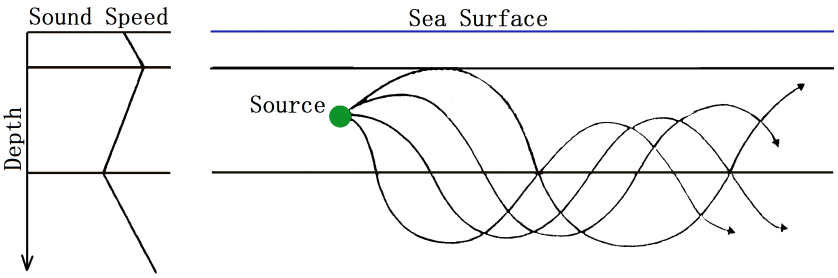

(b) Continuous change of sound velocity

Figure 2.4: Curvilinear propagation of acoustic ray. (a) Ray tracing with discontinuous change of sound velocity. (b) Ray tracing with continuous change of sound velocity

In water, the sound speed is affected by many factors, such as the temperature, water pressure and salinity. Usually, we could use a depth-velocity profile of acoustic wave to represent the changes of sound speed with respect to the depth of the water, as shown in the left part of Fig. 2.4(a) and Fig. 2.4(b).

As we know, the reflection and refraction of a plan wave occur if there is a change in sound velocity at the interface. According to the Snell-Descartes we have

$$\frac{\cos\beta_1}{c_1} = \frac{\cos\beta_2}{c_2}, \tag{2.1}$$

where β_1, β_2 and c represent the incidence angle, refraction angle and sound speed, respectively. Fig. 2.4(a) shows the refracted paths of acoustic ray in an idea situation, where the sound velocity changes with depth of water discontinuously. From this figure we observe that the sound tracing tends to propagate to the layer with smaller sound velocity. Fig. 2.4(b) demonstrates a more realistic profile of sound velocity, where the sound speed changes with depth of water continuously.

For short-range communications, the curvilinear propagation of acoustic signal is not significant, and could be neglected. For long-range communications, however, this phenomenon should be concerned carefully. By leveraging the knowledge of sound velocity profile over a particular area, the sound ray trajectories could be well compensated [30].

2.3 Summary

In this chapter, I first defined a UAN and gave a simple example to show how a typical UAN works in an underwater environment. After that several unique features, namely, the long propagation delay of acoustic signals, the narrow bandwidth of acoustic communications, the long preamble of acoustic modems and the the curvilinear propagation of sound ray was introduced. These features make a UAN very different from a terrestrial radio network. Conventional techniques designed for radio communications thus may need an overhaul before using in an acoustic network.

In the next chapter, I will analyze how above unique features challenge a UAN design in details.

Chapter 3

Challenges on UANs

In Chapter 2, I have introduced the unique features of UANs. In this chapter, I discuss how those features posed grand challenges on UANs, which promote us to study the techniques of cooperative, cognitive and coordinated communications in this dissertation.

3.1 Low channel utilization

The channel utilization is defined as the fraction of time used for data transmission in a certain channel. Due to the long propagation delay (Section 2.2.1), and the narrowband response of acoustic transducer (Section 2.2.2), the channel utilization in a UAN is very low, which challenges the throughput and the end-to-end relay of a network.

1) ***Low utilization in time domain***: In most of MAC protocols, the control packet, e.g. RTS and CTS, plays a crucial role in tacking the exposed terminal and the hidden terminal problems [39–42]. On one hand, a sender–receiver pair could utilize the control packet to well negotiate with each other, thereby considerably reducing the collisions among data packets in UANs. On the other hand, the time spend on sending

and waiting for the control messages inevitably reduces the utilization of an acoustic channel when considering the long preamble sequence and the large propagation delay of acoustic signal.

2) ***Low utilization in frequency domain***: The frequency band suitable for a mid-range acoustic communication is from 1 kHz to 40 kHz. However, as I have discussed in Section 2.2.2, the response bandwidth of an acoustic transducer is narrow, ranging from several kilohertz to tens of kilohertz. The following analyze will show that a single transducer may not be able to cover the whole mid-frequency.

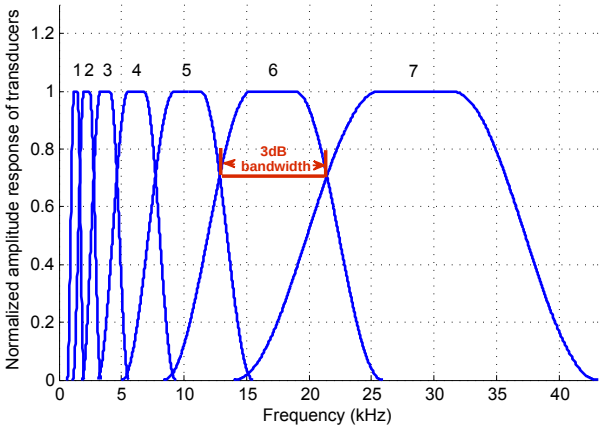

Figure 3.1: Narrowband response of acoustic transducers [15][1]. The number on each curve is the IDs of transducers.

Denote f_H^i, f_L^i, f_C^i and B_i as the lower 3 dB cutoff frequency, the upper 3 dB cutoff frequency, the central frequency and the bandwidth of transducer i, respectively, where

$$B_i = \frac{f_C^i}{Q}, \quad Q \in [2, 10]. \tag{3.1}$$

Substituting $f_C^i = \frac{1}{2}(f_H^i + f_L^i)$ and $B_i = f_H^i - f_L^i$ into (3.1), then we obtain

$$f_H^i = \frac{2Q+1}{2Q-1} f_L^i. \tag{3.2}$$

When $Q = 2$ (low quality factor), the transducer have a flat frequency response. Let $f_L^1 = 1$ kHz and $f_H^i = f_L^{i+1}$, and we have $f_H^i = (5/3)^i$. Therefore, $i = \log_{\frac{5}{3}} 40 \approx 7.22$

[1] © 2014 IEEE. Reprinted with permission from Yu Luo, Challenges and opportunities of underwater cognitive acoustic networks, IEEE Transactions on Emerging Topics in Computing, Jul. 2014

when $f_H^i = 40$ kHz. Now we obtain that at least 8 transducers are required to cover the whole mid-frequency band from 1 kHz to 40 kHz, as shown in Fig. 3.1.

Due to the size and the cost constraints, a commercial acoustic modem usually equips with a single transducer [33–35]. According to above analyze, they cannot cover a wide frequency band. Therefore, in addition to the frequency dependent attenuation, the narrowband response of an acoustic transducer further reduces the channel utilization of a UAN in the frequency domain.

3.2 Environment-friendly communications

As I have introduced in Section 2.2.4, an underwater channel is heavily shared. Now, imagine an underwater world with hybrid acoustic users, as illustrated in Fig. 3.2. An oil drilling installation system may employ a sensor network with acoustic modems to monitor the deflection of the drill. In the same area there could also exist a bottom mounted data collection system using another UAN to communicate with surface buoys. Meanwhile, there could be AUVs cruising in the water to inspect subsea oil pipelines and transmitting data wirelessly to their mothership [43]. In addition, a few marine mammals, e.g. dolphins and whales, might be playing in the neighborhood, using the same acoustic channel to communicate with each other and search for food via echolocation. Now the question is: Will existing UANs work well in this scenario? Unfortunately, the answer is "NO".

In fact, the design of existing UANs may cause significant scalability and sustainability issues, especially to the ocean ecosystem. First of all, traditional UANs assume full control over the acoustic spectrum they are operating in and do not consider the fact that multiple UANs could be deployed in a cross area. They are not able to share the spectrum with other networks even when it is possible. In other words, the static spectrum allocation will lead to the overall performance degradation

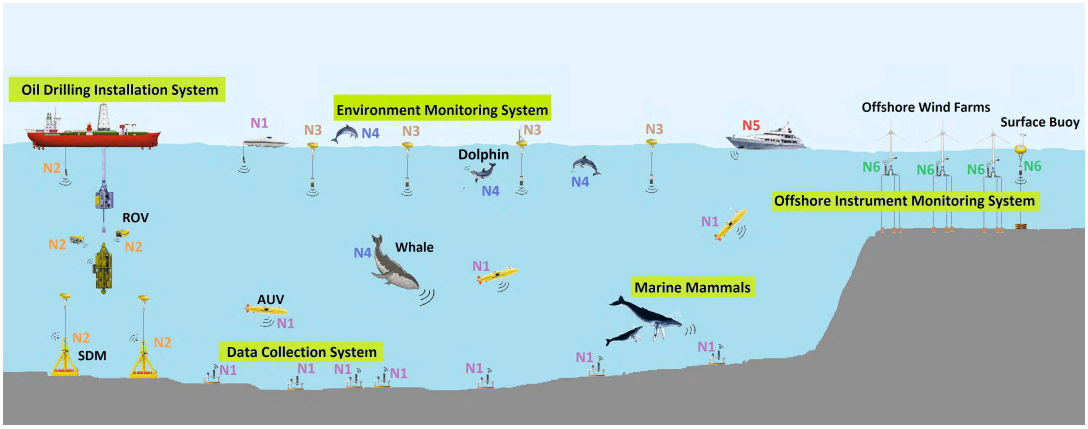

Figure 3.2: Underwater environment with hybrid acoustic users [15][2].

of all UANs and thus result in poor scalability. Secondly, there are also other acoustic systems, such as acoustic telemetry instruments. UANs operating without any awareness of these systems will face unexpected interference and undermined performance. Furthermore, many marine mammals share the same/similar acoustic spectrum with man-made acoustic systems including UANs (Fig. 2.3, Section 2.2.4). Recently, there are growing concerns about the effect of man-made noise (UANs, sonars, etc.) on marine mammals, implying greater sustainability issues on the ocean ecosystem.

Therefore, an ideal UAN should be able to detect other UANs (or man-made acoustic systems) and marine lives in its operating area, and perform wireless communications smoothly without affecting existing acoustic systems. Otherwise, not only the communication quality of UANs will be downgraded, but also the marine animals and the ecosystem will be largely affected.

[2] © 2014 IEEE. Reprinted with permission from Yu Luo, Challenges and opportunities of underwater cognitive acoustic networks, IEEE Transactions on Emerging Topics in Computing, Jul. 2014

3.3 High cost of overhearing traffic

In terrestrial radio network, a control packet is very short, usually less than one millisecond. In underwater communications, when taking into account the long preamble sequence of each packet (Section 2.2.3), the time and the energy consumption on transmitting a control message will be much larger than that in a radio network. In UANs, the overheard traffic, produced by sending and receiving control messages, could significantly increase the collision probability of packets, and dramatically reduces the lifetime of a network.

1) ***High collision probability***: As shown in Fig. 3.3, where node A and node C have the same distance to node B. Now, assume node A transmits a control packet, P_A, to node B. The transmission time of P_A is T. Usually, the interval marked at node C in this figure with $2T$ duration time is referred to as the *collision window*, during which the transmission of node C will disrupt the reception of packet P_A at node B. From Fig. 3.3 we observe that if the transmission probability of a control message in a certain period is a constant, the longer the collision window is, the higher the collision probability of control packets will have. Due to the long propagation delay and the low transmission ratio, the transmission time of control packets in a UAN is very long. Therefore, with the same network traffic, the collision probability of control message in UAN is much higher than that in a radio network.

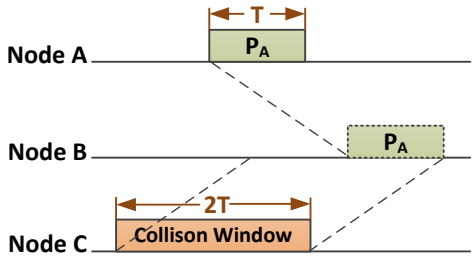

Figure 3.3: High collision probability of control packets

2) ***Short lifetime of network***: The overhead could reduce the lifetime of a UAN significantly. To make it straightforward, here I use a simple example regarding the time synchronization to clarify this problem.

The time synchronization amongst the network sometimes is required for a UAN. Now, suppose that we are using Teledyne Benthos ATM-885 modems for communication. The battery capacity of this modem is 300 Wh and the length of a preamble attached by it on each packet is 1.2 secs. Assume a UAN uses the classic two-way handshake method [44, 45] to synchronize the time every 15 secs. I further suppose that the size of each handshake packet (a kind of control message), transmission power and transmission rate of the ATM-885 modem are 40 B, 20 W (full transmission power) and 800 bits per second (MFSK with rate 1/2 convolutional coding mode), respectively. Then the network will die from the time synchronization after three days:

$$\begin{aligned} \text{Lifetime} &= \frac{300\,\text{W-hr} \times 60\,\text{mins/hr} \times 60\,\text{secs/min}}{A \times 60\,\text{mins/hr} \times 24\,\text{hrs/day} \times 20\,\text{W}} \\ &\approx 3\,days, \end{aligned} \tag{3.3}$$

where

$$A = 2\,\text{pkts/rnd} \times 4\,\text{rnds/min} \times \left(1.2\,\text{secs/pkt} + \frac{40\,\text{B/pkt} \times 8\,\text{bits/B}}{800\,\text{bits/sec}}\right). \tag{3.4}$$

However, if we do not consider the preamble sequence (remove the item, 1.2 secs/pkt, in (3.4)), then the lifetime of the network could extend to 12 days. Therefore, the long preamble of control packets significantly reduces the lifetime of acoustic node, and challenge a UAN, which needs to monitor an interesting area several weeks or even longer.

3.4 Summary

In this chapter, I introduced how the unique features of underwater communications challenge a UAN. According to the analysis I realized that the long propagation

delay of a sound signal and the narrowband response of an acoustic modem reduces the channel utilization of a UAN in the time domain and the frequency domain, respectively. Moreover, the marine animals who share the acoustic channel with artificial acoustic systems pose grand challenges on scalability and sustainability of a UAN. In addition, the long preamble sequence of an acoustic modem considerably increases the transmission time a short packet, thereby causing high collision probability and large overhead on transmitting control messages, which challenge the performance of a UAN in terms of throughput, lifetime and end-to-end delay.

In the following three chapters, I will introduce how to use the three techniques, namely, the COP-COM, COG-COM and COD-COM, to tackle the above challenges for a environment-friendly and channel efficient UAN.

Chapter 4

Underwater COP-COM

Due to the spatial diversity of wireless channel, nodes at different locations to a common receiver may have different channel qualities. Therefore, if a relay with a good channel helps the source node with a bad quality of channel to forward its data to the destination, the transmission performance could be enhanced. The technique of *cooperative communication* is proposed to achieve this goal. A good survey regarding the COP-COM could be found in [9].

In the last ten years, COP-COM has been well studied in radio networks. Nevertheless, due to the unique features of UANs discussed in Chapter 2, conventional cooperative scheme designed for radio network may work inefficient in underwater environment.

In order to make COP-COM feasible in UANs, in this chapter I first introduce a new best relay selection criterion, COBRA, for the purpose of improving the channel efficiency of underwater COP-COM. After that I propose a new cooperative scheme, called MNAC, to increase the channel utilization of cooperative acoustic networks.

4.1 COBRA

In this section, I introduce COBRA, a new best relay selection criterion for underwater cooperative acoustic networks. The new criterion aims to minimize one-way packet transmission (OPT) time instead of maximizing the transmission rate, which has been widely applied in terrestrial radio network. COBRA takes into account both the spectral efficiency and the long propagation delay of acoustic communication to improve the overall throughput performance of a network. The content in this section is mainly based on my previous work published in [13][1] .

4.1.1 Related work

Depend on the varied forwarding mechanisms, most of cooperative communication schemes could be classified into three categories: AF [46], DF [47] and CF [12]. In the first category, the relay node amplifies the noisy signal that it received from the source node directly and forward it to the destination without any processing. By contrast, the relay node in DF schemes decodes the received packet first, and then regenerates a new packet to the destination subsequently. In CF schemes, if a new codebook is utilized to produce the relayed message, we call it as the *space-time-coded cooperative communication*; otherwise it is referred to as *repetition-based cooperative communication*. In both schemes, the relay node retransmits a quantized or compressed version of the received message.

Although the cooperative communication has been a well explored research topic in terrestrial radio networks, little work has been conducted in underwater cooperative communications. In the literature, an AF based cooperative scheme with the time-reverse technique is proposed in [48]. In [49], the authors analyze the performance of several cooperative transmission schemes, which are originally designed for radio

[1] © 2013 IEEE. Reprinted with permission from Yu Luo, Effective relay selection for underwater cooperative acoustic networks, IEEE MASS, Oct. 2013

networks, in an underwater scenario. The multihop cooperative communication in an underwater grid network topology is investigated in [50].

The relationship between the communication range and the power consumption in underwater cooperative communications has been explored in [51]. The results demonstrate that when the communication distance is long enough, the cooperative communication could decrease the overall energy consumption significantly even if takes into account the additional overhead traffic of cooperative communications. This make cooperative communication a promising technique in UANs. A few energy efficiency based cooperative schemes have been proposed later in [52, 53].

In a cooperative communication network, one critical issue is how to select the best relay. In [54], it recommends to choose a relay with the best instantaneous channel state information (CSI), i.e., the relay with $\max\{\min\{|a_{sr_i}|^2, |a_{r_id}|^2\}\}$. Here, a_{sr_i} and a_{r_id} are the channel gain from the source to relay r_i and from r_i to the destination, respectively. In [55], the node with $\max\{|a_{r_id}|^2\}$ is selected as the relay. One advantage of [55] over [54] is that the source node could smartly switch between the cooperative mode and the non-cooperative mode (direct communication without the help of relay) to further improve the transmission rate. However, the aforementioned criteria are all designed for terrestrial radio networks and cannot be directly used into UANs due to the unique features of underwater channel.

4.1.2 Motivation

In COBRA, I focus on the DF repetition-based cooperative scheme, which generally consists of two phases, as shown in Fig. 4.1. In the first phase, the source node broadcasts data packets to the destination and all potential relays. In the second phase, the selected relays forward the re-encoded data to the destination. The destination node will not decode the data until received the copies from all relays.

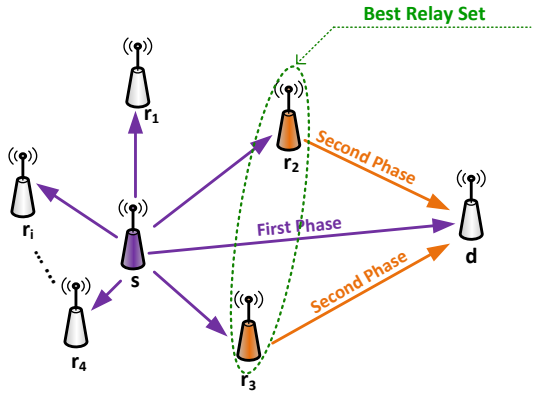

Figure 4.1: Two phases of DF repetition-based cooperative scheme, where $r_1, \ldots, r_i$ represent potential relays between the source s and the destination d. The destination node will receive three copies of data. One is directly from s in the first phase; another two are from the selected relays, r_2, and r_3, in the second phase.

Here, I define the time interval between the beginning of packet transmission at the source node and the end of last relayed packet reception at the destination as the OPT (one-way packet transmission) time. It consists of the overall transmission time and the propagation delay in a round of cooperative communication. The OPT time is a very straightforward metric to evaluate the performance of cooperative scheme — A receiver, which could obtain the data faster from a relay with a shorter OPT time, has higher throughput and shorter packet delivery delay.

In conventional criteria, the optimal relay is selected mainly based on the CSI [54, 55]. A node which has a the best channel quality to both the source and the destination is chosen as the best relay. This kind of criteria aim to maximize the channel capacity, thereby reducing the transmission time of a packet. In a radio network, it is reasonable because the propagation delay is ignorable. Therefore, the OPT time is approximate to the transmission time in cooperative communications. In underwater environments, however, the propagation delay is comparable to the transmission time of a packet due to the low speed of sound signal and the long distance among neighboring nodes (Section 2.2.1). Next, I introduce two factors that promote us to take into account not

only the channel quality, but also the location of a relay to optimize the OPT time in cooperative communications.

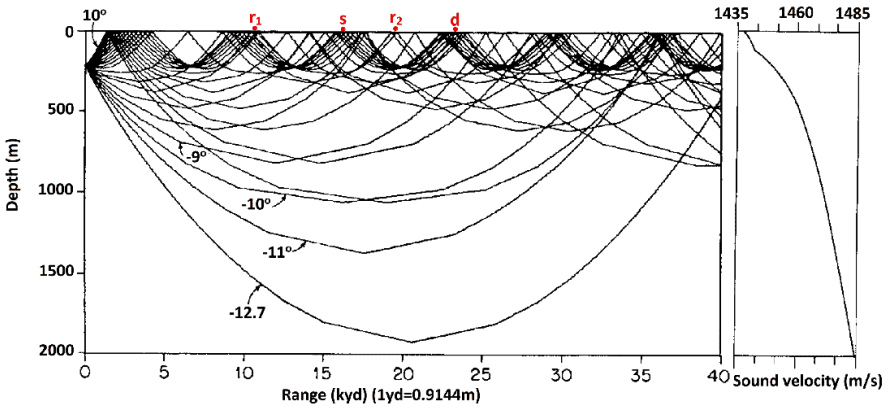

Figure 4.2: Curvilinear propagation of sound the Arctic region (Urick,1979 [56]). Sound velocity with depth (*right*) and the corresponding sound ray tracing(*left*).

Shadow zone of acoustic signal: As revealed in Section 2.2.5 one of the unique features of acoustic signal is its curvilinear propagation. With this propagation feature, a sound field may have multiple shadow zones and convergence zones in water, as shown in Fig. 4.2. In this circumstance, there is a probability that a relay near the source node has worse channel quality than the one far from the source node. Now, let s, d, r_1 and r_2 be the source, destination and two relays, respectively, and their positions are shown in Fig. 4.2. In this figure, r_1 has a better channel quality than r_2, since r_1 stays in the convergence zone the sound field. Therefore, CSI based criteria select it to relay the data. However, the OPT time of the cooperative communication with r_1 may be larger than that with r_2, since r_1 has a much longer propagation delay to the both the source and the destination than r_2.

Underwater obstacles: Underwater obstacles, such as fish school, also affect the result of best rely selection selection. As shown in Fig. 4.3, two fish schools block the signal from r_2 to the source and to the destination, resulting in a bad channel quality. However, the propagation distance of signal from s to d through r_1 is longer than that

through r_2. Therefore, r_1 offers a shorter transmission time but a longer propagation delay than r_2. In this circumstance, we could not arbitrarily conclude one relay is better than another unless compare the OPT time of two relays carefully.

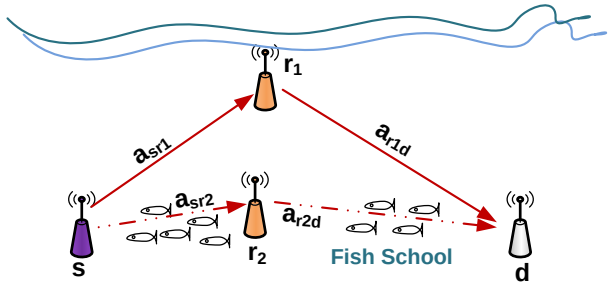

Figure 4.3: The impact of barrier on the best relay selection.

From the above discussion we obtain that the CSI based relay selection criteria proposed for radio network may work inefficiently in underwater environments due to the long propagation delay of sound signal. This promotes us to propose a new OPT time based criterion for the optimal relay selection.

4.1.3 System model

Assume all acoustic nodes work in the half duplex mode. The channel is supposed to be symmetric, i.e., the reciprocal channel from node A to B is the same as the channel from B to A. I consider an underwater network with a set of nodes denoted by $\mathcal{A}=\{s, d, r_1, r_2, \ldots, r_n\}$. The source node s has data to the destination node d. Let $\mathcal{R}$ be the relay set, where $\mathcal{R} \subset \mathcal{A}$.

During the first phase, the data signal received by relay r_i is

$$y_{sr_i}[k] = a_{sr_i} x_s[k] + n_{r_i}[k], \quad r_i \in \mathcal{R}, \tag{4.1}$$

where $x_s[k]$ is the raw data from the source node; $n_{r_i}[k]$ is a zero mean, independent and identically distributed circularly symmetric complex Gaussian noise with variance N_0, i.e., $n_{r_i}[k] \sim \mathcal{N}(0, N_0)$; a_{sr_i} is the channel gain between source and relay r_i.

Depending on the deployment, channel condition and modulation scheme, several distribution functions could be used to model the channel amplitude statistic characteristic, such as Rayleigh distribution [57], K-distribution [58] and Rice distribution [59]. Next, I use the Rayleigh channel as an example to show how COBRA criterion works.

Now, assume $|a_{sr_i}|$ in (4.1) follows Rayleigh distribution, and thus$|a_{sr_i}|^2$ is exponentially distributed with mean value $\lambda_{sr_i}^{-1}$, i.e. $|a_{sr_i}|^2 \sim Exponential(\lambda_{sr_i})$.

Let $y_{sd}[k]$ and $y_{r_id}[k]$ be the signal received at the destination and relay r_i, where

$$y_{sd}[k] = a_{sd}x_s[k] + n_d[k], \tag{4.2}$$

and

$$y_{r_id}[k] = a_{r_id}x_{r_i}[k] + n_d[k], \quad r_i \in \mathcal{R}. \tag{4.3}$$

In the DF repetition-based cooperative scheme, the relayed signal x_{r_i} is the same as the raw signal x_s. Moreover, a_{sd} and a_{r_id} are the channel gain from source to destination and from relay r_i to destination, respectively. Similar to $|a_{sr_i}|^2$, we have $|a_{sd}|^2 \sim Exponential(\lambda_{sd})$ and $|a_{r_id}|^2 \sim Exponential(\lambda_{r_id})$.

4.1.4 COBRA criterion description

In a cooperative communication scheme, one or more relays could be selected from the potential relay set $\mathcal{R}$ to forward the data packet. Denote the selected best relay set as $\mathcal{B}$, where $\mathcal{B} \subseteq \mathcal{R}$. Let $R_{\mathcal{B}}$ in bit/sec/Hz represent the spectral efficiency with the help of relay set $\mathcal{B}$, which is constrained by the following three factors:

1) ***Reliable reception at relay***: In DF-based cooperative communication, a relay would not forward the message to the destination if it fails to decode the data from the source node. Therefore, we should guarantee that the transmission rate will exceed the worst mutual information of the source-relay channels with a small probability at most

$$Pr[R_{\mathcal{B}} > \min\{I_{sr_i}\}] \leq P_{sr},\ r_i \in \mathcal{B}, \tag{4.4}$$

where I_{sr_i} is the mutual information between the source and the relay r_i, and P_{sr} is the predetermined outage probability.

2) ***Reliable reception at destination***: We should guarantee a reliable data reception at the destination with the help of relay. Hence, the transmission rate should not exceed the mutual information of the source-destination channel with a probability higher than

$$Pr[R_{\mathcal{B}} > I_{sd(\mathcal{B})} \,|\, \mathcal{B}] \leq P_{coop}, \tag{4.5}$$

where $I_{sd(\mathcal{B})}$ is the mutual information between the source and the destination with relay set $\mathcal{B}$, and P_{coop} is a predetermined outage probability.

3) ***Transmission power constraint***: In each round of cooperative communication, the total power consumed by the source and relays should be not higher than the non-cooperative scheme.

Now, we could express the relay selection problem to optimize the OPT time as:

$$\begin{aligned} &\arg\min_{\mathcal{B}\subseteq\mathcal{R}} \left\{ \frac{2L}{WR_{\mathcal{B}}} + \max\{T_{sr_i} + T_{r_i d}\} \right\}, \quad r_i \in \mathcal{B} \\ s.t. \quad &Pr[R_{\mathcal{B}} > \min\{I_{sr_i}\}] \leq P_{sr}, \\ &Pr[R_{\mathcal{B}} > I_{sd(\mathcal{B})} \,|\, \mathcal{B}] \leq P_{coop}. \end{aligned} \tag{4.6}$$

Here, L is the packet size in bits and W is the communication bandwidth in hertz. T_{sr_i} and $T_{r_i d}$ are the propagation delay from the source to relay r_i, and from relay r_i to the destination, respectively. The objective function of (4.6) includes the overall data transmission time and the maximum propagation delay of sound signal from the source to the destination through the relay.

We first derive the closed form of (4.4). The mutual information between source node and relay r_i is:

$$I_{sr_i} = \frac{1}{2}\log_2\left(1 + \frac{1}{(|\mathcal{B}|+1)} SNR|a_{sr_i}|^2\right), \tag{4.7}$$

where $SNR = P/N_0$ is the signal-to-noise ratio at the sender side[2]. P and N_0 are the transmission power and noise power, respectively. The coefficient $1/2$ indicates that an additional time slot (second phase) is required in DF-based cooperative communication. $|\mathcal{B}|$ is the number of relays in the relay set $\mathcal{B}$. The coefficient $1/(|\mathcal{B}|+1)$ indicates that the total power is equivalently assigned amongst the source and relays to meet the transmission power constraint. Substituting (4.7) into (4.4) and leveraging $|a_{sr_i}|^2 \sim Exponential(\lambda_{sr_i})$, we obtain

$$\begin{aligned} & Pr\left[R_{\mathcal{B}} > \min\left\{\frac{1}{2}\log_2\left(1+\frac{1}{(|\mathcal{B}|+1)}SNR|a_{sr_i}|^2\right)\right\}\right] \leq P_{sr} \\ \Rightarrow \quad & R_{\mathcal{B}} \leq \frac{1}{2}\log_2\left[\frac{-SNR\ln(1-P_{sr})}{\max\{\lambda_{sr_i}(|\mathcal{B}|+1)\}}+1\right],\ r_i \in \mathcal{B}. \end{aligned} \tag{4.8}$$

Now, we have the closed form of (4.4). Next, I derive the closed form of (4.5). Here, I first introduce a lemma [60] that will be used in the following derivation.

Lemma 1. *Let $(X_i)_{i=1,\ldots,n}, n > 1$, be independent exponential random variables with pairwise distinct respective parameters λ_i. Then the density of their sum is*

$$f_{X_1+X_2+\cdots+X_n}(x) = \left[\prod_{i=1}^{n}\lambda_i\right]\sum_{j=1}^{n}\frac{e^{-\lambda_j x}}{\prod\limits_{\substack{k=1\\k\neq j}}^{n}(\lambda_k-\lambda_j)}, x > 0. \tag{4.9}$$

At the destination, the receiver combines the packets it heard from the source and relays to enhance the receiving SNR. Therefore, the mutual information $I_{sd(\mathcal{B})}$ in (4.5) could be expressed as

$$I_{sd(\mathcal{B})} = \frac{1}{2}\log_2\left(1+\frac{SNR}{(|\mathcal{B}|+1)}|a_{sd}|^2+\sum_{r_i\in\mathcal{B}}\frac{SNR}{(|\mathcal{B}|+1)}|a_{r_id}|^2\right). \tag{4.10}$$

Substituting (4.10) into (4.5), we have

$$Pr\left[\left(|a_{sd}|^2+\sum_{r_i\in\mathcal{B}}|a_{r_id}|^2\right) < \frac{(|\mathcal{B}|+1)\,(2^{2R_{\mathcal{B}}}-1)}{SNR}\,|\,\mathcal{B}\,\right] \leq P_{coop}. \tag{4.11}$$

[2]The SNRs I used in COBRA are all signal-to-noise ratios at the sender side rather than at the receiver side.

Let λ_1 and λ_j re-represent λ_1 and $\lambda_{r_i d}$, respectively, where $r_i \in \mathcal{B}$ and $j = 2, 3, \ldots, |\mathcal{B}|+1$. Since $|a_{sd}|^2$ and $|a_{r_i d}|^2$ are two independent variables with exponential distribution, leveraging the conclusion of Lemma 1 and doing an integral operation, (4.11) becomes

$$\left[\prod_{j=1}^{|\mathcal{B}|+1}\lambda_j\right]\sum_{j=1}^{|\mathcal{B}|+1}\frac{e^{-\lambda_j\frac{(|\mathcal{B}|+1)(2^{2R_{\mathcal{B}}}-1)}{SNR}}-1}{-\lambda_j\prod\limits_{\substack{k=1\\k\neq j}}^{|\mathcal{B}|+1}(\lambda_k-\lambda_j)} \leq P_{coop}. \tag{4.12}$$

Then, I use $|\mathcal{B}|+1$ order Maclaurin series to approximate the exponential term in (4.12):

$$\begin{aligned}
&\left[\prod_{j=1}^{|\mathcal{B}|+1}\lambda_j\right]\sum_{q=1}^{|\mathcal{B}|+1}\frac{(\frac{(|\mathcal{B}|+1)\,(2^{2R_{\mathcal{B}}}-1)}{SNR})^q}{q!}\sum_{j=1}^{|\mathcal{B}|+1}\frac{(-\lambda_j)^{q-1}}{\prod\limits_{\substack{k=1\\k\neq j}}^{|\mathcal{B}|+1}(\lambda_k-\lambda_j)} \leq P_{coop}\\
\Rightarrow &\left[\prod_{j=1}^{|\mathcal{B}|+1}\lambda_j\right]\frac{(\frac{(|\mathcal{B}|+1)\,(2^{2R_{\mathcal{B}}}-1)}{SNR})^{|\mathcal{B}|+1}}{(|\mathcal{B}|+1)!} \leq P_{coop}\\
\Rightarrow &R_{\mathcal{B}} \leq \frac{1}{2}\log_2\left[\left(\frac{(|\mathcal{B}|+1)!\,P_{coop}}{\prod_{j=1}^{|\mathcal{B}|+1}\lambda_j}\right)^{\frac{1}{|\mathcal{B}|+1}}\frac{SNR}{(|\mathcal{B}|+1)}+1\right]\\
\Rightarrow &R_{\mathcal{B}} \leq \frac{1}{2}\log_2\left[\left(\frac{(|\mathcal{B}|+1)!\,P_{coop}}{\lambda_{sd}\prod_{r_i\in\mathcal{B}}\lambda_{r_i d}}\right)^{\frac{1}{|\mathcal{B}|+1}}\frac{SNR}{(|\mathcal{B}|+1)}+1\right],
\end{aligned} \tag{4.13}$$

It is worth noting that for the exponential function $e^x, x \in (-\infty, \infty)$, the remainder of a k-order Maclaurin series is $E_{|\mathcal{B}|}(x) = e^{\xi}x^{|\mathcal{B}|+1}/(|\mathcal{B}|+1)!$, where ξ is a number between 0 and x. To make the left side of (4.13) smaller than or equal to its right side, $E_{|\mathcal{B}|}(x)$ needs to be larger than zero. This requests $|\mathcal{B}|+1$ to be an even number when $x < 0$. However, in (4.12), the parameter SNR is the signal-to-noise at the sender side (not the receiver side), which is high. Therefore, the remainder of a Maclaurin series will be a small value. In this situation, an odd $|\mathcal{B}|+1$ only sightly losses the boundary of $R_{\mathcal{B}}$, and the symbol "$\leq$" should be replaced by "$\approx$" in (4.13).

Now, replacing the constraint conditions in (4.6) with (4.8) and (4.13), we obtain

$$\begin{aligned} &\arg\min_{\mathcal{B}\in\mathcal{R}} \left\{ \frac{2L}{WR_{\mathcal{B}}} + \max\{T_{sr_i} + T_{r_i d}\} \right\}, r_i \in \mathcal{B} \\ s.t.\ R_{\mathcal{B}} \leq \min\Bigg\{ &\frac{1}{2}\log_2\left[\frac{-SNR\ln(1-P_{sr})}{\max\{\lambda_{sr_i}\}\,(|\mathcal{B}|+1)}+1\right], \\ &\frac{1}{2}\log_2\left[\left(\frac{(|\mathcal{B}|+1)!\,P_{coop}}{\lambda_{sd}\prod_{r_i\in\mathcal{B}}\lambda_{r_i d}}\right)^{\frac{1}{|\mathcal{B}|+1}}\frac{SNR}{(|\mathcal{B}|+1)}+1\right]\Bigg\}. \end{aligned} \tag{4.14}$$

From (4.14) we observe that the spectral efficiency $R_{\mathcal{B}}$ in the DF-based cooperative scheme is constrained by the worst source-to-relay channel ($\max\{\lambda_{sr_i}\}$) and all relay-to-destination channels ($\prod_{r_i\in\mathcal{B}}\lambda_{r_i d}$). Fig. 4.4 demonstrates the $R_{\mathcal{B}}$ with resect to $\max\{\lambda_{sr_i}\}$ and $\prod_{r_i\in\mathcal{B}}\lambda_{r_i d}$, where I set $\lambda_{sd} = 0.5$, $SNR = 5$ dB, $P_{coop} = P_{sr} = 10^{-2}$. From this figure, we observe that:

1. Both bad source-to-relay channel (large $\max\{\lambda_{sr_i}\}$) and relay-to-destination channels (large $\prod_{r_i\in\mathcal{B}}\lambda_{r_i d}$) could reduce the spectral efficiency considerably.
2. When relay-to-destination channels are bad (large $\prod_{r_i\in\mathcal{B}}\lambda_{r_i d}$), the flat area in Fig. 4.4 illustrates that the spectral efficiency will not increase no matter how good the source-to-relay channel (small $\max\{\lambda_{sr_i}\}$) is, but limited by the poor relay-to-destination channels.
3. If the quality of a source-to-relay channel is poor ($\max\{\lambda_{sr_i}\} > 0.01$), the spectral efficiency barely changes with the variation of relay-to-destination channels. On another hand, with fixed relay-to-destination channels ($\prod_{r_i\in\mathcal{B}}\lambda_{r_i d}$)), the spectral efficiency improves significantly with the increase of $\max\{\lambda_{sr_i}\}$. These observations indicate that COBRA is resilient to a bad relay-to-destination channel, but susceptible to a poor source-to-relay channel. This is because in a DF-based cooperative scheme, each selected relay should be able to decode the raw packet. In this case, the spectrum efficiency in (4.8) is constrained by a relay with the worst channel to the source node. On the contrary, as expressed in (4.13), the

spectrum efficiency between the source and destination through the selected relay set is affected by the quality of source-to-destination channel and that of all relay-to-destination channels. The quality degradation of a few of these channels will not affect the spectrum efficiency in (4.13) too much.

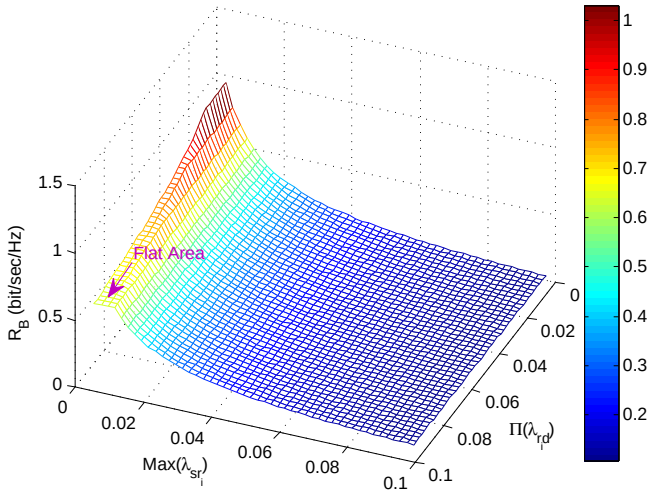

Figure 4.4: R_i with respect to λ_{sr_i} and λ_{r_id}, where $\lambda_{sd} = 0.5$.

4.1.5 Best relay selection

In the previous section, I have introduced the details of COBRA. In this section, I introduce how to select the best relay set based on the COBRA criterion.

Denote the OPT time, i.e., the objective function in (4.14), with relay set $\mathcal{B}$ as $F_{\mathcal{B}}$. We select the best relay set to minimize $F_{\mathcal{B}}$ through the following algorithm:

1. First of all, I select a single node, r_1^*, as the best relay based on (4.14) and set $\mathcal{B}_1 = \{r_1^*\}$.
2. Then, I add a new relay, r_2^*, into the previous relay set to minimize $F_{\mathcal{B}_2}$, where $\mathcal{B}_2 = \{r_1^*, r_2^*\}$.
3. Repeat Step 2, adding a new relay in each time until all potential relays are involved into the relay set.

4. Finally, I search for the minimum $F_{\mathcal{B}_n}$ from $\{F_{\mathcal{B}_1}, F_{\mathcal{B}_2}, \ldots, F_{\mathcal{B}_{|\mathcal{R}|}}\}$ calculated in previous steps, and the corresponding relay set, $\mathcal{B}_n$, is the best relay set, i.e., $\mathcal{B} \triangleq \mathcal{B}_n$.

It is worth nothing the OPT time in a COBRA based cooperative network is not monotonically decreasing function of number of relays joined in the communication. This is because COBRA equally allocates power among relays. The more relays we use, the higher the risk is to select a relay with a bad channel quality or a long propagation delay, which incurs higher energy consumption but without significant contribution on reducing the OPT time. Therefore, in the above algorithm, a source node needs to calculate all $F_{\mathcal{B}_n}$, $n = 1, 2, \ldots, |\mathcal{R}|$, and selects the best relay set with the minimum $F_{\mathcal{B}_n}$.

4.1.6 Cooperative or non-cooperative transmission

The performance of a cooperative communication is susceptible a poor quality of source-to-relay channel. Hence, in some circumstances, the performance of a network with a cooperative scheme not be better than that without it. In this section, I study when should a source node starts a cooperative communication and when it needs to send the data directly to the destination without the help of relay nodes.

Let R_{non} and P_{non} be the spectral efficiency and the outage probability of a non-cooperative communication, respectively. Then we have

$$\begin{aligned} & Pr[R_{non} > I_{sd}^{'}] \leq P_{non} \\ \Rightarrow \;& Pr[R_{non} > \log_2(1 + SNR|a_{sd}|^2)] \leq P_{non} \\ \Rightarrow \;& R_{non} \leq \log_2\left[\frac{-SNR\ln(1 - P_{non})}{\lambda_{sd}} + 1\right], \end{aligned} \tag{4.15}$$

where $I_{sd}^{'}$ is the mutual information between the source and the destination without the cooperative scheme. Compared with (4.7) and (4.10), the coefficients $1/2$ and $|\mathcal{B}| + 1$

have been removed in (4.15), since all channel and power resource could be assigned to the source node for its packet transmission.

When the best relay set is employed, denote the corresponding spectrum efficiency, maximum propagation delay from the source to the relay set and from the relay set to the destination as R^*_{coop}, T^*_{sr} and T^*_{rd}, respectively. Let ΔT be the difference of propagation delay between the relay path and direct path, i.e., $\Delta T = T^*_{sr} + T^*_{rd} - T_{sd}$. The OPT time of a non-cooperative scheme is superior when

$$\begin{aligned} &\frac{L}{WR_{non}} \leqslant \frac{2L}{WR^*_{coop}} + \Delta T \\ \Rightarrow\ &\frac{\Delta T}{L} \geq \frac{1}{W}(\frac{1}{R_{non}} - \frac{2}{R^*_{coop}}); \end{aligned} \tag{4.16}$$

otherwise, the cooperative scheme is preferred.

Here, I call $\Delta T/L$ as the ΔTL ratio — a metrics for the source node to choose the appropriate transmission scheme. Now, I use an example, where I set $W = 5$ kHz, $SNR = 5$ dB, $P_{non} = P_{coop} = P_{sr} = 10^{-2}$, to demonstrate the impact of the ΔTL ratio. Fig. 4.5 shows the threshold of ΔTL ratio, when the left side of (4.16) is equivalent to the right side, with respect to λ_{sr_i}, λ_{r_id} and λ_{sd}. From this figure we observe that the cooperative scheme will outperform the non-cooperative one once the ΔTL ratio is smaller than the threshold; otherwise, the non-cooperative scheme obtains shorter OPT time.

Now, I give an insight into Fig. 4.5. As we know, the cooperative communication could increase the transmission rate of a source node through improving the spectrum efficiency, thereby reducing the transmission time of a data packet. Compared with the non-cooperative scheme, however, a packet in the cooperative communication experiences larger delay, since the source-relay-destination path is always longer than the source-to-destination path. Hence, the reduction of transmission time in an underwater cooperative network is at the cost of longer propagation delay. In order to use

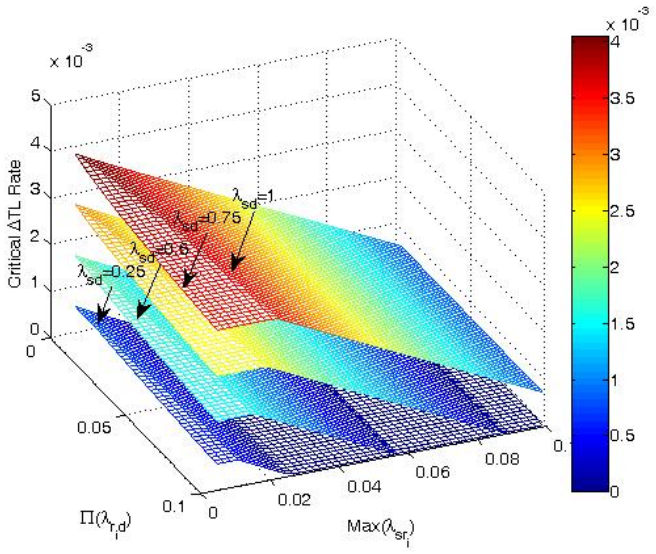

Figure 4.5: Threshold of the ΔTL ratio as a function of λ_{sr_i}, λ_{r_id} and λ_{sd}.

cooperative scheme more efficiently, we could decrease the threshold of ΔTL ratio by increasing the packet size, L. The larger the packet size is, the more the transmission time could be saved in cooperative communications, and thus the higher the resilience of ΔT is.

In addition, Fig. 4.5 illustrates that although the deterioration in the quality of both source-to-relay (larger λ_{sr_i}) and relay-to-destination (larger λ_{r_id}) channel will decrease the threshold of ΔTL ratio, ΔTL ratio is more sensitive to the variation of λ_{sr_i} than that of λ_{r_id}, which is similarly demenstrated in Fig. 4.4.

Moreover, when the quality of source-to-destination channel becomes better (smaller λ_{sd}), the threshold of ΔTL ratio will decrease, and the source node will tend to send the data straightforwardly without the help of relays.

4.1.7 Cooperative MAC

In this section, I provide a handshake based MAC protocol for an underwater cooperative network with COBRA criterion.

At the beginning of a round of cooperative communication, the source node broadcasts a request-to-send (RTS) packet first. The RTS has two functions: one is to reserve the channel for collision avoidance and to estimate the channel gain a_{sd} and propagation delay T_{sd} at the receiver side; another one is to help with the relay selection by measuring the channel gain a_{sr_i} and propagation delay T_{sr_i} at relay r_i. After receiving RTS, the receiver replies with a clear-to-send (CTS) packet if it is free to receive the data. Relay r_i could measure the parameters a_{r_id} and T_{r_id} by overhearing the CTS packet. Only a node that hears both the RTS and CTS messages could work as a potential relay.

In radio network, the instantaneous channel gains, a_{sd}, a_{r_id} and a_{sr_i}, may be available. In underwater environment, however, these parameters are usually out of data owing to the large propagation delay, long transmission time of a packet and high dynamic of an acoustic channel [61]. Nevertheless, a node could get the statistical feature of a channel, i.e., λ_{sd}, λ_{r_id} and λ_{sr_i} by utilizing historical measurements of the channel gain in COBRA.

After potential relays updating the parameters λ_{r_id} and λ_{sr_i} according to the latest measurements of the channel gain, they attach these parameters into a prepare-to-help (PTH) packet and send it to the source node. When the source node received PTH packet, it measurements a new channel gain a_{sr_i} and uses it to update λ_{sr_i}. Now, the source node obtains all statistical channel information in (4.14) for the optimal relay select selection.

It is worth noting that a relay does not need to send a PTH packet in each round of communication, unless in the following two situations:

1. At the beginning of the protocol. At the first several periods of the protocol, λ_{sr_i}, λ_{r_id} and λ_{sd} may change a lot before obtaining enough historical value of channel gain for an accurate statistical measurement.

2. The statistical feature of an underwater channel changes significantly. In this situation, a relay retransmits the parameters λ_{r_id} and λ_{sr_i} to the source node through the PTH packet. The source node will update the corresponding channel information of potential relays for the future optimal relay selection.

From the above description we know that a relay node will not send a PTH frequently in a stable underwater environment. The overhead on sending PTH messages thus is negligible in the MAC protocol.

After receiving the PTH packets, the source node chooses the best relay set based on the COBRA algorithm described in Section 4.1.5, and calculates the corresponding ΔTL ratio. According to the analyze in Section 4.1.6, the source node will sent the data to the destination directly if the ΔTL ratio is higher than the threshold; otherwise, it will start the DF-based cooperative transmission described in Section 4.1.2.

4.1.8 Performance evaluation

In this section, I investigate the performance of COBRA criterion through simulations. Both the CSI based criterion [54] and the maximum transmission rate based criterion [55] are implemented for comparison. The CSI based criterion selects the relay with the best channel quality, i.e., $\min\{\max\{\lambda_{sr_i}, \lambda_{r_id}\}\}$, while the maximum transmission rate based criterion chooses the relay to optimize the spectrum efficiency, i.e., $\max\{R_{\mathcal{B}}\}$. Simulation results show the superior of an underwater cooperative network with the COBRA criterion in terms of OPT time, throughput and packet delivery ratio.

4.1.8.1 Point-to-point performance

I first compare the spectrum efficiency and OPT time of different criteria with respect to the number of relays and SNRs in point-to-point cooperative communications,

as shown in Fig. 4.6 and Fig. 4.7, respectively. In these two figures, the distance from the source to the destination is 2 km. There are a total number of 10 potential relays deployed between the source and the destination. The transmission power is equally allocated to the source and relay nodes. I model the underwater channel as a Rayleigh fading channel, and assume $\lambda_{r_i d} \sim U(5 \times 10^{-3}, 1 \times 10^{-1})$ for relay r_i, where U represents an uniform distribution. The communication bandwidth, sound speed in water and SNR at the sender side are 5 kHz, 1500 m/sec and 5 dB, respectively. I assume the quality of source-to-relay channel is poor, where $\lambda_{sd} = 0.5$. The size of data packet, and outage probability for both P_{sr} and P_{coop} are set to 100 B and 10^{-2}, respectively.

From Fig. 4.6(a) I observer that the spectrum efficiency of COBRA is lower than another two criteria when the quality of source-to-relay channels is good (small λ_{sr_i}). This is because COBRA need to take into account not only the spectrum efficiency but also the propagation delay for optimizing the OPT time. This implies that a node with a good channel quality but a long distance to the source and the detonation may not be chosen as a relay in COBRA, which decreases the spectrum efficiency. In addition, the $R_{\mathcal{B}}$ in the figure is not a monotonically increasing function. That is why a source node needs to select the best relay set from potential relays for efficient cooperative communication, as I discussed in Section 4.1.5.

Fig. 4.6(b) shows the variation of $R_{\mathcal{B}}$ with respect to the number of relays in a poor source-to-relay channels (λ_{sr_i}). Compared with Fig. 4.6(a), $R_{\mathcal{B}}$ in Fig. 4.6(b) is much small, and the spectral efficiency is a monotonically decreasing function of the size of relay set in all three cooperative criteria. This observation verify that the performance of DF-based cooperative scheme is susceptible to a poor source-to-relay channel. In this situation, the spectral efficiency is most likely constrained by $\max\{\lambda_{sr_i}\}$ rather than $\prod_{r_i \in \mathcal{B}} \lambda_{r_i d}$ in (4.14). When more relays are selected, the power assigned to each

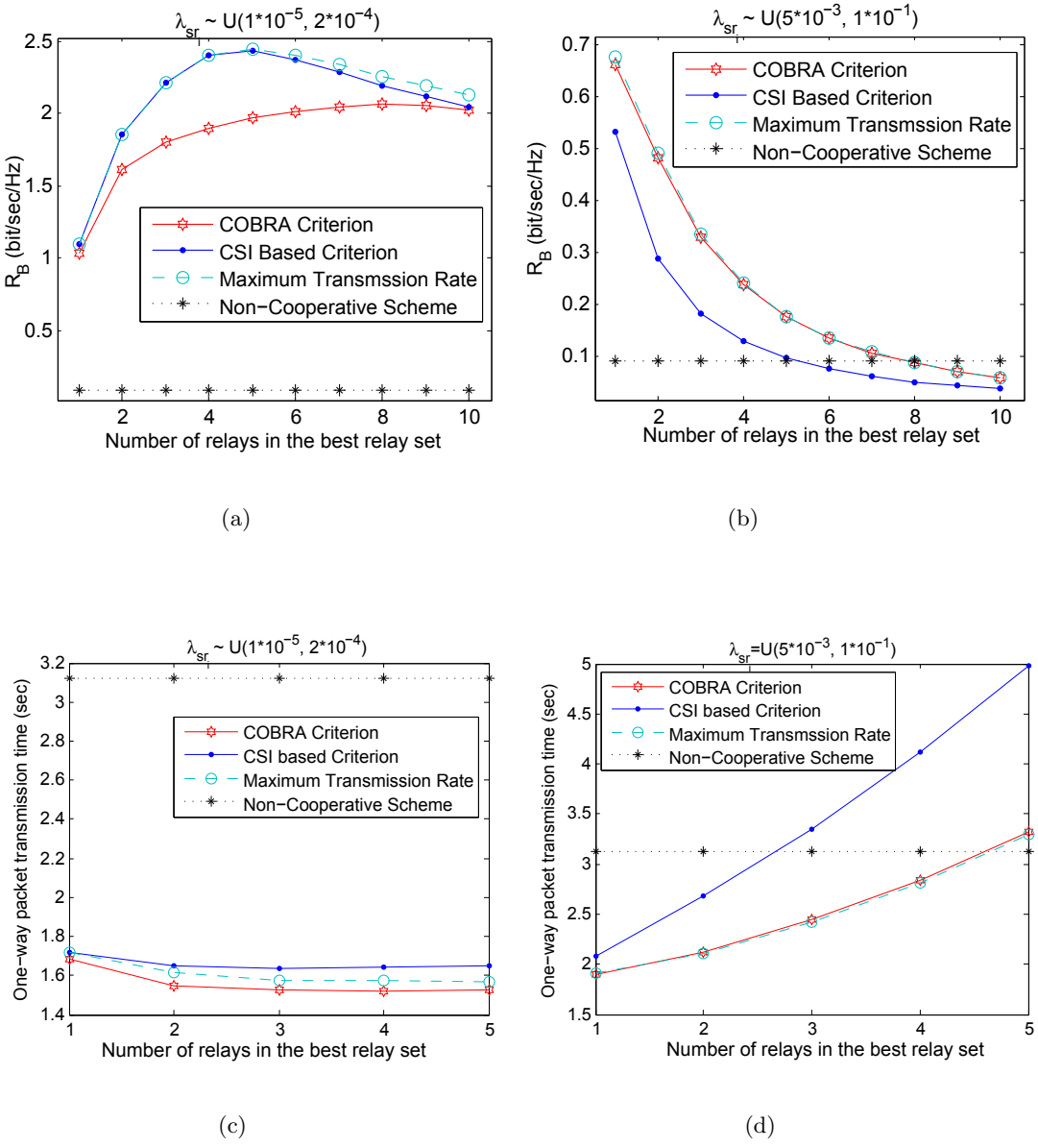

Figure 4.6: Performance comparison among different criteria with respect to the number of relays. (a) Spectrum efficiency with small λ_{sr_i}. (b) Spectrum efficiency with large λ_{sr_i}. (c) OPT time with small λ_{sr_i}. (d) OPT time with large λ_{sr_i}.

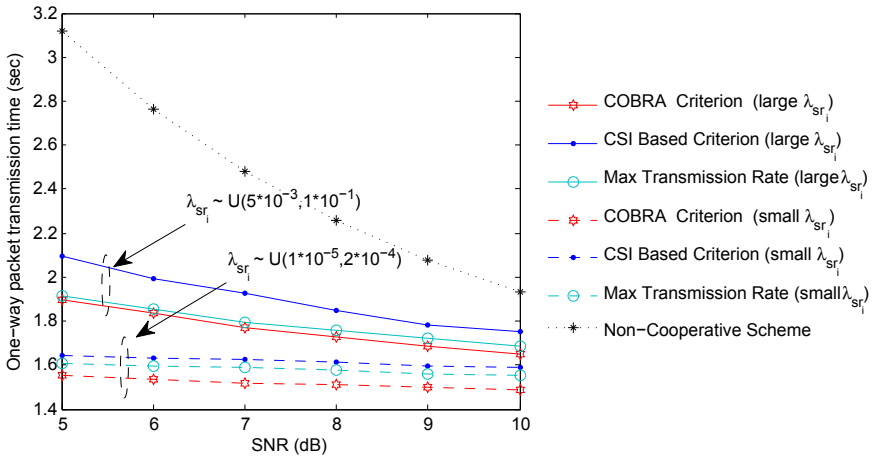

Figure 4.7: OPT time comparison between different criteria as a function of SNR with the best relay set.

node will reduce, and $\max\{\lambda_{sr_i}\}$ may increase, which finally decreases the spectrum efficiency in a cooperative scheme.

Fig. 4.6(c) and Fig. 4.6(d) illustrate the OPT time of the three criteria. The performance of COBRA is better than another two criteria at different λ_{sr_i}, since COBRA considers both the spectrum efficiency and the propagation delay. In addition, with a good source-to-relay channel (small λ_{sr_i}), a DF-based cooperative scheme with all three criteria outperforms the non-cooperative one, as shown in Fig. 4.6(c). Moreover, COBRA achieves the shortest OPT time amongst all three criteria with arbitrary number of relays. Increasing the size of relay set in this scenario could reduce the OPT time. On another hand, if the source-to-delay channel is bad, the OPT time will increase with the number of relays, as demonstrated in Fig. 4.6(d). This is because a large number of relay cases a low spectrum efficiency and a long propagation delay, which have been analyzed in Fig. 4.6(b).

Fig. 4.7 shows the OPT time with respect to the SNR when the best relay set is selected through (4.14). From this figure we obtain that the OPT time in all communication schemes decreases with a growing SNR. Moreover, COBRA achieves a shorter OPT time than other schemes, especially when SNR is low. In a high SNR situation,

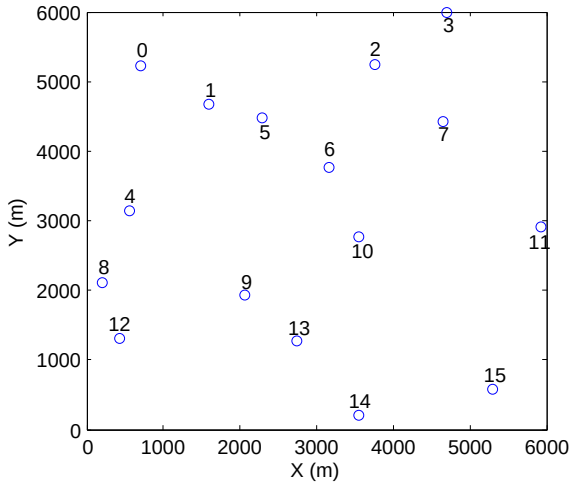

Figure 4.8: Deployment of nodes . (Nodes 0–14 communicate with Nodes 1–15 respectively.)

the propagation delay dominates the OPT time, while an improvement of the transmission time obtained from a cooperative communication is negligible. Therefor, the OPT time of an noncooperative transmission becomes comparable with a cooperative one with a high SNR.

4.1.8.2 Network performance

We use Aqua-Sim to evaluate the throughput and delivery ratio of different cooperative and non-cooperative schemes in UANs. In the the previous section, we observe that the maximum transmission rate criterion is superior to the CSI based one on both the spectrum efficiency and the OPT time. Therefore, I compare COBRA with the maximum transmission rate criterion in this section.

In a network, I assume 16 nodes are randomly distributed in a 6000 m $\times$6000 m rectangular area, as shown in Fig. 4.8. Nodes with even ID run a Poisson traffic generator and send packet to the nodes at their right hand with odd ID. All nodes in the communication range (2 km) of a sender-receiver pair are considered as potential

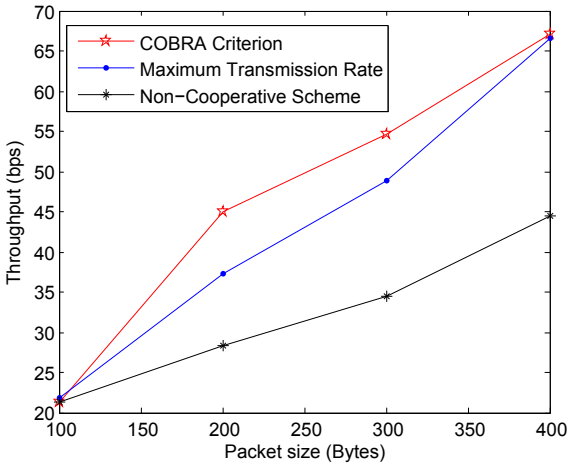

Figure 4.9: Throughput comparison between different criteria with respect to packet size.

relays. Each point in Fig. 4.9 or Fig. 4.10 is the average of 10 random deployments, and each deployment repeat 20 times.

According to the analysis in Section 4.1.5, the efficiency of a underwater cooperative communication depends on the packet transmission time and the propagation delay. Here, I change the transmission time by increasing the packet size in the simulation and show the throughput in Fig. 4.9. The traffic load per node in this test is 0.025 packet/second. The SNR and channel settings are the same as Fig. 6(b). This figure illustrates that with moderate packet sizes, there is more significant throughput improvement of COBRA criterion than both the non-cooperative scheme and the conventional cooperative scheme.

In addition, when the packet size is small, the propagation delay dominates the OPT time. The benefit on reducing the packet transmission time is overwhelmed by the increased propagation delay in a cooperative communication. In this situation, COBRA will smartly switch to a noncooperative scheme to increase the throughput and the delivery ratio of the network. With the growth of a packet size, the OPT time decreases significantly in COBRA criterion, thereby achieving considerably throughput

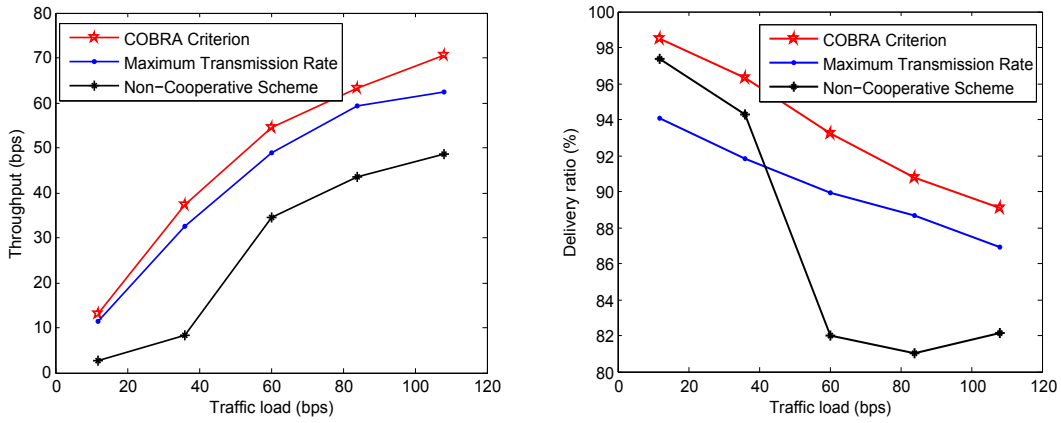

(a) (b)

Figure 4.10: Performance comparison between different criteria with respect to the network traffic load. (a) Throughput. (b) Delivery ratio.

improvement. Compared with the maximum transmission rate criterion, which chooses relays with a higher spectrum efficiency but much longer propagation delay, COBRA has as much as 20% throughput improvement. When the packet size in the simulation is larger than 400 B, the throughput of COBRA and maximum transmission rate criterion become comparable, since the reducing of a transmission time overwhelms a propagation delay.

Fig. 4.10 presents the throughput and delivery ratio of different communication schemes with a varying traffic load, where the packet size is set to 300 B. The throughput of all three schemes increases with the growth of a traffic load. By contrast, the delivery ratio decreases significantly due to the high collision probability at a heavy traffic load scenario.

COBRA offers the highest throughput performance, along with better delivery ratio as illustrated in Fig. 4.10. Owning to the optimized OPT time, the average time on delivering a data packet in COBRA is much shorter than the maximum transmission rate criterion and an non-cooperative communication. Moreover, the maximum transmission rate criterion shows a superior throughput performance than the non-cooperative

one, since a cooperative scheme could dramatically decrease the transmission time of a packet with a large packet size (300 B). Nevertheless, it is still less than the COBRA criterion, since it omits the propagation delay in the relay selection.

In Section 3.3, I introduced that the long transmission time of a packet would case a high collision probability among messages by increasing the length of the collision window. Through the transmission of relay nodes increases the traffic load of a network, a short packet transmission time obtained from a cooperative communication still reduces the collisions even in a high traffic load scenario. This could be observed in Fig. 4.10(b), where the packet delivery ratios of COBRA and maximum transmission rate based cooperative schemes are much higher than the non-cooperative scheme. When the traffic load increases to 60 bps, the collision avoidance mechanism in the non-cooperative scheme stops the collision probability further decreasing with the cost of increasing of throughput.

4.2 MNAC

In the previous section, I have introduced a new criterion, COBRA, for the best relay selection in a DF-based underwater cooperative network. In this section, I propose a new cooperative scheme, called MNAC, for UANs.

In MNAC, I select a proper mirror node for each specific source node, and make the signals from the source and the mirror node add destructively at a certain receiver that we want to protect. In this way, the protected node could receive data from its intended sender, while not be interfered by other mirror-assisted nodes, even if they transmit simultaneously. With the proposed technique, multiple data streams could be sent in parallel without causing any collisions, thereby improving the channel efficiency of UANs. I also design a simple MAC protocol, called the mirror node assisted MAC (MNA-MAC), for MNAC. In addition to guarantee a strong destructive interference at

the protected receiver, MNA-MAC could select the best mirror node to maximize the channel capacity from the cooperative communication point of view.

4.2.1 Motivation

Here, let us consider a common application of a UAN. As shown in Fig. 4.11, multiple underwater sensor nodes are deployed in oceans to monitor an interesting area. Through acoustic communications, they could send the collected data to surface nodes (sink nodes) in real-time. In order to reduce the shadow zone (the region not covered by sensors) in the monitoring area, the coverage range of neighboring surface nodes overlaps with each other properly.

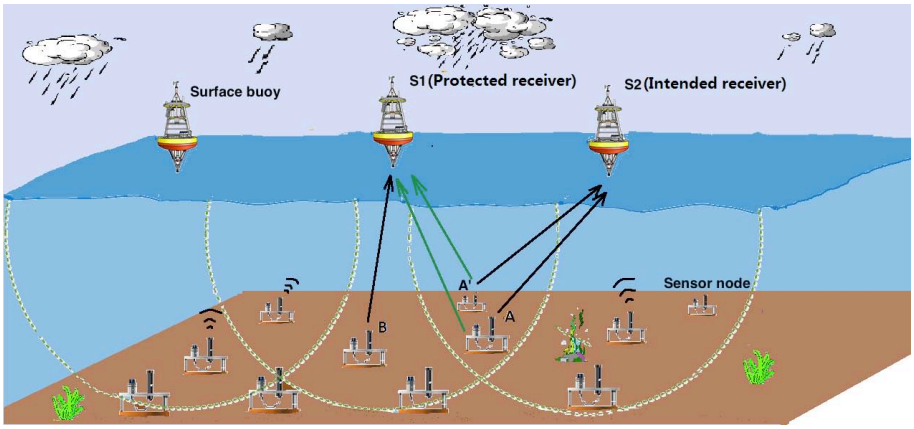

Figure 4.11: Underwater sensor network, where a semicycle represents the coverage of a surface node.

In the network depicted in Fig. 4.11, suppose each node is equipped with a single half-duplex transducer. Sensor node A is in an overlapping area of surface nodes S_1 and S_2, i.e., both S_1 and S_2 could hear the signal from node A. Now, assume that nodes A and B plan to send their data to S_2 and S_1, respectively. In this scenario, to prevent the node A's signal from interfering with the data reception at S_1, nodes A and B have been generally assumed that one should keep quiet while another is transmitting.

MNAC challenges that assumption, and shows via analysis that it is possible to let node B transmit with node A simultaneously without causing any collisions at S_1, while improving the SNR at S_2[3] . I leverage the destructive interference of acoustic waves to achieve this goal.

4.2.2 Destructive interference benefits

Destructive interference is a common phenomenon, which could be observed with all types of waves, such as light, electromagnetic and acoustic waves. In this section I give a brief description on this phenomenon, and then introduce how to harness the destructive interference for improving the performance of UANs.

4.2.2.1 What is destructive interference

According to the principle of superposition [62], if multiple waves of same type are incident on a certain point, the displacement at that point is equal to sum of the displacements of the individual waves. As shown in Fig. 4.12, if the crests of two waves meet with each other, then *constructive interference* occurs. If the crest of a wave meet the trough of another one, then *destructive interference* occurs.

At a certain point, the destructive interference is most effective when the amplitudes of two signals are equivalent while the phase difference between them is π. In this situation, two signals add destructively, thus each completely cancels out the other.

4.2.2.2 Making destructive interference useful

In a wireless communication, the signal from a transmitter may arrive at a receiver through multiple paths if there are reflectors in the environment, for example, cloud, ground, sea surface and barriers. Signals from different paths experience differences in

[3]In the rest of the section, I call S_1 and S_2 as the protected receiver and the intended receiver of node A, respectively.

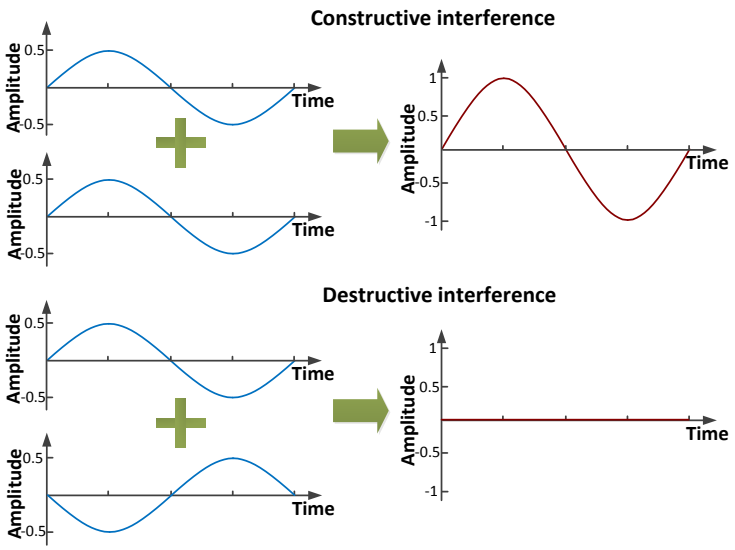

Figure 4.12: Constructive and destructive interferences.

attenuation, phase shift and delay when traveling from the source to the destination. If two or more of these signals meet the requirement of destructive interference, an attenuation of the signal power would be observed at the receiver. A strong destructive interference is usually referred to as the deep fading, which may cause a sharp decrease in receiving SNR.

In most of applications, we should avoid the deep fading, since it may result in a failure of communication [63]. However, in MNAC I propose to take advantage of the strong destructive interference in a completely new way, which enables multiple nodes to transmit at the same time without interfering with the data reception of each intended receiver.

More specifically, as shown in Fig. 4.11, before a data transmission, the sink node selects a mirror node, which is denoted by A′, for node A. When A is transmitting, A′ is also arranged to send the same data with node A after a certain delay. By adjusting the transmission delay and the transmission power of A′ carefully, it is possible to make the amplitudes of the signals from A and A′ be equivalent at S_1, and the phase difference between them be π. In this way, the source and the mirror signals are cancelled out with

each other. Therefore, the signal from node A would not disrupt the data reception at the protected receiver, S_1. With this approach, nodes A and B could send their data simultaneously without causing any collisions.

4.2.3 Performance of MNAC

If we use the MNAC in a real UAN, its performance may be affected by many factors, such as the error of distance measurement, the bandwidth of a signal and the location of a mirror node. In this section, I give an insight into these problems.

4.2.3.1 Distance measurement error

In order to well protect a specific receiver, the amplitudes of signals from the source and its mirror node should be the same at the protected receiver, but their phases should differ by π.

Now, I use Fig. 4.11 as an example to analyze the effect of distance measurement error on MNAC. Denote the signals from the source node A and the mirror node A$'$ by $s_A e^{j(2\pi f_A t+\phi_A)}$ and $s_{A'} e^{j(2\pi f_{A'} t+\phi_{A'})}$, respectively. Here s, f and ϕ represent the amplitude, frequency and phase of a signal, respectively. Let a_{AS_1} and $a_{A'S_1}$ be the attenuation coefficients of acoustic signals from A and A$'$ to the protected node S_1, respectively. Therefore, the received signal of S_1, which is represented as $r(t)$, is

$$r(t)=\frac{s_A}{a_{AS_1}} e^{j(2\pi f_A t+\phi_A+\phi_{AS_1})}+\frac{s_{A'}}{a_{A'S_1}} e^{j(2\pi f_{A'} t+\phi_{A'}+\phi_{A'S_1})}, \tag{4.17}$$

where ϕ_{AS_1} and $\phi_{A'S_1}$ are the phase shifts of signals traveling from nodes A and A$'$ to S_1, respectively.

To obtain a strong destructive interference, in (4.17) s_A/a_{AS_1} should equal to $s_{A'}/a_{A'S_1}$, and the difference between $\phi_A+\phi_{AS_1}$ and $\phi_{A'}+\phi_{A'S_1}$ should be π. However, a real system inevitably introduces some errors on the amplitude and phase of a signal owning to the hardware constraints. Now, denote the mismatch of amplitude and phase

between signals from nodes A and A′ at S_1 as $\Delta s(t)$ and $\Delta\phi$, respectively. Then, we have

$$\frac{s_{A'}}{a_{A'S_1}} = \frac{s_A}{a_{AS_1}} + \Delta s, \tag{4.18}$$

and

$$\phi_{A'} + \phi_{A'S_1} = \phi_A + \phi_{AS_1} + \pi + \Delta\phi. \tag{4.19}$$

Let p_{recv} be the instantaneous power of signal $r(t)$. Assume the source and its mirror node have the same transmission frequency, i.e., $f_A = f_{A'}$. According to (4.17), (4.18) and (4.19), after a simple derivation, we obtain that

$$\begin{aligned} p_{recv} &= r(t)\,\overline{r(t)} \\ &= \Delta s^2 + 2\frac{s_A}{a_{AS_1}}\Big[\frac{s_A}{a_{AS_1}} + \Delta s\Big](1 - \cos\Delta\phi), \end{aligned} \tag{4.20}$$

where $\overline{r(t)}$ represents the complex conjugation of $r(t)$.

In a real application, Δs and $\Delta\phi$ usually result from the error of distance measurements. More specifically, according to (4.18), in order to make $\Delta s = 0$, a mirror node should adjust its transmission power to offset the difference of propagation attenuations between the source and the mirror signals, i.e.,

$$s^*_{A'} = \frac{a_{A'S_1}}{a_{AS_1}} s_A, \tag{4.21}$$

where $s^*_{A'}$ represents the idea $s_{A'}$.

The attenuation coefficients, $a_{A'S_1}$ and a_{AS_1}, could be calculated through the geometrical spreading losses and Thorp's formula of an acoustic wave [64], which are distance-dependented parameters. $s_{A'}$ may deviate from the idea value if there are any errors in a distance measurement, which results in a nonzero Δs.

In (4.19), if the distances from nodes A and A′ to S_1 are different, ϕ_{AS_1} and $\phi_{A'S_1}$will be different. In this situation, A′ should rotate its initial phase to compensate for the difference of the phase shifts. This could be done by adding a certain delay on A′,

which is denoted by $\tau_{A'}$, before its data transmission. In (4.19), let $\phi_A = 0$, then it is easy to obtain that the idea $\tau_{A'}$ is

$$\tau^*_{A'} = \frac{1}{2f_A} + \frac{d_{AS_1} - d_{A'S_1}}{c}, \tag{4.22}$$

where c is the sound speed in water, d_{AS_1} and $d_{A'S_1}$ are the distances from nodes A and A$'$ to S_1, respectively. From (4.22) we observe that if there are any errors in a distance measurement, $\tau_{A'}$ may deviate from the ideal value, causing a nonzero $\Delta\phi$ in (4.19).

In Fig. 4.13, I consider the effect of destructive interference and show the attenuation of receiving signal power at S_1 with respect to the percentage of phase mismatch and amplitude mismatch. From this figure we observe that there is a deep null of receiving signal power exists if the mirror node transmits with the optimal signal strength and transmission delay as expressed in (4.21) and (4.22), respectively. After that the growth of mismatch in amplitude and phase weaken the effect of destructive interference. This increases the interference on a protected receiver, and thus hurts the performance of MNAC. For instance, assume the power and frequency of a signal that S_1 received from node A is 1 W and 17 kHz, respectively. If the phase mismatch and amplitude mismatch are both 1%[4] , then the attenuation of receiving signal at S_1 could reach 43 dB. In this case, the remaining interference produced by node A decreases from 1 W to 0.0037 W at S_1. When this mismatch increases to 5%, the attenuation reduces to 9.9 dB. In this circumstance, the interference left at S_1 raises to 0.1 W, 27 times higher than that in the previous situation.

4.2.3.2 Wideband communications

In the previous section, I analyzed the performance of MNAC for any signals with single frequency. In some applications, however, a wideband modulation scheme, like

[4]That is $\Delta s = 0.01 * s_A/a_{AS_1}$ and $\Delta\phi = 0.01 * \pi$.

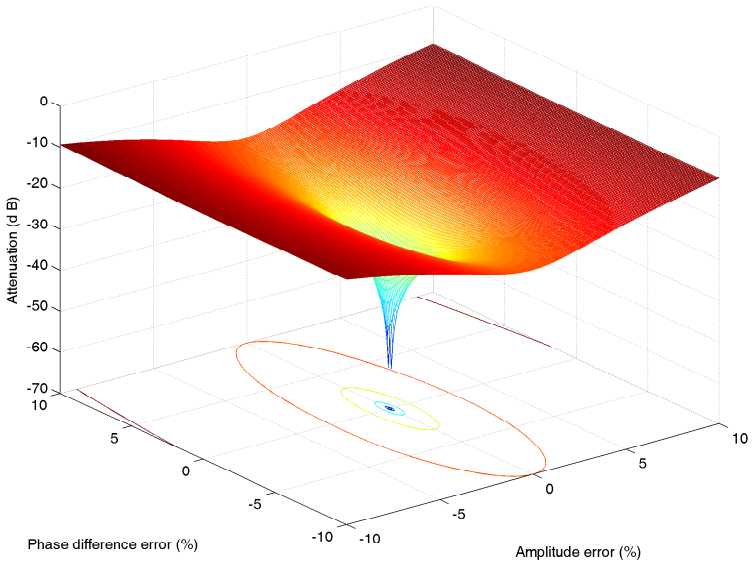

Figure 4.13: Attenuations of the MNAC with respect to the percentage of errors.

the orthogonal frequency-division multiplexing (OFDM), may be applied in a UAN for high-speed communications [65, 66]. Next, I study the impact of wideband signal on MNAC.

From (4.22) we obtain that the optimal transmission delay of a mirror node is calculated for a certain frequency f_A. If the transmission signal contains multiple frequency components, the phase mismatch presented in (4.19) may occur at the protected receiver.

Let f_c and f_i represent the central frequency and the i^{th} frequency component of a wideband signal, respectively. We create the strong destructive interference at f_c by making $f_A = f_c$ in (4.22). Denote the phase mismatch between the source and the mirror signals on the i^{th} frequency component as $\Delta\phi_i$, then we have

$$\Delta\phi_i = \pi\left(\frac{f_i}{f_c} - 1\right). \tag{4.23}$$

Substituting (4.23) into (4.20), I could calculate the remaining power on each frequency component at the protected receiver with the assistance of a mirror node.

In Fig. 4.14, I use an OFDM-BPSK signal as an example to show the performance of MNAC with a wideband signal. The original sound wave was collected from the real acoustic modem, which consists of one preamble sequence (first block) and six data blocks. The frequency band is from 14 to 20 kHz, and the central frequency is $f_c = 17$ kHz. The mirror signal is a copy of the original wave but with a delay of $1/(2f_c)$ secs.

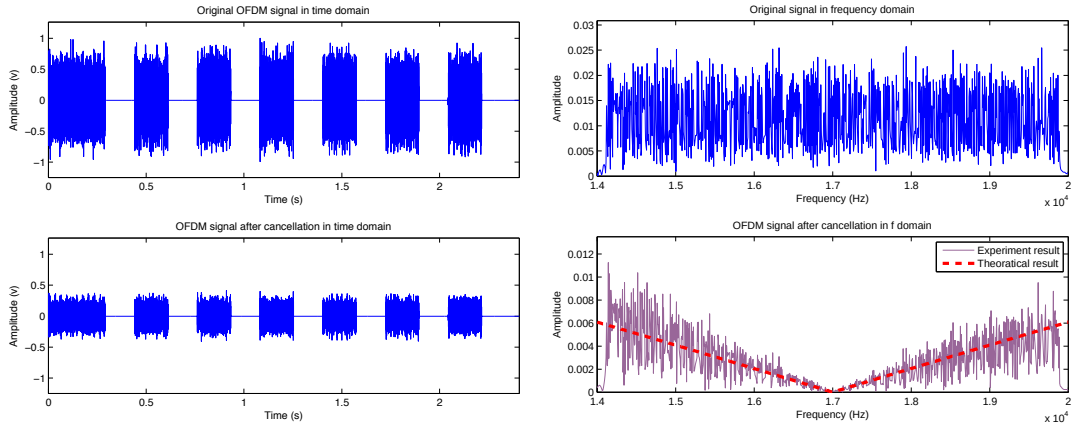

(a) Time domain (b) Frequency domain

Figure 4.14: Effect of MNAC on a wideband signal.

As demonstrated in Fig. 4.14(a), due to the phase mismatch, the mirror signal cannot completely cancel out the source signal on all frequencies. For example, the average power of the first data block in the raw wave is 0.07 W. With the assistance of mirror node, the remaining power reduces to 0.0081 W significantly, but not zero.

I draw the spectrum of the first data block with and without MNAC In Fig. 4.14(b), where the theoretical result is calculated via (4.20) and (4.23). The figure illustrates that MNAC does not provide a flat frequency response for a wideband signal at the protected receiver. Particularly, there is a strong destruction at the central frequency (17 kHz), where the amplitude of the original signal is cancelled out by the mirror signal. However, when the frequency component deviates from the central frequency, the phase mismatch occurs, causing an incomplete interference cancellation.

We can tackle the problem of phase mismatch in a wideband OFDM signal by applying a pre-filter to line up the phase of each subcarrier [67]. More specifically, before a data transmission, the mirror node first calculates $\Delta\phi_i$ on each sub frequency based on (4.23), and then rotates the phase by $-\Delta\phi_i$ for each subcarrier through a pre-filter. After that, the mirror node could almost line up the phases on all frequency components, and a strong destructive interference for a wideband signal is available at the protected receiver.

4.2.3.3 Location of mirror node

In MNAC, I need to ensure that the source and its mirror signals do not cancel out with each other at the intended receiver. Using Fig. 4.11 as an example, for the signal from node A, I aim to reduce its strength at the protected receiver S_1, meanwhile increasing or at least not reducing that strength at the intended receiver S_2. Otherwise, a wrong cancellation scheme may block the data sent from node A to its intended receiver unintentionally, which hurts the performance of a network. We could solve this problem by selecting a proper mirror node in each round of communication.

In the following discussions, I will first guarantee that signals from the source and its mirror node could completely cancel out each other at the protected receiver. Then, I analysis how the location of a mirror node affects the receiving signal power at the intended receiver. I first set the transmission power of the source node as a constant and discuss the case of variable transmission power later.

Let $\mathbf{L}_n = (x_n, y_n, z_n)$ be the coordination of node n, where x-y plane and z-axis represent the sea surface and the depth of water, respectively. Here, x_n, y_n and z_n are expressed in meters. Let $p_{AA'}(x_i, y_i, z_i)$ be the power of superposed signals from nodes A and A$'$ at the point (x_i, y_i, z_i) after considering the acoustic attenuation, the constructive and destructive of acoustic waves. Denote the power of signal from the

source node at the point (x_i, y_i, z_i) as $p_A(x_i, y_i, z_i)$, which takes the acoustic attenuation into account.

Here, I assume the spreading factor of an acoustic wave is 1.5, the transmission power of node A is 1 W, the signal frequency is 17 kHz, and location of the protected receiver S_1 and the intended receiver S_2 are at $\mathbf{L}_{S_1} = (100, 0, 10)$ and $\mathbf{L}_{S_2} = (450, 0, 10)$, respectively. The transmission power and the initial delay of a mirror node is calculated from (4.21) and (4.22), respectively.x

Now, I define $p_{dif}(x_i, y_i, z_i)$ as the ratio of receiving power with and without MNAC at the point (x_i, y_i, z_i), where

$$p_{dif}(x_i, y_i, z_i) = 10 \log \left(\frac{p_{AA'}(x_i, y_i, z_i)}{p_A(x_i, y_i, z_i)} \right). \tag{4.24}$$

Compared with a non-mirror node assisted situation, if a mirror node enhances the power of a signal at the point (x_i, y_i, z_i), p_{dif} is larger than 0 dB; otherwise it is smaller than or equal to 0 dB.

In Fig. 4.15, I plot $p_{dif}(x_i, 0, z_i)$ in three typical scenarios: (a) the source node A is closer to the protected receiver S_1 than the mirror node A$'$; (b) the mirror node A$'$ is closer to the protected receiver S_1 than the source node A, and (c) the source node A and the mirror node A$'$ are close to each other.

In scenario 1 of Fig. 4.15, we could use the perpendicular of the line segment AA' to roughly divide the figure into two parts, where colors of the right part is dominated by warm tones. This indicates that the power of a signal from node A is enhanced by its mirror node at S_2, as I expected. Since node A$'$ is closer to the intended receiver S_2 than the source node A, i.e., $a_{A'S_2} < a_{AS_2}$, but node A's transmission power is larger than the source node, i.e., $s_{A'} > s_A$. More specifically, according to (4.21), A$'$ in each data transmission use higher power than the source node to create the destructive interference at the protected receiver S_1. Therefore, considering the propagation attenuation, a signal from node A will be much weaker than that from A$'$ at any point

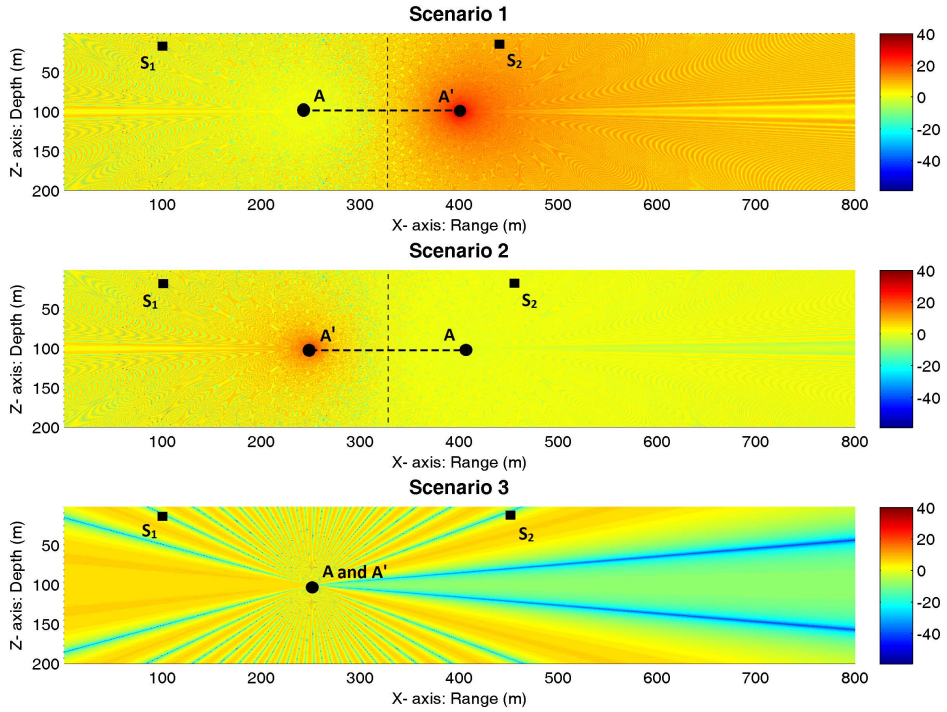

Figure 4.15: Interference pattern of MNAC in different scenarios, where $\mathbf{L_{S_1}} = (\mathbf{100}, \mathbf{0}, \mathbf{10})$ and $\mathbf{L_{S_2}} = (\mathbf{450}, \mathbf{0}, \mathbf{10})$. Scenario 1: $\mathbf{L}_A = (250, 0, 100)$ and $\mathbf{L}_{A'} = (400, 0, 100)$. Scenario 2: $\mathbf{L}_A = (400, 0, 100)$ and $\mathbf{L}_{A'} = (250, 0, 100)$. Scenario 3: $\mathbf{L}_A = (250, 0, 100)$ and $\mathbf{L}_{A'} = (251, 0, 100)$.

$P = (x_p, y_p, z_p)$ in the right side of the figure. Then, we have

$$\frac{s_A}{a_{AP}} \ll \frac{s_{A'}}{a_{A'P}}. \tag{4.25}$$

According to (4.18) and (4.25), we obtain

$$\Delta s \approx \frac{s_{A'}}{a_{A'P}}. \tag{4.26}$$

Substituting (4.26) into (4.20), we have

$$p_{AA'}(x_p, y_p, z_p) \geq \left[\frac{s_{A'}}{a_{A'P}}\right]^2. \tag{4.27}$$

Finally, substituting (4.25) and (4.27) into (4.24), we obtain

$$p_{dif}(x_p, y_p, z_p) \gg 0. \tag{4.28}$$

Above analysis gives us an insight into the scenario 1 of Fig.4.15. If a mirror node is closer to the intended receiver than a source node, the signals from A and A′ could

cancel out each other at the protected receiver S_1, but are enhanced at the intended receiver S_2 significantly.

In scenario 2 of Fig. 4.15 I show an opposite situation of scenario 1, where the mirror node A$'$ is closer to the protected receiver S_2 than the source node A. In this case, the strength of a signal from node A is much stronger than that from A$'$ in the right side of the figure. Therefore, the signal from node A dominates $p_{AA'}(x_p, y_p, z_p)$. This implies that MNAC neither significantly increases nor decreases the receiving power at the intended receiver S_2. We could verify this conclusion from the right side of Fig. 4.15, the color of which is in-between status of a warm tone and a cool tone, i.e., $p_{dif}(x_p, y_p, z_p)$ is around 0 dB.

In some applications, the deployment of underwater nodes are random. In this case, there is a probability that some mirror nodes are close to the source node. In scenario 3 of Fig. 4.15, I show this situation, where A$'$ is only 1 m away from node A. From this figure, we observe that the pattern of interference consists of multiple beams. In addition to at the protected receiver S_1, there exist several shadow zones (green and blue region) in the right side of the figure. If the intended receiver is deployed in one of these regions, the signal from the source node would be blocked by its mirror signal, which hurts the performance of a network.

To summarize, when the mirror node is far from the source node, e.g., scenario 1 and scenario 2 of Fig. 4.15, even if the phase difference between signals from the two nodes meets the require of destructive interference, a significant mismatch of the signal strength could prevent the mirror signal from canceling out the source signal at the intended receiver. However, if the mirror node is close to the source node, the interference pattern becomes symmetric beams. In this situation, there is a probability that a mirror signal unintentionally blocks the source signal at both intended receiver and protected receiver, which we should avoid in a real application.

In Section 4.2.5, I will study how to select the best mirror node in a more complicated situation, where the problem is analyzed from a cooperation communication point of view.

4.2.4 MNA-MAC protocol

To make MNAC works efficiently in a UAN, it is crucial to guarantee that both the source and the mirror node have identical data to send. In this section, I design a MAC protocol, called MNA-MAC to achieve this goal.

4.2.4.1 Spatially-correlated observation

In most of sensor networks, in order to detect the target events reliably, sensors in the immediate vicinity are deployed to observe highly correlated data. After the data fusion, the probability of a false detection from any single sensor node could be considerably reduced through the collaborative sensing. Therefore, the data collected by the sensors are *spatially-correlated* [68].

In the last ten years, people have leveraged the feature of spatial correlation to improve the performance of MAC protocols for a sensor network [68–70]. The main idea of these protocols are saving energy and reducing the collision probability among packets by suppressing the transmission opportunities among correlated observations. More specifically, due to the spatial correlation, neighboring nodes in a sensor network are most likely aware of the same event, hence a MAC protocol could select only a portion of nodes to report their sensing results. With this strategy, a network can reduce its traffic load and extend its lifetime dramatically.

Different from existing researches, I utilize the property of spatial correlation for a completely different purpose — maintain the identity of the data collected by the source node and the mirror node. To achieve this, in MNAC I always select a mirror

node from the observation correlation area of a source node to guarantee that they have the same sensing data to transmit.

How to divide the correlation area dynamically in a complex underwater environment, however, is a challenge. Particularly, the correlation region in a UAN may change with the time, e.g., when tracking a moving target or measuring the water temperature from different seasons. In this situation, a network should be capable of re-identify the correlation area in a varying environment for appropriate mirror node selection. Next, I introduce how to implement this function in MNA-MAC.

4.2.4.2 Assumptions

Here, I assume the network is static[5] and non-synchronized. All nodes use a single channel for control message and data packet transmissions. I further assume that each sensor node knows the distance to its nearby buoys, which could be measured at the initial stage of the network through the classic two-way handshake method [71]. Similar distance measurement approach has been successfully tested in the sea experiment [72].

Furthermore, I suppose that surface nodes realize whether a sensor node is in their overlapping coverage area or not by sending test packets. If a sensor node hears test packets from different buoys, then it is in an overlapping coverage area of neighboring buoys; otherwise, it belongs to a single buoy.

Finally, I assume that surface nodes cannot hear the acoustic signals from each other, a transmission of one buoy thus will not disrupt the data reception of another. This assumption is based on the fact that surface nodes usually use the RF modem for internode communications [73], and thus the distance among neighboring buoys could be longer than the rage of acoustic communications.

[5]The random drift of sensor nodes with the ocean current may result in a mismatch of the phase and the amplitude, especially the phase, between the source signal and the mirror signal, effects of which have been studied in Section 4.2.3.

4.2.4.3 Protocol description

MNA-MAC consists of two stages for the correlation area detection and re-identification, respectively. In the first stage, each buoy divides sensor nodes in its coverage range into different clusters based on the cross-correlation coefficient among the collected data. In the second stage, the buoy involves new nodes into or removes old ones from a cluster with the variation of environments to re-identify the correlation area. Next, I introduce these two stages in detail.

Correlation area detection: In this stage, since the surface node has little knowledge regarding the correlation area of a network, it cannot select the mirror node rashly; otherwise, the data collected by the source and the mirror node may have some differences, resulting in a packet collision at both the protected receiver and the intended receiver. Therefore, a surface node in this stage considers each acoustic node as an independent one, and then applies a conventional underwater MAC protocol for the data transmission [74, 75].

Each time when a surface node receives the data from sensor nodes, it measures the similarity among these data by calculating their cross-correlation coefficients. If the coefficient among any data packets over a certain threshold, the buoy divides the corresponding nodes into the same correlation area, and then groups them into the same cluster. This process will repeat several times for a reliable clustering.

Correlation area re-identification: In this stage, a source node sends out an RTS packet to reserve the channel before its data transmission. Once a buoy received the RTS, it first checks whether the source node is in an overlapping area of its neighboring buoys or not. If yes, the buoy selects a node from the cluster of the source node as a mirror node, and sends a CTS and an assist-to-send (ASTS) message to the source and the mirror node, respectively. Otherwise , the buoy simply replies with a CTS message to the source node, since its transmission would not disrupt other buoys.

The CTS and ASTS packets attach the time information to tell the source and the mirror node how long they should wait for the following data transmission, respectively. Using the scenario depicted in Fig. 4.11 as an example, when node A and A$'$ receive CTS and ASTS from buoy S_2, they are requested to wait for t_{A_wait} and $t_{A'\_wait}$ secs, respectively, before their data transmission. Therefore, we have

$$t_{A'\_wait} - t_{A\_wait} + \frac{d_{A'S_2} - d_{AS_2}}{c} + t_{ASTS} = \tau^*_{A'}, \tag{4.29}$$

where $d_{A'S_2}$ and $d_{A'S_2}$ are the distances from nodes A$'$ and A to buoy S_2, respectively; t_{ASTS} is the transmission time of an ASTS packet, and $\tau^*_{A'}$ is the optimal delay expressed in (4.22) to create a strong destructive interference. Let

$$T_{wait} \triangleq \tau^*_{A'} - t_{ASTS} + \frac{d_{AS_2} - d_{A'S_2}}{c}, \tag{4.30}$$

then we obtain

$$t_{A'\_wait} = \begin{cases} T_{wait}, & T_{wait} > 0, \\ 0, & \text{otherwise}, \end{cases} \tag{4.31}$$

and

$$t_{A\_wait} = \begin{cases} T_{wait}, & T_{wait} \leq 0, \\ 0, & \text{otherwise}. \end{cases} \tag{4.32}$$

After a successful data reception, the buoy replies with an acknowledgement (ACK) message for a reliable communication.

Other nodes that do not win the contention for the following data transmission will enter the receive model. They overhear the packet sent from the winner and compare it with their local data. If a node collected the same data with the one it overheard, it discards the local data to avoid a redundant transmission; otherwise, it sends an RTS message to initiate a new round of communication after hearing ACK for the current winner.

Each time when a buoy receives data from the sensor nodes, it calculates the cross-correlation coefficients among them, and then classifies the nodes into different clusters.

In this way, each buoy could re-identify correlation area in a varying environment and maintain the identity of the data from the source and the mirror node.

4.2.5 Power management and mirror selection

In Section 4.2.3.3, I have introduced how to select a proper mirror node. However, that discussion is based on the assumption that the transmission power of a source node is a constant. In that case, once a mirror node joins a communication, the total energy consumption in a network would be higher than that without the assistance of mirror node. In this section, I study how to select the best mirror node under the constraint of power consumption.

Using Fig. 4.11 as an example, let P_0 be the maximal transmission power allowed for each round of communication, i.e., $s_{A'}^2 + s_A^2 = P_0$. Substituting (4.21) into it, then we have the transmission power assigned to the source node A and mirror node A$'$, which are denoted by P_A and $P_{A'}$, are

$$P_A = P_0 \frac{a_{AS_1}^2}{a_{A'S_1}^2 + a_{AS_1}^2}, \tag{4.33}$$

and

$$P_{A'} = P_0 \frac{a_{A'S_1}^2}{a_{A'S_1}^2 + a_{AS_1}^2}. \tag{4.34}$$

The intended receiver S_2 could calculate the attenuation coefficients $a_{AS_1}^2$ and $a_{A'S_1}^2$ based on the distance from nodes A and A$'$ to the protected receiver S_1, and then attaches the values of P_A and $P_{A'}$ into the CTS and ASTS packets, respectively. Particularly, if the source node is not in the overlapping area of neighboring buoys, none of mirror nodes would be selected, and P_A is set to P_0.

In MNAC, we could expect a spatial diversity gain of the signal strength at the intended receiver, since the behaviors of the source and its mirror node could be considered as a special case of cooperative communication. More specifically, when a mirror

node joins a data transmission, it works as a relay to enhance the signal strength at the destination (intended receiver), which is similar to a DF based cooperative communication [10].

To optimize the channel capacity of a conventional DF-based cooperative communication, the problem of optimum power allocation is formulated as [10]

$$C_{DF} = \max_{\{P_S,P_R\}} \min\Big\{\frac{1}{2}\log(1+|h_{SR}|^2P_S), \\ \frac{1}{2}\log(1+|h_{SD}|^2P_S+|h_{RD}|^2P_R)\Big\} \tag{4.35}$$

where C_{DF} is the channel capacity, h_{SD}, h_{SR} are the channel gains of the source-relay and source-destination links, respectively. P_S and P_R are the transmission power of the source and the relay, respectively.

In MNAC, the source and a mirror node inherently have the same data to send, which is equivalent to a perfect source-relay link in a cooperative communication, i.e., $|h_{SR}| \to \infty$. Therefore, MNAC does not require the first phase of the DF-based cooperative communications , in which relay hears raw data from the source node. This implies that the factor 1/2 in (4.35) could be removed. Finally, (4.35) degenerates to a very simple optimization problem that

$$C_{DF} = \max_{\{P_A,P_{A'}\}}\Big\{\log(1+|h_{AS_2}|^2P_A+|h_{A'S_2}|^2P_{A'})\Big\}, \tag{4.36}$$

where $P_A+P_{A'}=P_0$. It is easy to obtain that the optimal power allocation of (4.36) is

$$\begin{cases} P_A^* = P_0 \quad \text{and} \quad P_{A'}^*=0, & |h_{AS_2}| > |h_{A'S_2}|, \\ P_{A'}^* = P_0 \quad \text{and} \quad P_A^* = 0, & |h_{AS_2}| \le |h_{A'S_2}|. \end{cases} \tag{4.37}$$

From (4.37) we observe that in order to maximize the channel capacity, all power should be allocated to either the source or the mirror node, which one has a better channel quality to the destination than another. However, I cannot simply apply this optimum power allocation strategy in MNAC, since the power assigned to the source

and the mirror nodes needs to meet the requirement that $P_{A'}/P_A = a^2_{A'S_1}/a^2_{AS_1}$ as expressed in (4.33) and (4.34) first for interference cancellation at the protected receiver. This implies that MNAC cannot reach the maximal channel capacity. Nevertheless, the loss of channel capacity could be minimized by choosing the best mirror node.

Denote the set of potential mirror nodes for the source node A as $\mathbf{M}_A$. Considering the sound attenuation as the main factor[6] that affects the quality of acoustic channels, then we have

$$|h_{AS_2}| = \frac{1}{a_{AS_2}} \quad \text{and} \quad |h_{A'S_2}| = \frac{1}{a_{A'S_2}}. \tag{4.38}$$

Substituting (4.33), (4.34) and (4.38) into (4.36), then the optimal mirror node should be

$$\begin{aligned} C_{DF} &= \max_{A'_i \in \mathbf{M}_A} \log \left[1 + \frac{P_0}{a^2_{A'_iS_1} + a^2_{AS_1}} \left(\frac{a^2_{AS_1}}{a^2_{AS_2}} + \frac{a^2_{A'_iS_1}}{a^2_{A'_iS_2}} \right) \right] \\ &= \max_{A'_i \in \mathbf{M}_A} \log \left[1 + P_0 \left(1 + \frac{a^2_{A'_iS_1}}{a^2_{A'_iS_1} + a^2_{AS_1}} \right) \left(\frac{1}{a^2_{A'_iS_2}} - \frac{1}{a^2_{AS_2}} \right) \right] \\ &\triangleq \max_{A'_i \in \mathbf{M}_A} \log \left[1 + P_0(1+\nu)\xi \right]. \end{aligned} \tag{4.39}$$

From (4.39), we obtain the following observations. First of all, if $a^2_{A'_iS_2} < a^2_{AS_2}$, then ξ is a positive value. In this case, we should maximize ν to optimize C_{DF}. This could be achieved by choosing a mirror node with the largest propagation attenuation to the protected receiver, i.e., $\max\{a^2_{A'_iS_1}\}$. Secondly, if $a^2_{A'_iS_2} > a^2_{AS_2}$, then ξ is a negative value. In this situation, we should minimize ν to maximize C_{DF}. This could be done by selecting a mirror node with the smallest propagation attenuation to the protected receiver, i.e., $\min\{a^2_{A'_iS_1}\}$. Finally, if $a^2_{A'_iS_2} = a^2_{AS_2}$, then ξ is equal to 0, and C_{DF} is a constant. In this circumstance, any entity in $\mathbf{M}_A$ could work as the best mirror node to maximize C_{DF}.

[6] How to model the gain of an underwater channel when considering other factors, such as multipath and curvilinear propagation of acoustic wave, has been studied in [57] and [59], which is out of the scope of this dissertation.

To summarize, let $d_{A'_i S_i}$ be the distance from the mirror node i to receiver S_i, where $A'_i \in \mathbf{M}_A$. According to the previous discussions, we could select the mirror node quickly based on the following criteria:

1): If $d_{A'_i S_2} > d_{AS_2}$, $\forall\, A'_i \in \mathbf{M}_A$, then a good mirror node is the one far from the intended receiver, but close to the protected receiver.

2): If multiple mirror nodes in $\mathbf{M}_A$ meet the requirement that $d_{A'_i S_2} < d_{AS_2}$, then we should choose a one close to the intended receiver, but far from the protected receiver.

3): If the distance from multiple mirror nodes to the buoy S_1 satisfied $d_{A'_i S_2} = d_{AS_2}$, meanwhile these mirror nodes are the closest ones to S_2 in $\mathbf{M}_A$, then we can select any one of them as the best mirror node.

4): In order to prevent strong destructive interference at the intended receiver, the mirror node should not be close to the source node, as described in Section 4.2.3.3.

Essentially, above criteria guarantee that most of power are allocated to either the source or the mirror node in the set $\mathbf{M}_A$, which has the best link quality (lowest attenuation) to the intended receiver, while meeting the requirement of a strong destructive interference at the protected receiver.

Fig. 4.16 gives an example of the best mirror node selection in MNA-MAC. Let S_1 and S_2 be the protected receiver and intended receiver of source node A, respectively. A'_1 to A'_4 are four potential mirror nodes of A. In scenario (a), A'_1 is the best mirror node based on the criterion (1). According to the criterion (2) and (4), we select A'_2 as the best mirror node in scenario (b). In scenario (c), A'_1, A'_2 and A'_3 could all work as the best mirror node as described in criterion (3).

4.3 Summary

In this chapter, I introduced a new best relay selection criterion, COBRA, and a new cooperative transmission scheme, MNAC, for UANs.

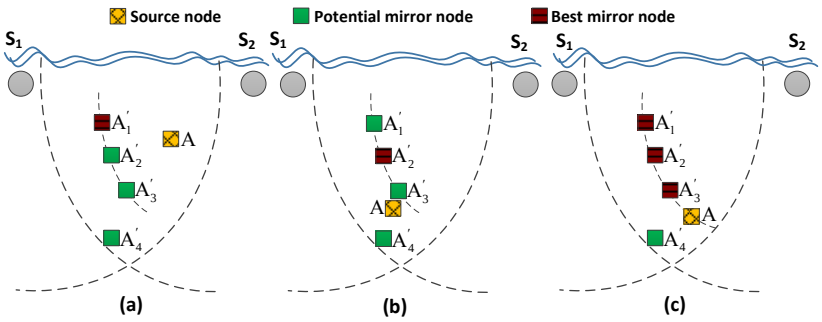

Figure 4.16: **Best mirror selection**. (a) source node closer to the intended receiver than all potential mirror nodes; (b) three potential mirror nodes (A'_1, A'_2 and A'_3) closer to the intended receiver than the source node; (c) the source and three potential mirror nodes (A'_1, A'_2 and A'_3) have the same distance to the intended receiver.

In COBRA criterion, a source node takes into account not only the channel quality but also the propagation delay to select the best relay set for its cooperative communication. COBRA aims to optimize the OPT time instead of the maximum transmission rate. Therefore, its spectrum utilization may be lower than a conventional CSI based relay selection criterion, but the overall network performance in terms of throughput and end-to-end delay is much higher. I also designed a simple handshake based MAC protocol for COBRA. In the new protocol, the transmission of a source node could switch between a cooperative scheme and a non-cooperative scheme smartly based upon the packet size, channel quality and the position of the potential relays in each round of communications. Therefore, the new criterion guarantees that the throughput and the end-to-end delay of a cooperative communication is higher than or at least equal to a non-cooperative communication.

To further improve the channel utilization, I proposed MNAC, a new cooperative scheme for UANs. Different from traditional cooperative schemes which leverage the spatial diversity in wireless network to improve the receiving signal-to-noise ratio (SNR) at the destination, MNAC aims to increase the channel efficiency by allowing multiple nodes to send their data simultaneously without casing any collisions. I achieved this through selecting a mirror node for each specific source node, and made signals from

the source and the detonation add destructively at a protected receiver. Therefore, the data from an intended receiver to the protected receiver would not be disrupted by the mirror assisted source node, several independent data stream thus could travel in the same channel without interfering each other. However, from the analysis we observed that MNAC is sensitive to the error of distance measurement. How to improve the reliability of the new cooperative scheme in a real underwater application is still an open issue.

Chapter 5

Underwater COG-COM

As I discussed in Section 3.3, underwater environment, where multiple networks coexist, usually features high competition for acoustic spectrum (channel) among different users. Meanwhile, available communication frequencies in water are quite limited, due to the severe frequency dependent attenuation and narrowband response of an acoustic transducer. Therefore, the spectrum is a scarce resource for underwater acoustic systems.

To improve the efficiency of spectrum utilization in a complex underwater environment, UCAN is advocated as a promising technique to achieve both the environment-friendly and spectrum-efficient communications over acoustic channels [15, 76, 77].

In UCANs, acoustic nodes are capable of sensing the surrounding environment first, and then dynamically configure their operating frequency, transmission power or other system parameters to avoid the interference with other acoustic systems. In Fig. 5.1, I show the three major components of a CA system: a spectrum sensing mechanism, a dynamic power control algorithm and a spectrum management system.

- *Spectrum sensing mechanism*: It plays a crucial role in detecting the presence of other acoustic users and identifying the idle channel for UCANs. Spectrum

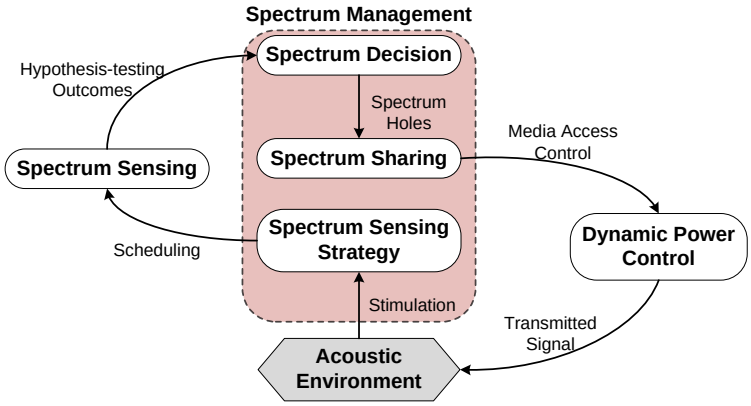

Figure 5.1: Architecture of UCANs.

sensing could be performed in frequency, time, space and code domains. In addition, users can sense the spectrum independently to increase the channel access opportunity, or cooperatively to improve the sensing accuracy.

- *Dynamic power control*: In a UCAN, users could adopt a dynamic power control algorithm to improve the channel capacity and energy efficiency of the network. This could be done by assigning proper power to each user on different channels, while maintaining a constant energy consumption over the whole spectrum.
- *Spectrum management system*: It allows acoustic nodes to intelligently detect whether any portion of the acoustic spectrum is vacant, and change their transmission frequencies, power or other operating parameters to temporarily use the idle frequency for communications without interfering other acoustic systems.

In this chapter, I first introduce an efficient spectrum management system, called RISM, for UCANs. After that, I propose a new MAC protocol, DCC-MAC, to solve the congestion problem of CCC in a cognitive network.

5.1 RISM

RISM seeks to significantly improve the performance of UANs through a collaboration of the physical layer and MAC layer. It aims to provide low collision probability data transmissions and efficient spectrum utilization for CA nodes, while avoiding harmful interference with both "natural acoustic systems", such as marine mammals, and "artificial acoustic systems" like sonars and other UANs. In addition, to solve the unique challenge of deciding when receivers start to retrieve data from their neighbors, I propose to use a traffic predictor on each receiver to forecast the traffic load of surrounding nodes. This allows receivers to dynamically adjust their polling frequency according to the variation of a network traffic. The content in this section is mainly based on my previous work published in [17][1] .

5.1.1 Related work

A spectrum management system generally contains three key components, including the spectrum sensing, spectrum sharing and spectrum decision. The spectrum sensing aims to detect the presence of primary user (PU) reliably and to maximize the spectrum access opportunity of cognitive nodes. The spectrum sharing scheme is to handle self-coexistence of cognitive nodes with a low collision probability for data transmission. The goal of a spectrum decision algorithm is to allocate the frequencies and transmission power properly to improve the resource utilization. In the last ten years, many spectrum management methods have been proposed for cognitive radio networks.

In [78], a dynamic frequency hopping communication (DFHC) scheme is proposed for centralized spectrum management. In this scheme, each CR node is supposed to work on two separate sub-channels simultaneously. During the data transmission on

[1] © 2014 IEEE. Reprinted with permission from Yu Luo, RISM: An efficient spectrum management system for underwater cognitive acoustic networks, IEEE SECON, Jun. 2014

one frequency band, the node could sense the other intended channel in parallel. The cognitive nodes in DFHC provide the sensing results and the spectrum usage of their neighbors to the leader, while the leader is responsible for calculating the hopping patterns for all cognitive nodes. In oder to maximize the opportunity to discover a vacant channel while minimizing the average time taken to sense the spectrum, an optimal spectrum sensing method is proposed in [79]. In this method, each node has two different sensing patterns: the reactive sensing and the proactive sensing. Nodes in the proactive sensing mode detect different channels periodically, and the idle channels will be added into idle channel list for switching. Once the current channel is occupied by PUs and there is no available channel in the idle channel list, the reactive sensing mode will be trigged for an opportunistic spectrum access.

In [80] the authors propose a protocol called cognitive medium access control (C-MAC) for distributed CR networks. Each channel in C-MAC is divided into recurring superframes, each of which consists of a a slotted beaconing period (BP) and a data transfer period (DTP). A node transmits a beacon in the designated beacon slot during the BP for multi-channel rendezvous and collision avoidance, and sends the data in DTP. In [81], the implementation of a spectrum management is divided into two levels. At the first level, each node does the optimized spectrum sensing based on the traffic rate of the cognitive network. At the second level, a random access based MAC called CR-ALOHA and a carrier-sensing called CR-CSMA are developed to deal with the packet scheduling of the cognitive nodes.

In order to mitigate the congestion on the CCC of a spectrum management system, the authors propose MMAC-CR. MMAC-CR is a conventional sender-initiated protocol, extending IEEE 802.11 to support cognitive communications. This protocol consists of two phases: an ad hoc traffic indication message (ATIM) phase and a data phase. In the ATIM phase, users communicate on the CCC to decide which channel

to use in the following data phase, i.e., channel rendezvous. In the data phase, nodes that are assigned the same channel compete for the channel access using traditional handshake approach similar to IEEE 802.11.

In most of the aforementioned approaches, a sender initiates the negotiation for a spectrum usage. The components in these spectrum management systems are considered as separate parts, and optimization is performed on each individual components. The overhead issue for integrating all units of the system, however, is usually overlooked, especially when taking into account the long propagation delay, the long preamble and the bandwidth constraints in acoustic communications [16]. This promotes us to design a new receiver-initiated spectrum management system, RISM, for UCANs.

Compared with sender-initiated systems, we could obtain several benefits by staring a handshake process at the receiver. Specifically, each receiver in RISM could run as a "semi-center" collecting local sensing information from neighboring nodes for a reliable PU detection, and performing joint channel and power allocation for surrounding senders. Therefore, the spectrum sensing mechanism, the spectrum sharing scheme and the spectrum decision algorithm could be considered as a whole in the new system. In addition, the control packets are shared amongst different components, thereby significantly reducing the overhead and improving the channel utilization.

5.1.2 Receiver-initiated spectrum sharing

I first introduce the receiver-initiated spectrum sharing (RISS) scheme, the backbone of RISM. In RISS, a handshake process is initiated at the receiver side to negotiate the vacant spectrum sharing.

5.1.2.1 Description of RISS

In RISS, a node needs to know the propagation delay to its neighbors, which could be measured at the initialization stage of a network through the classic two-way handshake approach that has been tested in the sea experiment [72]. Furthermore, I assume that there is a CCC, which is physically separated from the in-band data channel, as it is widely accepted in cognitive networks [82]. RISS involves six phases, as shown in Fig. 5.2.

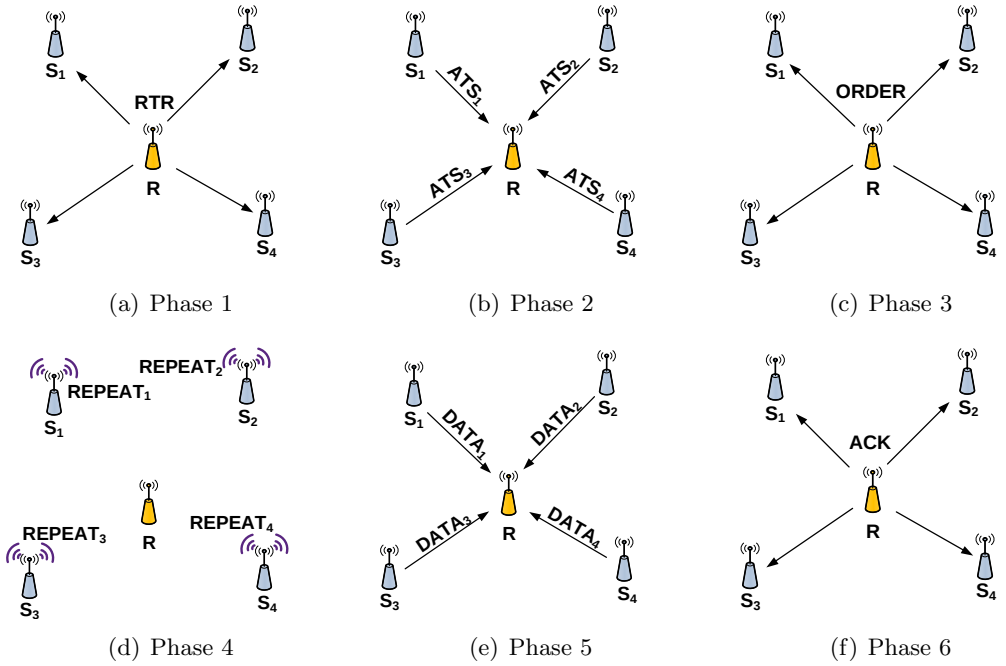

(a) Phase 1 (b) Phase 2 (c) Phase 3

(d) Phase 4 (e) Phase 5 (f) Phase 6

Figure 5.2: Six phases of the RISS scheme. R is a receiver and S_i is sender i.

Phase 1: The receiver, which intends to collect data, sends out a request-to-receive (RTR) packet to its neighbors to start a handshake process. Here, the RTR message has three functions: (a) to help the receiver request data from neighborhoods, (b) to arrange the transmissions of available-to-send (ATS) packets for neighboring senders, and (c) to inform its neighbors of the frequency each node to sense.

Phase 2: The invited senders, which successfully received an RTR and have data to send, will first sense the frequency arranged by the receiver. Then the senders

respond with `ATS` messages to establish connections with the receiver. In order to avoid collisions among `ATS` packets, senders transmit `ATS` following the schedule ordered in RTR. Here, the `ATS` has four functions: (a) to establish a connection with the receiver, (b) to inform the receiver of its number of data packets to send, (c) to notify the receiver about the spectrum usage of other active neighboring receivers for collision avoidance, which will be introduced in Section 5.1.4.2, and (d) to send back the local sensing result for a collaborative PU detection.

Phase 3: After `ATS` packet reception, the receiver fuses local sensing outcomes from its neighboring senders for the final spectrum decision. Then it broadcasts an `ORDER` packet, which includes information about the frequency allocation and the transmission power assignment for its neighbors.

Phase 4: If a sender successfully receives the `ORDER` message, it extracts its own schedule information and broadcasts this information through a `REPEAT` packet to its neighborhood. This process is to avoid a data collision with other receivers, which will be discussed in Section 5.1.4.2.

Phase 5: After the `REPEAT` packet transmission, each sender sends out its `DATA` packet at the scheduled time and frequency band according to the `ORDER` message it received in Phase 3.

Phase 6: Finally, for the purpose of reliable transmission, the receiver replies with a common ACK to all senders after the data reception.

Here, RTR, `ATS`, `ORDER`, `REPEAT` and `ACK` are all control packets and thus, share the CCC. From the above description, it is easy to obtain that though there are six phases in RISS, each round of negotiation allows multiple senders to reserve the channel. This is an advantage comparing with conventional sender-initiated approaches. In addition, the receiver in RISS can effectively work as a fusion center to schedule the sensing pattern and to collect local sensing results for collaborative PU detections, and it could

also play a role as the control center to arrange the data transmission of its surrounding senders. This is why I call RISM as a "semi-centralized" system.

5.1.2.2 Scheduling of ATS transmission

As introduced in Phase 1 in Fig. 5.2, each receiver in RISS needs to schedule the transmission of `ATS` messages for its neighbors. In order to avoid `ATS` collisions, the arriving time of `ATS` packets from different senders to a common receiver should be staggered. Moreover, a minimal `ATS` reception time is preferred to reduce the overhead on handshake and to improve the utilization of control channel.

Now, denote the receiver and its i^{th} neighboring sender as r and s_i, respectively. Let $\mathcal{S}$, L and τ_i be the set of s_i, the size of $\mathcal{S}$ and the propagation delay between r and s_i, respectively. Assume at t_0, a receiver transmits an `RTR` packet, and then receives $\texttt{ATS}_\texttt{i}$ from s_i at the receiver's local time t_i, where $i \in \{1, \ldots, L\}$. The transmission time of `RTR` and `ATS` are denoted by $T_{\texttt{RTR}}$ and $T_{\texttt{ATS}}$, respectively. Let w_i represent the time difference between the `RTR` reception and the $\texttt{ATS}_\texttt{i}$ transmission on s_i.

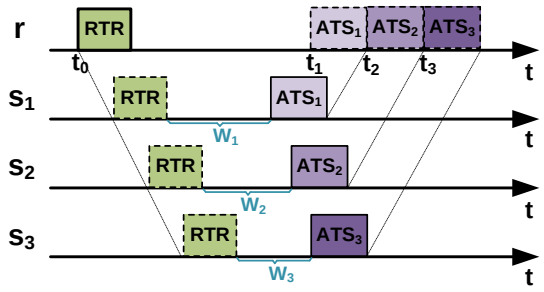

Figure 5.3: The schedule of `ATS` transmissions. A square with solid line and dash line represent a transmission and a reception, respectively.

The receiver calculates w_i for each sender to minimize the total time for all `ATS` receptions, while avoiding collisions among `ATS` messages. In Fig. 5.3, I use three senders as an example to show the optimal scheduling for `ATS` transmissions. Next, I introduce how to calculate w_i.

According to the propagation delay between the receiver and the sender i, we have

$$w_i = t_i - (t_0 + T_{\texttt{RTR}}) - 2\tau_i, \;\; i \in \{1, \ldots, L\}. \tag{5.1}$$

Then, I sort senders in $\mathcal{S}$ by the propagation delay in an ascending order. Let T_m be the local time that the last `ATS` packet arriving at the receiver, i.e., $T_m = \max\{t_i\}$, $i \in \{1, \ldots, L\}$. Now, optimizing the total reception time of all `ATS` packets is equivalent to minimizing T_m.

Suppose $\texttt{ATS}_i$ is the l^{th} of L `ATS` packets arriving at the receiver, then (5.1) can be written as:

$$w_i = T_m - (L-l)T_{\texttt{ATS}} - (t_0 + T_{\texttt{RTR}}) - 2\tau_i, \;\; i \in \{1, \ldots, L\}. \tag{5.2}$$

Note that $w_i \geq 0$, so from (5.2) we have

$$T_m \geq (L - l)\, T_{\texttt{ATS}} + (t_0 + T_{\texttt{RTR}}) + 2\tau_i, \;\; i \in \{1, \ldots, L\}. \tag{5.3}$$

From (5.3) we observe that in order to minimize T_m, the order of `ATS` reception should follow the order of senders in $\mathcal{S}$. More specifically, an `ATS` packet from a sender with a larger propagation delay (larger τ) should come after the one from a closer sender (smaller τ), and vice versa. Therefore, let $l = i$ and we have the minimum T_m is

$$T_m = \arg\max_i \big\{(L - i)T_{\texttt{ATS}} + (t_0 + T_{\texttt{RTR}}) + 2\tau_i\big\}, \; i \in \{1, \ldots, L\}. \tag{5.4}$$

Finally, the receiver calculates t_i by $t_i = T_m - (L - i)T_{\texttt{ATS}}$ for each sender, and then attaches the scheduled time $[t_0, t_1, \ldots, t_L]$ and the MAC addresses of corresponding senders on an `RTR` packet. After the `RTR` reception, sender s_i delays for $w_i = t_i - t_0 - 2\tau_i$ before replying its `ATS`.

From above descriptions we have that at the sender side, the wait time, w_i, before an `ATS` transmission is the time difference, $t_i - t_0$. Therefore, the knowledge of receiver's local time is not necessary at the sender side, which allows the above `ATS` scheduling to operate in a non-synchronized UCAN.

5.1.3 Spectrum sensing

Generally speaking, a CA node may not be able to sense all frequencies in one sensing period, since a full-band spectrum sensing is not only energy and time inefficient, but also hardware demanding, which make it impractical for battery-powered underwater equipments. Thereafter, I consider the scenario that each CA node could only sense one or several subset frequency bands in one sensing period. In this section, I elaborate how nodes in a UCAN identify signals from a PU and perform collaborative spectrum sensing in an RISM system.

5.1.3.1 Spectrum usage realization

In an asynchronous UCAN, when a node is sensing the spectrum, other senders may be transmitting on the same channel, which will interfere with the sensing process. Nodes in RISM are thus required to distinguish signals of PUs from that of CA nodes. Here, I advocate *cyclostationary* based spectrum sensing approaches to achieve this goal.

Different man-made communication signals natually have cyclostationary features at different cyclic frequencies [83]. By recognizing the cyclostationary pattern during spectrum sensing, CA nodes can distinguish between received signals from different systems.

However, one objective of UCANs is to share the acoustic spectrum with marine animals in an environment-friendly manner. Hence, PU in oceans may involve not only "artificial acoustic systems", like UANs and sonars, but also "natural acoustic systems", such as whales and dolphins. One important question coming up is that whether signals from "natural acoustic systems" and from CA nodes can be told apart by applying a cyclostationary based sensing technique. Here, I compare the cyclostationary based

time-smoothed cyclic cross periodogram [84], $S_x^\alpha[k]^2$, of different acoustic signals in Fig. 5.4. The results may help us to answer this question.

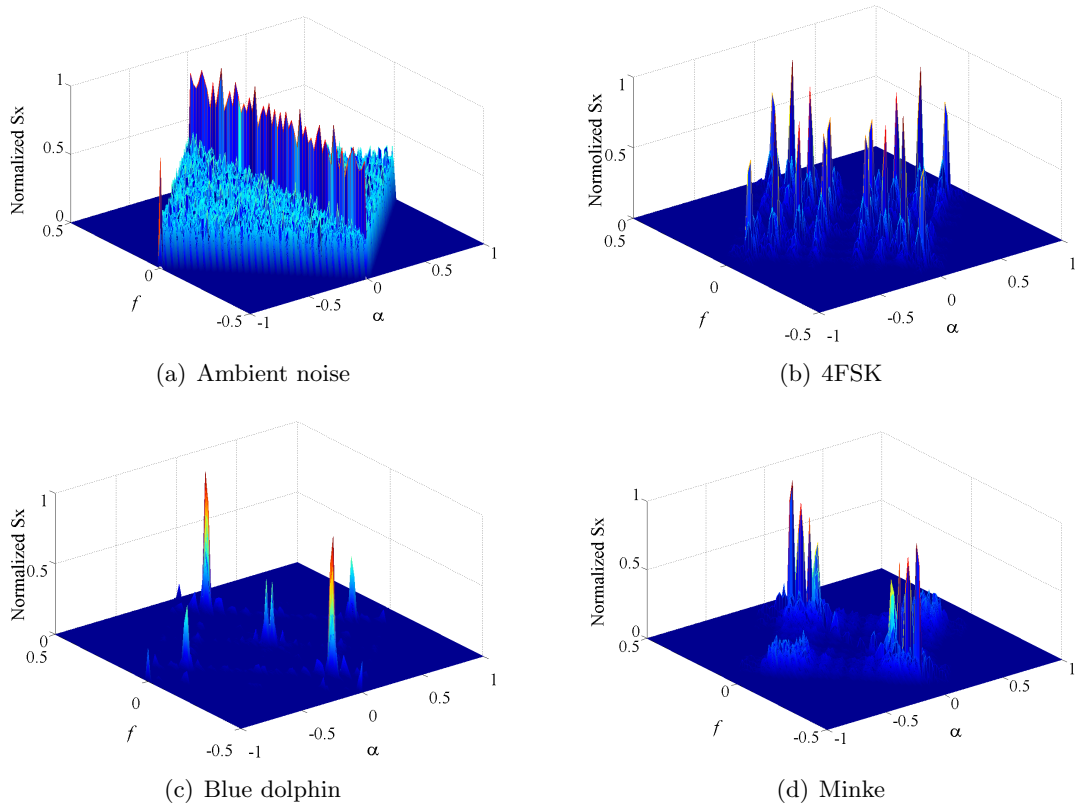

(a) Ambient noise (b) 4FSK

(c) Blue dolphin (d) Minke

Figure 5.4: Normalized cyclic cross periodogram of different acoustic signals in oceans with Hamming window. This figure demonstrates that the ambient noise does not exhibit the cyclostationary feature, since its cyclic cross periodogram has no peaks if $\alpha \neq 0$. By contrast, $S_x^\alpha[k]$ of 4FSK, blue dolphin and minke signals show additional peaks at different α, where $\alpha \neq 0$. A node could use the position of these peaks to identify sensed signals.

Fig. 5.4 includes 4FSK signal, which is common man-made communication systems, and voice signals from two different marine mammals. This figure illustrates that both 4FSK and voice signals from marine mammals exhibit cyclostationary feature on multiple cyclic frequencies. Moreover, it is easy to observe the obvious differences

[2] $S_x^\alpha[k]=\frac{1}{D}\sum_{d=0}^{D-1} X_l[k]X_l^*[k-\alpha]W[k]$, where α, D, M, $W[k]$ and $X_l[k]$ are the cyclic frequency, the number of windows, the number of samples, the smoothing spectrum window and the Fourier transform of the sensed signal $x[n]$, respectively.

among cyclostationary patterns of different signals, which could be used in RISM for local spectrum sensing.

5.1.3.2 Collaborative spectrum sensing

After local sensing, senders transmit their sensed outcomes to the receiver via `ATS` packets. The receiver fuses these local results together for a collaborative PU detection. An example of a cyclostationary based collaborative spectrum sensing, which is well supported by the RISM system, could be found in [85].

In order to maximize the channel access opportunities while preventing intrusions to PUs, it is important to design an efficient sensing pattern [18]. Owing to the "semi-centralized" feature of an RISM system, the receiver could choose different sensing patterns to achieve varied goals:

1) ***Maximize spectrum access opportunity***: In order to maximize the probability to discover vacant spectrum, senders in this pattern are assigned to detect different frequency bands for increasing the sensing coverage.

2) ***Maximize sensing accuracy***: To overcome the fading and shadowing effects, a collaborative sensing strategy could be exploited for a reliable PU detection. Neighboring senders in this case are arranged to sense the same frequencies.

3) ***Hybrid spectrum sensing***: This sensing pattern is a trade-off between maximizing the channel access opportunity and maximizing the sensing accuracy. Neighboring senders in this pattern are divided into multiple groups. Different groups take charge of different subsets of frequencies, while senders in the same group sense the same frequency.

Depending on application requirements, RISM system could easily support all above sensing patterns by leveraging its "semi-centralized" structure. More specifically, as a control center, the receiver schedules the sensing pattern for its neighbors through an

`RTR` message, and then collects and fuses local sensing results from neighboring nodes through `ATS` packets.

5.1.4 Spectrum decision

When assigning vacant frequencies for communication, receivers need to schedule the data transmission for its intended senders carefully to avoid potential collisions. In addition, CA nodes in underwater environment usually experience severe frequency selective fading. However, a frequency which appears in deep fading to a node may be of good quality for other nodes. Therefore, a receiver should dynamically allocate the frequency and power to senders based on their channel situations. In this section, I introduce how to take advantage of a dedicated collision avoidance mechanism with a dynamic spectrum decision algorithm to achieve the aforementioned goals.

5.1.4.1 Channel model

In this section, I use the following multi-channel model. Each CA node has a single half-duplex acoustic transducer, which can switch to different channels for either transmission or reception. Let N and K be the number of available data channels and the amount of surrounding senders, which have replied `ATS` for data transmission, respectively. Let t represent a local time of the receiver.

The frequency allocation matrix at time t is represented as $\mathbf{A}^t$, where each entry $a^t_{nk} \in \{0, 1\}$. If channel n is assigned to node k, then I set $a^t_{nk} = 1$, otherwise $a^t_{nk} = 0$. The transmission power and data transmission rate of sender k on channel n is denoted by p^t_{nk} and R^t_{nk}, respectively, which will be jointly allocated by the receiver. Let P_k be the total transmission power assigned to sender k.

In a communication system, if the instantaneous channel state information (CSI) is available, the receiver could schedule sender k to transmit at the maximum rate

$R^t_{nk}=C^t_{nk}$. Here, C^t_{nk} is the channel capacity of node k on channel n at time t, which is expressed as

$$C^t_{nk} = a^t_{nk} B_n \log_2(1 + \frac{p^t_{nk}|h^t_{nk}|^2}{N_0 B_n a^t_{nk}}), \tag{5.5}$$

where h^t_{nk} is the instantaneous channel gain between sender k and the receiver on channel n, B_n is the bandwidth of channel n, and N_0 is the noise spectral density.

However, the real-time channel gain is usually unavailable in UCANs due to the long propagation delay of acoustic signal and the high dynamic of underwater channel. Therefore, I use the *outage probability*[3] , which only requires the statistical knowledge of h^t_{nk}, to calculate the channel capacity. The statistical information of h^t_{nk} is stable in underwater communications.

Depending on the quality of service (QoS) requirement, the packet loss ratio between sender k and the receiver on channel n should be equal to or less than a predetermined outage probability β_{nk}. That is

$$Pr[R^t_{nk} > C^t_{nk}] = \beta_{nk}. \tag{5.6}$$

Now, let $f(|h^t_{nk}|^2)$ represent the probability distribution function (PDF) of $|h^t_{nk}|^2$. Depending on the real deployment of a network and the certain ocean environment as well as the specific modulation scheme, the channel gain could be modeled as Rayleigh distribution [57], K-distribution [58] or Rice distribution [59]. RISM system is generic to arbitrary channel models. In this section, I use Rayleigh distribution as an example to show how the proposed spectrum decision mechanism works.

Assume that $|h^t_{nk}|$ follows Rayleigh distribution, then $f(|h^t_{nk}|^2)$ is an exponential distribution with mean value λ_{nk}. Substituting (5.5) into (5.6) and using the exponential expression of $f(|h^t_{nk}|^2)$, we have

$$R^t_{nk} = a^t_{nk} B_n \log_2\left[1 + \frac{p^t_{nk}\lambda_{nk}\ln(\frac{1}{1-\beta_{nk}})}{N_0 B_n a_{nk}}\right], \tag{5.7}$$

[3]If one packet is transmitted with spectral efficiency $S(\rho)$ (in bit/sec/Hz) and SNR ρ, the probability that this packet will be correctly decoded is $1-\beta$, i.e., $P_e(\rho, S(\rho)) = \beta$. Then $P_e(\rho, S(\rho))$ is called as the outage probability [86].

which will be used for the spectrum decision in Section 5.1.4.3.

5.1.4.2 Collision avoidance in channel allocation

In UCANs, multiple CA nodes may need to share a limited number of vacant frequency bands. When assigning frequencies to neighboring senders, a receiver in RISM should take into account the sending and receiving actions of the nodes within its two hops to mitigate the *hidden terminal problem*.

Here, I introduce a collision avoidance matrix, which will be used in the spectrum decision algorithm for the collision-free data transmission. I define $\mathbf{C}^t$ to be the collision avoidance matrix, with each entry $c_{nk}^t \in \{0, 1\}$. Here, $c_{nk}^t = 1$ identifies that the channel n is not available for sender k at the receiver's local time t. If any `DATA` packet of sender k is arranged to transmit on this channel at time t, collisions would happen. Let τ_k be the propagation delay between the sender and the receiver k. Next, I present how to calculate the value of each entry in $\mathbf{C}^t$ based on three constraints.

Packet forwarding constraint: As described in Section 5.1.2.1, a sender needs to forward a `REPEAT` packet before its `DATA` transmission. Therefore, when scheduling the sending time of `DATA` packet for a transmitter, the receiver should leave enough time to this sender for its `REPEAT` packet transmission. Let t_0 be the local time when a receiver sends out an `ORDER` packet. Denote the transmission time of `ORDER` packet and `REPEAT` packet by $T_{\texttt{ORDER}}$ and $T_{\texttt{REPEAT}}$, respectively. Then, we have $c_{nk}^t = 1$, if $t < t_0 + 2\tau_k + T_{\texttt{ORDER}} + T_{\texttt{REPEAT}}$.

Transmission constraint: When a receiver schedules a `DATA` transmission for an intended sender, it should prevent this transmission from interfering with other receivers' receptions. As shown in Fig. 5.5, receiver r_2 is planing to collect `DATA` from sender s, where s is in the communication range of both r_1 and r_2, but r_1 and r_2 cannot hear from each other. The receiver r_1 reserved channel n from its local time t_a

to t_b to receive data from neighboring senders (not s). In order to avoid interference to r_1, s cannot transmit on channel n from its local time t'_a to t'_b. Here, I call this as *transmission constraint*.

Senders in RISM need to inform the receiver of their transmission constraints by following the steps below. Upon overheard $\texttt{ORDER}_1$ from r_1, s calculates t'_a and t'_b based on $t'_a = t'_0 + t_a - t_0 - 2\tau_1$ and $t'_b = t'_a + t_b - t_a$, where t_0, t_a, t_b are included in $\texttt{ORDER}_1$, t'_0 is the local time when s overhears the $\texttt{ORDER}_1$, and τ_1 is the propagation delay between s and r_1. The time stamps t'_1, t'_a and t'_b will be sent to r_2 through $\texttt{ATS}$ so that r_2 could update the collision avoidance matrix accordingly. More precisely, I set $c^t_{ns} = 1$ on receiver r_2 if $t \in [t''_a, t''_b]$, where $t''_a = t''_1 + t'_a - t'_1$ and $t''_b = t''_a + t'_b - t'_a$. Here t''_1 is the local time when r_2 receives the $\texttt{ATS}$ packet.

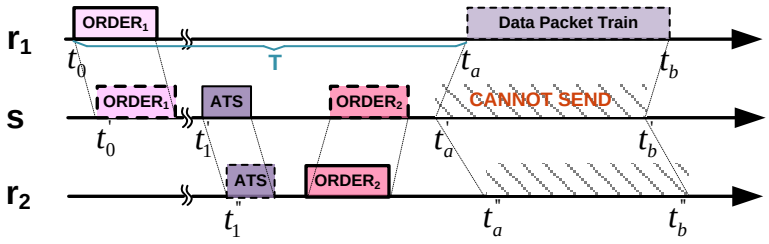

Figure 5.5: When receiver r_2 schedules a data transmission for its intended sender s, it should prevent interference to any other receivers, such as r_1.

Reception constraint: When arranging a data reception, the receiver should guarantee that it will not be interfered by neighboring senders' transmissions. As shown in Fig. 5.6, receiver r_1 has scheduled to receive data from sender s on channel n from its local time t_a to t_b and announced the arrangement through $\texttt{ORDER}_1$. When the sender receives $\texttt{ORDER}_1$, it transfers the time stamps (t_0, t_a and t_b) to its local time (t'_1, t'_a and t'_b) and attaches the information in $\texttt{REPEAT}_1$. Since r_2 is also in the communication range of s, r_2 cannot use channel n to receive $\texttt{DATA}$ from its local time t''_a to t''_b for collision avoidance purposes. I call it as *reception constraint*. The entry in the

collision avoidance matrix of r_2 is thereby set $c^t_{ns}=1$, if $t \in [t''_a, t''_b]$, where $t''_a=t''_1+t'_a-t'_1$ and $t''_b=t''_a+t'_b-t'_a$. Here t''_1 is the local time when r_2 overhears $\texttt{REPEAT}_1$.

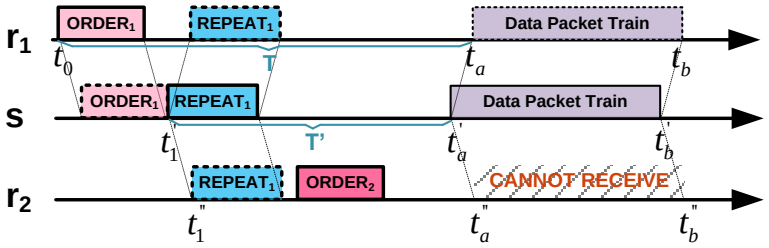

Figure 5.6: When receiver r_2 schedules its packet reception, it should guarantee that there is no interference from any other surrounding senders, like s.

From the above descriptions we observe that the calculation of entries in $\mathbf{C}^t$ is completely based on the local time of a receiver, which does not necessitate the absolute time of neighboring senders. Therefore, it can work in a non-synchronized UCAN.

5.1.4.3 Joint channel and power assignment

From the collaborative spectrum sensing, each receiver obtains the IDs of vacant channels. In this section, I introduce how to jointly allocate channel and power to maximize the spectrum utilization.

In RISM, senders inform the receiver of how many data packets will be sent out through their `ATS` messages. Different nodes may send out different numbers of data packets in each transmission. Now, let Q and T_r denote the total bits of data a receiver will receive and the time spent on receiving these data, respectively. Then, we have

$$Q=\int_0^{T_r} \sum_{n=1}^{N} \sum_{k=1}^{K} R^t_{nk}\, dt, \tag{5.8}$$

where R^t_{nk} is the assigned data rate to sender k on channel n at time t.

I aim to minimize T_r in (5.8), which is equivalent to maximizing $\sum_{n=1}^{N}\sum_{k=1}^{K} R^t_{nk}$ as Q is fixed. Therefore, I formulate the joint power and frequency allocation as the

following optimization problem:

$$\begin{aligned}
&\textbf{Prob.1} \qquad \arg \max_{\substack{p_{nk}^t>0 \\ a_{nk}^t \in \{0,1\}}} \sum_{n=1}^{N}\sum_{k=1}^{K} R_{nk}^t, \\
&\textbf{where} \quad R_{nk}^t = a_{nk}^t B_n \log_2\left[1+\frac{p_{nk}^t \lambda_{nk} \ln(\frac{1}{1-\beta_{nk}})}{N_0 B_n a_{nk}^t}\right]. \\
&\textbf{s.t.} \\
&\textbf{C1:} \ \textstyle\sum_{k=1}^{K} a_{nk}^t = 1, \quad n \in \{1,\ldots,N\}, \\
&\textbf{C2:} \ \textstyle\sum_{n=1}^{N} p_{nk}^t \le P_k, \quad k \in \{1,\ldots,K\}, \\
&\textbf{C3:} \ a_{nk}^t = 0, \text{ if } c_{nk}^t = 1, \ n \in \{1,\ldots,N\}, k \in \{1,\ldots,K\}.
\end{aligned} \tag{5.9}$$

In Prob.1, C1 is the channel allocation constraint which ensures that each channel is assigned to no more than one CA sender; C2 is the power constraint to guarantee that the overall transmission power of each sender does not exceed the maximum power supply, and C3 is the collision avoidance constraint.

As introduced in Section 5.1.4.2, C3 is the combination of three constraints, namely, packet forwarding constraint, transmission constraint and reception constraint. It is an unique constraint condition in Prob.1, which integrates the collision avoidance mechanism on the MAC layer with the power and channel assignment on the physical layer closely.

Solving Prob.1 without the constraint condition C3, I can use a similar approach proposed in [87] and [88]. I first relax the requirement $a_{nk}^t \in \{0, 1\}$ to allow a_{nk}^t to be a real number within the interval [0, 1]. Then, the objective function of the problem follows the form of $f(x, y) = \mu x \log_2(1 + \nu y/x)$, where μ and ν are constants. Its easy to prove that the Hessian matrix of this function is negative semidefinite for all x and y. Therefore, the objective function is concave. Finally, Prob.1 could be solved through

the following classic method of Lagrangian multipliers:

$$\begin{aligned}\mathcal{L}(a_{nk}^t, p_{nk}^t) = &\sum_{n=1}^{N}\sum_{k=1}^{K} B_n a_{nk}^t \log_2\left[1+\frac{p_{nk}^t \lambda_{nk} \ln(\frac{1}{1-\beta_{nk}})}{N_0 B_n a_{nk}^t}\right] \\ &- \phi_k\left(\sum_{n=1}^{N} p_{nk} - P_k\right) - \varphi_n\left(\sum_{k=1}^{K} a_{nk}^t - 1\right),\end{aligned} \tag{5.10}$$

where ϕ_k and φ_n are the Lagrangian multipliers of the constraints C1 and C2, respectively.

Calculating the partial derivatives of $\mathcal{L}(a_{nk}^t, p_{nk}^t)$ with respect to a_{nk}^t and p_{nk}^t, we have

$$\frac{\partial \mathcal{L}}{\partial p_{nk}^t} = \frac{a_{nk}^t B_n \theta_{nk}}{\ln(2)(a_{nk}^t B_n + \theta_{nk} p_{nk}^t)} - \phi_k, \tag{5.11}$$

and

$$\begin{aligned}\frac{\partial \mathcal{L}}{\partial a_{nk}^t} = &B_n \log_2(1 + \frac{p_{nk}^t \theta_{nk}}{a_{nk}^t B_n}) \\ &- \frac{p_{nk}^t B_n \theta_{nk}}{\ln(2)(a_{nk}^t B_n + \theta_{nk} p_{nk}^t)} - \varphi_n,\end{aligned} \tag{5.12}$$

where

$$\theta_{nk} = \frac{\lambda_{nk} \ln(\frac{1}{1-\beta_{nk}})}{N_0}. \tag{5.13}$$

Now, let (5.11) and (5.12) equal to zero, we have

$$p_{nk}^t = \frac{a_{nk}^t B_n}{\phi_k \ln(2)} - \frac{a_{nk}^t B_n}{\theta_{nk}}, \tag{5.14}$$

and

$$\ln\left(\frac{1}{1+X_{nk}}\right) - \frac{1}{1+X_{nk}} = -\left[\frac{\ln(2)\varphi_n}{B_n} + 1\right], \tag{5.15}$$

where

$$X_{nk} = \frac{p_{nk}^t \theta_{nk}}{B_n a_{nk}^t}. \tag{5.16}$$

I note that the subscripts of variables at the left side of (5.15) include n and k, but those at the right side of the equation only contain n. This implies that X_{nk} is independent with k and thus, we have

$$X_{n1} = X_{n2} = \cdots = X_{nK}. \tag{5.17}$$

According to (5.16) and (5.17), I conclude that a_{nk}^t should be proportional to $p_{nk}^t \theta_{nk}/B_n$.

Now, we rethink the original constraint C2 of requiring a_{nk}^t to be a binary value. With this constraint, channel n would be allocated to the sender $\hat{k}$, which has the largest a_{nk}^t. Therefore, the optimal values of a_{nk}^t and p_{nk}^t are

$$\hat{a}_{nk'}^t = 1, \;\; \hat{a}_{nk}^t = 0 \quad \text{for all} \;\; k \neq k', \tag{5.18}$$

where

$$k' = \arg\max_k \frac{p_{nk}^t \theta_{nk}}{B_n}, \quad k \in \{1, \ldots, K\}, \tag{5.19}$$

and

$$\hat{p}_{nk}^t = \begin{cases} 0, & \phi_k \geq \dfrac{\theta_{nk}}{\ln(2)} \;\; \text{or} \;\; a_{nk}^t \neq 1 \;\; \text{or} \;\; c_{nk}^t = 1, \\ \min\left\{ \dfrac{B_n}{\phi_k \ln(2)} - \dfrac{B_n}{\theta_{nk}}, \, P_k \right\}, & \text{otherwise.} \end{cases} \tag{5.20}$$

Let vector $\mathbf{A}_k^t$ be the channel assignment to sender k at time t, which is a collection of row indexes with nonzero elements in the k^{th} column of $\hat{\mathbf{A}}^t$. Substituting (5.20) into constraint C2 of Prob.1, we have

$$\phi_k = \frac{\sum_{n \in \mathbf{A}_k^t} B_n}{\ln(2) \left[P_k + \sum_{n \in \mathbf{A}_k^t} \dfrac{B_n}{\theta_{nk}} \right]}. \tag{5.21}$$

Finally, we get the optimal transmission power, $\hat{p}_{nk}^t$, by substituting (5.21) into (5.20).

Next, I take into account the constraint condition C3 and use an iterative algorithm to compute $\hat{p}_{nk}^t$ and $\hat{a}_{nk}^t$ in RISM.

Algorithm 1

Initialization: Based on the infromation of spectrum usage collected from ATS and REPEAT packets, the receiver generates its collision avoidance matrix $\mathbf{C}^t$.

Iterative Calculations:

do

for $n = 1$ to N

Step 1: Let $a_{nk}^t = 1$ for each sender, k, in turn for the channel, n, with $c_{nk}^t \neq 1$, and calculate ϕ_k according to (5.21). In this step, previous channel allocation $a_{n'k}$, $n' \neq n$ remains unchanged.

Step 2: Use (5.20) to calculate p_{nk}^t.

Step 3: Pick out the best sender, $\hat{k}$, based on (5.19), and set $a_{n\hat{k}}^t = 1$.

end for

Step 4: Calculate $\sum_{n=1}^{N}\sum_{k=1}^{K} R_{nk}^t$ in Prob.1.

while The increment of $\sum_{n=1}^{N}\sum_{k=1}^{K} R_{nk}^t$ is larger than a predetermined threshold.

After running Algorithm 1, the receiver attaches the sending time of data packets, the channel assignment, transmission power and data rate into an `ORDER`, and delivers the packet to intended senders.

5.1.4.4 An insight into collision avoidance matrix

The matrix $\mathbf{C}^t$ in the RISM system is a critical "bridge" to connect the joint channel and power allocation algorithm on the physical layer with the collision avoidance mechanism on the MAC layer. In each round of communication, a receiver needs to update its $\mathbf{C}^t$ according to the occurrence of certain events. Next, I introduce how a specific event triggers a change of collision avoidance matrix by affecting the status of channel usage.

In RISM, there are a total number of six specific events that may change the channel status (idle or busy). Here, I use Fig. 5.7 as an example to introduce these events. In the figure, I have two senders, s_1 and s_2, and a common receiver, r_1. The propagation delay from s_1 to r_1 is shorter than that from s_2. Assume r_1 arranges s_1 and s_2 to send

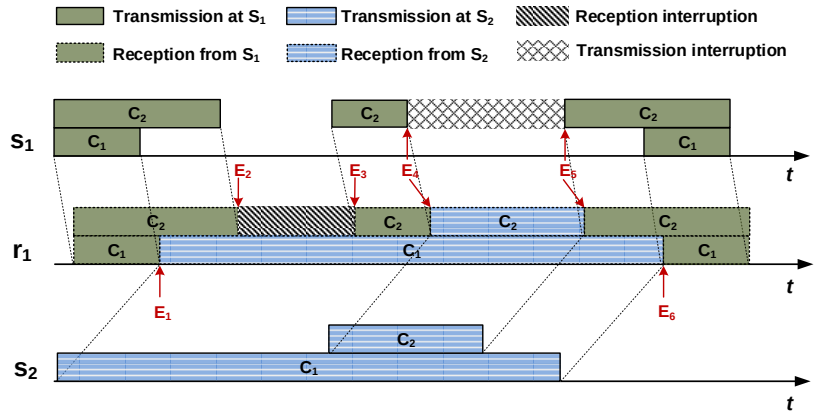

Figure 5.7: The events that affect the channel status. $\mathbf{E_1}$: s_2 joins the channel allocation; $\mathbf{E_2}$: reception at r_1 interrupted on c_2; $\mathbf{E_3}$: reception interruption released on c_2; $\mathbf{E_4}$: transmission at s_1 interrupted on c_2; $\mathbf{E_5}$: transmission interruption released on c_2; $\mathbf{E_6}$: transmission completed at s_2 and c_1 released.

the data simultaneously. I further assume that s_1 has a good channel quality on c_2 whereas s_2 prefers channel c_1. The six events are introduced as follows.

a) ***Sender join*** **($\mathbf{E_1}$)**: The event that a new sender joins the channel allocation. Particularly, in a network, the distances from senders to a common receiver may be different. Hence, senders in RISM usually join a channel allocation one by one. Each time when the packet from a new sender coming, a receiver recalculates its collision avoidance matrix to allocate the channel and power optimally.

b) ***Reception interruption*** **($\mathbf{E_2}$)**: The event that a receiving process is interrupted on a specific channel. According to the reception constraint introduced in Section 5.1.4.2, a receiver may suspend its data reception on a certain channel for a while to avoid the interference from other transmitters.

c) ***Reception interruption release*** **($\mathbf{E_3}$)**: The event that the interruption is end and a receiver can resume its data reception.

d) ***Transmission interruption*** **($\mathbf{E_4}$)**: The event that a sender suspends its data transmission on a specific channel to prevent its sending activity from interrupting the reception of neighboring receivers.

e) ***Transmission interruption release*** *(**$\mathbf{E_5}$**)*: The event that the potential interruption to surrounding receiver is end and the sender can resume its data transmission on the channel again.

f) ***Sender leave*** *(**$\mathbf{E_6}$**)*: The event that a sender completes its data transmission and leaves the channel. More specifically, in each round of communication, senders usually finish their data transmission at different time, since both the amount of data packets and the transmission rate of different senders are different. Therefore, when a node finishes its data transmission, the channel will be available to other senders.

It is worth noting that a receiver in RISM knows the occurrence of above events before they happen, as the channel usage is up to date by overhearing `ORDER` and `REPEAT` messages and by calculating the constraints described in Section 5.1.4.2. Once an event happens, the status of the channel will change. In this situation, the receiver flips the corresponding elements in its collision avoidance matrix $\mathbf{C}^t$ between 1 and 0. Thereafter it needs to run Algorithm 1 for a new round of channel and power allocation. Finally, as shown in Fig. 5.7, once the packet reception starts, the data streams from different senders will arrive at the receiver seamlessly. This allows CA nodes to fully utilize the channel resource for a data reception.

5.1.5 Adaptive polling in RISM

In receiver-initiated approaches, there is a unique challenge that receivers need to decide when to poll the neighboring senders blindly. It becomes a big problem in a distributed network, since receivers usually lack in the current status e.g., having packets to send or not, of its intended senders. In this section, I discuss how to handle this problem in RISM with a traffic predictor.

5.1.5.1 Why polling senders adaptively

Adjusting the polling frequency of a receiver will cause a trade-off between the queuing delay and the energy efficiency. Initiating handshake over frequently results in resources (spectrum, energy and time) waste for transmitting control messages, whereas slowing down the polling rate occasionally leads to larger queuing delay such that the data cannot be delivered timely. In a receiver-initiated protocol, a receiver should adjust its polling frequency, i.e., the time interval between successive `RTR` requests, to match the traffic loads on its intended senders [89].

However, it is a challenge for a receiver to poll surrounding senders adaptively due to the following reasons. First of all, the receiver has no prior knowledge regarding the number of data packets cumulated on the intended senders. Intuitively, a sender could inform the receiver its current status by sending some specific messages. However, considering the long preamble in acoustic modems and the energy constraint in UCANs, such a strategy would generate extra overhead traffic and reduce the lifetime of the network. Therefore, senders in RISM have to passively wait for the receiver to initiate the handshake process. Secondly, the traffic load is generally heterogeneous in a network. It becomes more difficult to decide the optimal polling frequencies for different senders. Finally, the traffic load of a node may change with the time. For example, in a target tracking network, nodes generate bursty traffic to report their observations whenever the presence of a target is detected, while keeping quiet for the rest of time to save the energy.

In order to tackle the above challenges, each receiver in RISM system needs to decide its data polling frequency independently to match the heterogenous and varying traffic of a network. A smart polling strategy thus is required to improve the network throughput, energy efficiency and delivery delay.

5.1.5.2 Smart polling scheme

In RISM, I adopt the traffic prediction to implement the smart polling scheme. By using the traffic predictor, a receiver could estimate the current traffic loads of its intended senders through historical traffic measurements. Whenever the total traffic of neighboring senders exceeds a threshold, the receiver sends out an `RTR` packet to request for data.

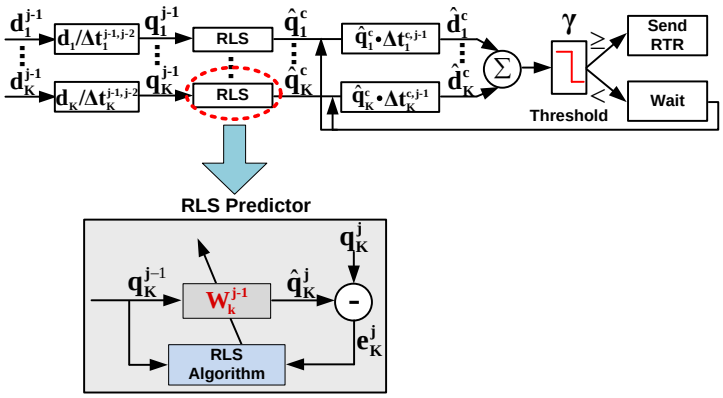

Figure 5.8: An RLS based adaptive polling scheme for RISM system.

In the literature, a number of algorithms, such as the adaptive filter [90] and artificial neural network [91] have been proposed for predicting the network traffic. In RISM, we could choose an appropriate method depending on the demand of an application. For instance, in a target detection network, the traffic load of a sensor node may change quickly with the entering and leaving of a target. In this scenario, a receiver could employ a recursive least squares (RLS) filter, which has a fast convergence, to track the traffic variation of its neighbors. Moreover, if the traffic of a UCAN is non-linear, non-stationary and non-Gaussian but changes slowly, a receiver could use a finite-impulse-response artificial neural network (FIR-ANN) [92] for an accurate traffic prediction.

In Fig. 5.8, I use the RLS filter as an example to introduce how to design a smart polling scheme for the RISM system. Here, I call the time interval for a receiver and its

intended senders completing a round of communication (Phase 1 to Phase 6 in RISS) as a period, and then the details of a smart polling scheme are as follows:

(a) Before transmitting an `RTR` message, the receiver first estimates the number of data packets, $\sum_{k=1}^{K} \hat{d}_k^c$, currently cumulated on all K intended senders, where $\hat{d}_k^c = \hat{q}_k^c \times \Delta t_k^{c,j-1}$. Here, $\hat{q}_k^c$ is the estimation of current traffic load on sender k, and $\Delta t_k^{c,j-1}$ is the elapsed time since receiving the $\texttt{ATS}_k^{j-1}$ packet. The receiver initiates a handshake if $\sum_{k=1}^{K} \hat{d}_k^c$ exceeds the threshold, which is denoted by γ, otherwise it will wait for longer time.

(b) Based upon $\texttt{ATS}_k^j$, the receiver calculates the average traffic rate, q_k^j, of sender k during the last period according to $d_k^j / \Delta t_k^{j,j-1}$, where $\Delta t_k^{j,j-1}$ is the time interval between the receptions of $\texttt{ATS}_k^j$ and $\texttt{ATS}_k^{j-1}$. Then the receiver uses the latest l measurements, $\{q_k^j, \ldots, q_k^{j-l+1}\}$, to update the weight vector, which is denoted by $\mathbf{W}_k^j$, of its RLS filter. Here, l is referred to as the order of a RLS filter.

(c) The receiver applies the new weight, $\mathbf{W}_k^j$, to predict $\hat{q}_k^{j+1}$ — the traffic rate of sender k in the next period.

By adjusting the threshold γ in the traffic predictor, a UCAN could achieve a tradeoff between the queuing delay and the energy efficiency. More specifically, with a small γ, the data produced by each sender could be sent out timely, whereas with a large γ, each round of communication could carry more data packets, which saves the energy consumption on transmitting control messages.

5.1.6 Simulations and analysis

In this section, I conduct simulations to evaluate the performance of RISM system. The simulation platform is Aqua-Sim [93], an NS-2 based underwater network simulator. We extend Aqua-Sim to support multi-channel communications, dynamic power

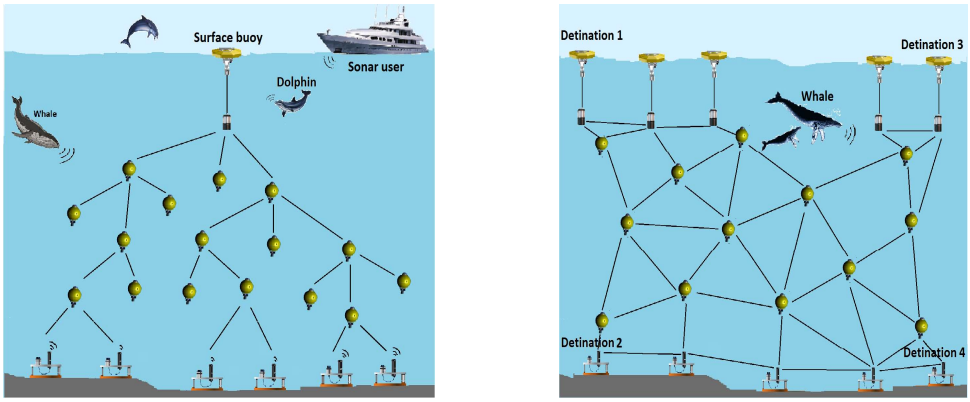

(a) Tree topology (b) Mesh topology

Figure 5.9: Two network topologies used in simulations. (a) In the tree topology, 20 underwater nodes in the network deliver their data to a surface buoy. (b) In the partially connected mesh topology, 16 underwater nodes randomly select a node at four corners as the destination for data transmission.

and channel assignments. Simulation results verify the enhanced network throughput, delivery delay and energy efficiency with smart polling, than RISM with constant polling. We also compare RISM with MMAC-CR [20] in different network settings. All results presented in this section are the average outcomes of multiple simulations.

One of the real applications I considered in the simulation is an underwater target tracking network, where a UCAN with the bottom nodes, autonomous underwater vehicles (AUVs) and surface nodes is deployed in oceans to detect the presence of interesting targets, e.g., marine animals or submarines. If the nodes have not sensed any specific target yet, they stay in the sleep mode to save power. In this case, each node generates only a few packets periodically to update the routing table or to synchronize time. The sensor nodes become busy once any target enters the network, thereby creating a bursty traffic. In this application, an UAN becomes active when the interesting targets enter the network. In order to prevent the UAN from interfering surrounding underwater systems, like sonar or marine animals, we can apply the cognitive technique for environment-friendly data transmissions.

We evaluate the performance of RISM in two typical network topologies, as shown in Fig. 5.9. The tree network is usually applied for underwater data collection while the mesh topology network is a general example of ad hoc UANs. In the tree topology, we have 20 sub-sea nodes collecting and forwarding data to the sink node on the surface of the oceans, as illustrated in Fig. 9(a). In the partially connected mesh network, I deploy four hydrophones at four corners as sink nodes, as shown in Fig. 9(b). In the network, 16 sub-sea nodes generate and deliver data to a randomly selected hydrophone. In both topologies, the size of data packets is 250 B.

The average distance among neighboring nodes is 1 km (uniformly distributed between 800 m to 1200 m) in both topologies. I set the maximum transmission range and the maximum transmission power of each node as 1.5 km and 20 W, respectively. The overall available channel bandwidth in the simulation is 30 kHz (from 1 kHz to 31 kHz), which is evenly divided into six subbands. I assign the lowest subband (1 kHz to 6 kHz) to be the CCC and assume this channel is not occupied by any PUs in the area. The remaining five subbands are used as data channel. In the network, I also deploy two PUs. Each of them randomly selects one amongst five data channels for its communication, and switches the communication channel every 60 secs.

5.1.6.1 Performance evaluation

I first evaluate the joint channel and power assignment in RISM by comparing the transmission rates in scenarios with and without optimal resource allocation. In this comparison, I set four vacant channels, and three intended senders requiring data transmission to a common receiver.

Fig. 5.10 illustrates the average transmission rate of three senders. In the random allocation strategy, the receiver randomly allocates one channel to each sender with the maximum transmission power. The optimal assignment with continuous a_{nk}^t supposes

that multiple senders could share one channel simultaneously, which is unrealistic in the real world, but could be considered as an upper bound of the transmission rate. The channel allocation algorithm applied in RISM is a sub-optimal solution, in which one channel is allocated to no more than one sender. From this figure, it is easy to observe a significant improvement on the average transmission rate in RISM system over the random assignment. In addition, the sub-optimal channel allocation is only slightly lower than the optimal solution. This verifies that RISM could utilize the channel and energy resources efficiently on the physical layer.

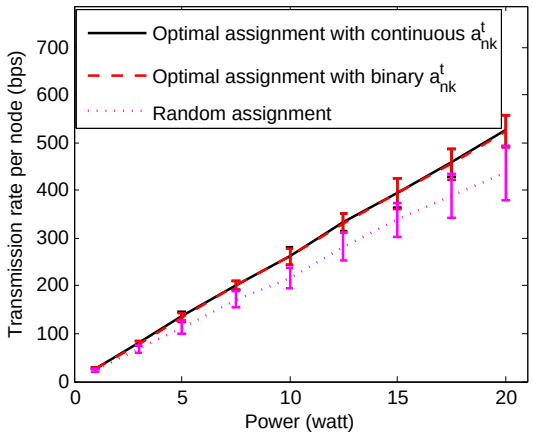

Figure 5.10: The average transmission rate comparison among different resource allocation approaches.

As I introduced in previous sections, RISM aims to eliminate the collisions caused by the hidden terminal problems. However, I observe the existence of collisions in RISM when a) the node fails to overhear the transmission scheduling of surrounding users due to the collision of `ORDER` or `REPEAT` with other control packets; and b) the node does not overhear the `ORDER` or `REPEAT` packets on time due to the long propagation delay in underwater communications. I plot the delivery ratio of data packets with respect to the variation of a traffic load in different networks. Here, the packet delivery ratio is defined as the number of packets successfully received by receivers divided by the total packets sent by senders.

Fig. 5.11 demonstrates that RISM achieves 90% – 95% delivery ratio when there is no channel loss caused by the factors other than collisions. RISM can get higher delivery ratio, which means lower data collisions, in the mesh topology than in the tree network. In the tree topology, the data flow is gradually aggregated to the upper nodes in the network causing higher collision probabilities than the case in the mesh topology where the destination of data packets is one of a random node located in the four corners resulting in the scattered data flow. When the probability of packet decoding failure caused by the poor channel quality is 10% or 20% in my simulations, the high channel loss becomes the dominated reason for a low packet delivery ratio, as shown in Fig. 5.11. However, it is worth noting that the end-to-end reliability of RISM can be guaranteed by the acknowledgment and retransmission mechanism regardless the packet loss on the hop-by-hop delivery.

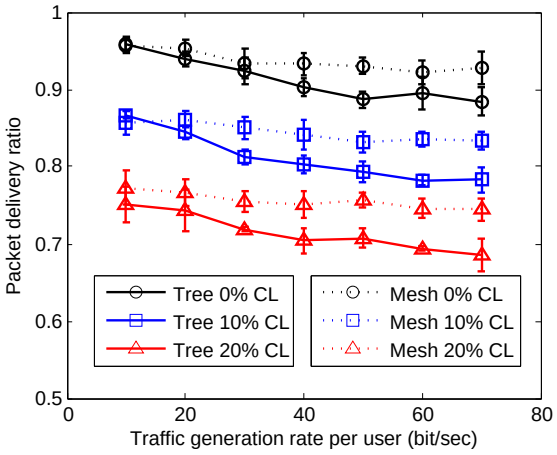

Figure 5.11: Packet delivery ratio of RISM.

In RISM, a tradeoff exists between the packet delivery delay and the overhead of control messages through changing the polling frequency of receivers. More specifically, if a receiver polls its intended senders frequently, data packets on a seder will have a short queuing delay, but at the cost of a low handshake efficiency, since each round of communication carries only a small number of data packets. On the other hand, if a

receiver waits for a long time before requesting data, the queuing delay on the senders would be significant. However, a low polling frequency guarantees that enough data packets could be delivered in each round of handshake process, which improves the efficiency of a negotiation.

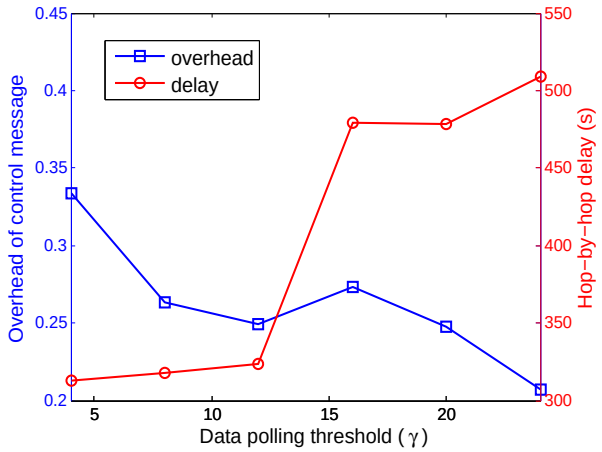

Figure 5.12: Tradeoff between the delay and the overhead of control messages.

For RISM with the smart polling scheme, a receiver would not send `RTR` until it predicts that the total number of packets accumulated on its intended senders goes over the polling threshold. Therefore, we could change the polling frequency of a receiver by simply adjusting the parameter γ. In Fig. 5.12 I set the traffic generation rate as 40 bit/sec and show the tradeoff between the overhead of control messages and the hop-by-hop delay of RISM in the tree topology with respect to γ. In this figure, the overhead of control messages represents the percentage of energy consumption on control packets for each successful data transmission. It is a ratio of energy consumption on transmitting control messages to that on all packets (control plus data). The results depict that when γ is small, frequent handshake consumes considerable energy on control message transmissions. The energy consumption remarkably reduces with the increment of γ, but results in a larger delivery delay, especially when γ is over 13. Hence, in the rest

of this section, I set the threshold for the adaptive polling as $\gamma = 13$ unless stated otherwise.

In order to give an insight into the overhead of RISM, I show the average number of control packets sent for each successful data transmission in Fig. 5.13. From this figure we could observe a considerable decrease in the average number of control messages with the growth of traffic generation rate. Intuitively, when the traffic is light, the time it takes for senders to cumulate enough data packets for being polled will be inevitably long, which is not desirable in a delay sensitive application. To tackle this problem, I set a maximal polling interval for the RISM system. When either the polling interval exceeds the maximal value or the number of cumulated packets reaches γ, the receiver will initiate a request for the data reception. For this reason, in a situation of low traffic rate, a handshake is most likely triggered by the maximal polling interval, at which time senders may have only a few data to send. On the other hand, when the traffic rate is high, the threshold, γ, controls the polling frequency. The average number of control packets used for each data transmission becomes stable as traffic generation rate grows.

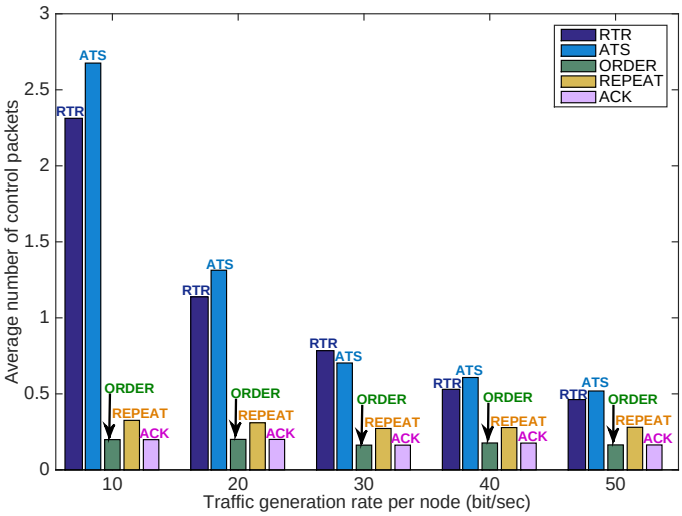

Figure 5.13: The average number of control packets used for each successful data transmission in the tree topology.

5.1.6.2 performance comparison

To verify the advantages of the proposed system, I compare RISM with MMAC-CR [20], a representative MAC protocol for CR networks. A brief introduction on MMAC-CR has been presented in Section 5.1.1. I also run RISM with and without smart polling to validate the effectiveness of the adaptive data retrieving mechanism. In RISM without smart polling, the polling frequency is determined based upon the traffic rate measured at the initialization stage of a network. In this scheme, receivers sends `RTR` periodically, and thus could not self-adapt to the variation of the network traffic.

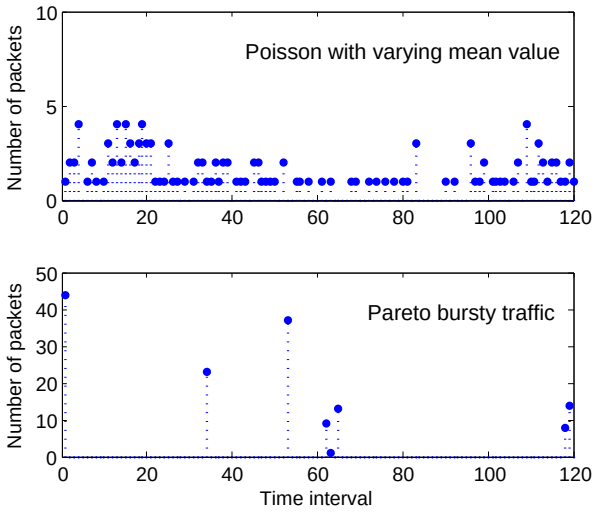

Figure 5.14: An example of traffic patterns. (Average traffic generation rate is 0.02 packet per second for both scenarios. Each time interval is 50 secs.)

The performance metric I focus on in the comparison are network throughput, delay and overhead of control packet. The throughput is bits per second successfully received by each node in a network. The delay consists of queueing delay, transmission delay and propagation delay. Considering the low throughput and the high collision probability among control messages in UANs, the queuing delay waiting for channel access is considerable and dominates the packet delivery delay. The overhead is calculated as

the ratio of energy consumption on transmitting control messages to that on all packets (control plus data).

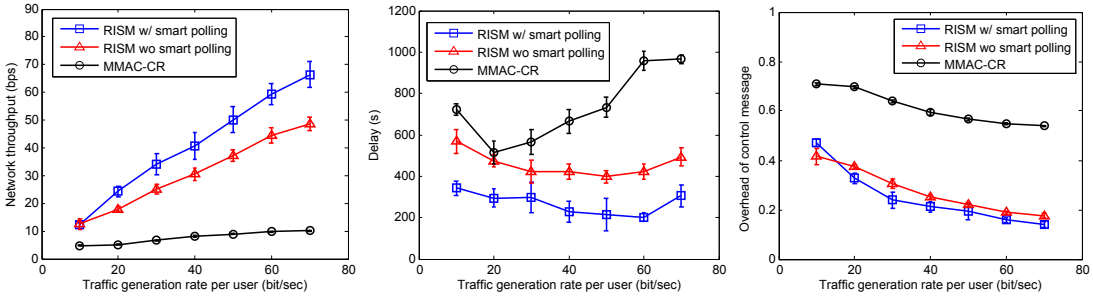

(a) Network throughput (b) Delay (c) Overhead

Figure 5.15: Performance comparison for Poisson traffic with slowly varying mean value in tree topology.

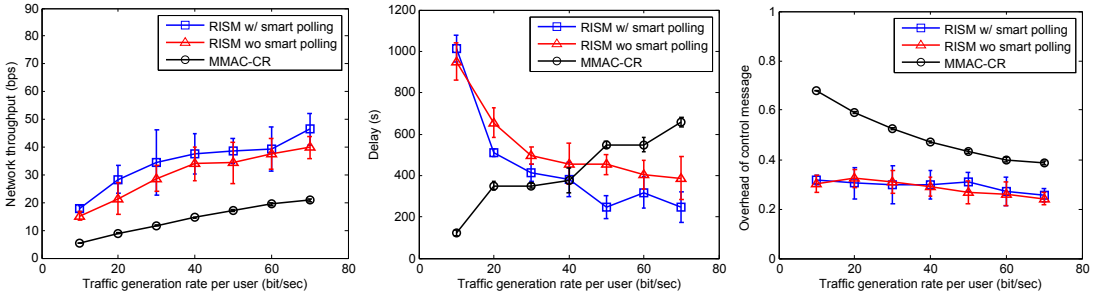

(a) Network throughput (b) Delay (c) Overhead

Figure 5.16: Performance comparison for Poisson traffic with slowly varying mean value in mesh topology.

In order to give comprehensive comparisons, I test the protocols with two different traffic patterns, namely, the Poisson process with slowly varying mean value and a Pareto busty traffic, as shown in Fig. 5.14. The Poisson traffic is generally used to model the arrival process of a traffic in sensor networks where the data traffic is barely bursty. A varying mean value in the Poisson process can simulate the temporal variation of data collection rate. The Pareto traffic generator could well capture the traffic features of an event-driven sensor network, where sensor nodes generate a large amount of observations whenever a target event is detected.

Fig. 5.15 demonstrates the performance comparison in the tree network (Fig. 9(a)) where the data generation rate follows Poisson process. From Fig. 5.15 we observe that RISM outperforms the conventional sender-initiated MMAC-CR in all aspects. More specifically, smart polling assisted RISM achieves the highest throughput benefiting from the parallel reservation. By allowing receivers to negotiate with multiple senders in parallel, RISM mitigates the problem of a low handshake efficiency in UCANs caused by the long propagation delay and the long preamble in acoustic modems. Moreover, as shown in Fig. 15(a), the throughput improvement of RISM dramatically increases with the growth of network traffic generation rate. In applications with heavy traffic loads, RISM could provide high network throughput, which makes it a promising solution for efficient spectrum management. Compared to RISM without smart polling, the traffic prediction scheme grants receivers the capability to dynamically poll senders with the varying mean value of Poisson traffic, thereby leading to a significant throughput enhancement.

Furthermore, RISM with smart polling allows a network to accommodate a high traffic rate with relatively low delivery delays, as shown in Fig. 15(b). In a UCAN with heavy traffic load, the packet queuing delay is the main source of packet delivery delays in RISM without smart polling. The traffic prediction enables each receiver to retrieve data from surrounding senders not only more efficiently but also more timely than the RISM without smart polling, thereby significantly reducing the delivery delay in scenarios with high traffic generation rates.

Another advantage of RISM over sender-initiated protocols is the low overhead on control messages. When receivers start negotiation with their surrounding senders, RISM works as a "semi-centralized" system, where the spectrum sensing, spectrum sharing and dynamic power control could efficiently share control packets with each other. As illustrated in Fig. 15(c), RISM with and without traffic prediction have

comparable control overhead, since both schemes tend to wait for enough cumulated data packets before starting a handshake process for better energy efficiency. MMAC-CR, by contrast, has almost twice larger overhead than RISM, as MMAC-CR has to schedule separate control messages for spectrum sensing, multi-channel rendezvous, and dynamic power control.

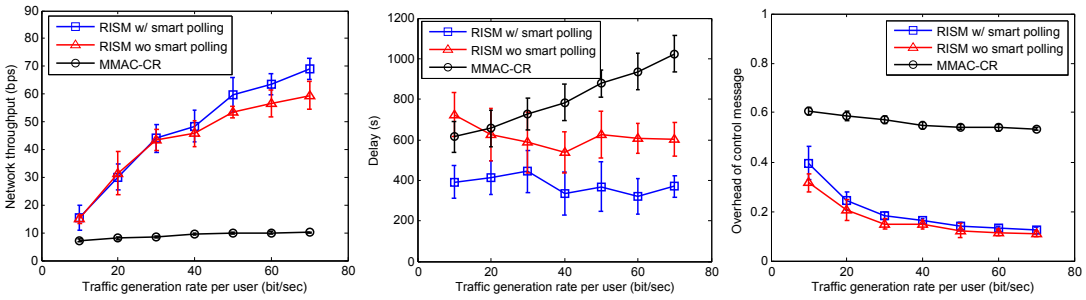

(a) Network throughput (b) Delay (c) Overhead

Figure 5.17: Performance comparison for Pareto bursty traffic in tree topology.

Fig. 5.16 uses the same setting as Fig. 5.15, but the network topology is changed from the tree network to the mesh network as shown in Fig. 9(b). By comparing the results in Fig. 5.15 and Fig. 5.16, we could observe that RISM has lower throughput in the mesh network than in the tree network. This is because in the tree topology, underwater nodes generate and forward data packets to a common destination, namely, the surface node resulting in the aggregated data flow. Therefore, a receiver could easily get a large amount of packets from nodes beneath it in each period, which improves the handshake efficiency. In the mesh network, on the other hand, the destination of data packets is one of a random node located in the four corners, which "diluents" the traffic. Therefore, a receiver usually retrieves less data packets within a given period in a mesh network than that in a tree network, which reduces the handshake efficiency and leads to a lower nodal throughput for RISM.

By contrast, MMAC-CR can achieve higher throughput in mesh networks than that in tree networks. Intuitively, in tree networks, multiple senders choosing the same relay

node causes heavy congestion for the channel access. In mesh network, however, the data packets are scattered resulting in lower collision probability on control messages. Due to the similar reason, RISM has a much longer delay in the mesh network than that in the tree network, whereas MMAC-CR can achieve a shorter delay in the mesh network. Although RISM works more efficiently in tree network, it still outperforms the sender-initiated MMAC-CR in terms of network throughput and energy efficiency in the mesh network.

By comparing the results in Fig. 5.15 and Fig. 5.17, we could realize how a traffic pattern affects the performance of different protocols. For Pareto bursty traffic, the instantaneous traffic is bursty but the average data generation rate is a constant in the simulation. As for Poisson traffic, I periodically change the average traffic generation rate from 0.5× to 1.5× of the mean value in each test. we observe that RISM with smart polling has comparable performance with both Poisson traffic and bursty traffic, i.e. RISM is barely affected by the traffic pattern. With an assistance of traffic prediction, the smart polling mechanism could capture the variations in the network traffic, thereby making receivers in RISM request data at a proper time. RISM without smart polling, on the other hand, has much lower throughput than RISM with smart polling when the network traffic varies with time, as shown in Fig. 15(a). The difference on throughput of RISM with and without smart polling becomes less significant with bursty traffic. This indicates that the adaptive polling could bring more enhancement to RISM when the average traffic rate is more dynamic.

5.2 DCC-MAC

In CR network, the CCC based MAC protocols are very popular due to their high reliability, easy implementation and low overhead. However, due to the frequency-dependent attenuation, a UCAN may not have enough frequency band to its CCC.

How to prevent the control channel from congesting in the applications with a heavy traffic load should be concerned carefully. With this in mind, in this section I propose, DCC-MAC, a new MAC protocol for distributed UCANs. The control channel in DCC-MAC consists of two parts: a dedicated CCC and one or more data channels. Once the acoustic nodes detected a congestion of CCC, they could flexibly select a proper data channel to extend their control channel, and return the excessive frequency bands back when the current control channel becomes idle. The content in this section is mainly based on my previous work published in [27][4] .

5.2.1 Related work

A MAC protocol in a cognitive network relies more on the control packets than that in a conventional single channel network. Cognitive nodes use these control packets for handshaking to avoid collisions, negotiating to decide the communication channel (multi-channel rendezvous), and collaborating to improve the sensing accuracy (co-operative sensing). In a cognitive network, people usually assign a dedicated CCC for control packets [17, 20, 94]. This channel is physically separated from the in-band channel where data transmission occurs.

However, the available spectrum resource is limited in an acoustic communication owing to the frequency-depended attenuation and narrowband response of acoustic modem. Hence, a UCNA may allocate a narrow frequency band for control messages, resulting in a congestion problem on CCC in a heavy traffic load situation. This reduces the performance of a cognitive network in terms of throughput, energy efficiency and end-to-end delay. To solve this problem, some excellent works have been done in recent years. Here, I classify these works into two categories as follows.

[4] © 2016 IEEE. Reprinted with permission from Yu Luo, Dynamic control channel MAC for underwater cognitive acoustic networks, IEEE INFOCOM, Apr. 2016 (Accepted)

CCC Workload Reduction: In this kind of MAC protocols, the cognitive network retains a CCC, but nodes transmit only part of control messages on it. In this way, the traffic load on the CCC could be reduced considerably. For example, in MMAC [94], only the packets for a channel rendezvous are transmitted on CCC. Other handshake packets, such as RTS, CTS and ACK, are sent on different in-band data channels. In [20], authors propose the MMAC-CR. Similar to MMAC, MMAC-CR also leverages CCC in each beacon period to handle the multi-channel rendezvous problem, and uses the in-band channels for handshake and data packet transmissions. Different from MMAC, in order to support the PU detection, MMAC-CR inserts a fast sensing and a fine sensing procedures into its beacon period and data period, respectively.

CCC Elimination: Cognitive MAC protocols in this category dedicate to completely remove the CCC. The main idea behind these protocols to address the channel rendezvous problem is that each node keeps tracking the receiving channel of its neighbors, and sends a notification regarding the ID of a new receiving channel to its neighbors when a PU reclaims the old one. Typical CCC elimination protocols include cognitive MAC (C-MAC) [80], single-radio adaptive channel (SRAC) [95] and synchronized MAC (SYN-MAC) [96]. In C-MAC [80], different channels are divided into multiple asynchronized beacon periods and data periods. If a node plans to switch its current operating channel, called the rendezvous channel (RC), it appends the ID of this new RC to a beacon signal and sends it in the beacon period on its current RC. Hence, a node could track neighbors' RC without CCC. SRAC [95] is another approach working in a cognitive network without CCC. It is designed as an independent module to let existing single-radio MAC protocols support the dynamic spectrum access. In this approach, each node monitors the spectrum usage through the background channel probes, and then chooses inactive frequencies as its operating channel. During a communication, a node utilizes a single-radio MAC protocol to transmit their control

or data packets on its neighbors' operating channel. If a node changes its operating channel, it sends ID of the new channel to its neighbors via a notification frame. In synchronized MAC (SYN-MAC) [96], control packets also share the channel with data packets to overcome the potential congestion on CCC. More specifically, SYN-MAC divides each frame into multiple slots, and assigns each channel a different one. Nodes are aware of the spectrum usage of their neighbors at the initial stage of a network. If a node would like to update the information regarding the spectrum sensing results, or to send a data, it first selects a vacant channel that it shared with the receiver. Thereafter the node sends a notification packet or starts a classic two-way handshake process in the corresponding time slot of the selected channel.

5.2.2 Motivation

Both the CCC workload reduction based and the CCC elimination based cognitive protocols may have some constraints when applying in an underwater environment. In this section I briefly analyze these constraints, which promote us to propose a more efficient MAC for UCANs.

5.2.2.1 Dynamic bandwidth of control channel

Currently, most of existing cognitive MAC protocols allocate static bandwidth to control packets [17, 20, 80, 95, 96]. However, next I introduce a common event-driven sensor network, where the nodes need to smartly adjust the bandwidth of their control channel with a variation of network traffic.

Imaging a UAN with the bottom nodes, AUVs and surface nodes is deployed in oceans to detect the presence of interesting targets. If the nodes have not sensed any specific target yet, they stay in the sleep mode to save the energy. In this case, each node generates only a few packets periodically to update the routing table or to

synchronize time. Therefore, a narrow frequency band could meet the requirement of sending control messages with a low collision probability. In this case, the rest of vacant frequencies could be saved for a data transmission to reduce the end-to-end delay. The nodes become busy once a target enters the network, thereby creating a bursty traffic. In this situation, the nodes should extend the bandwidth of their control channel to prevent control messages from colliding with each other, otherwise the low delivery ratio of control packets would become the bottleneck of the network performance by affecting the transmission opportunity of data packets.

In order to achieve a good network performance in terms of throughput, end-to-end delay and energy efficiency, an underwater cognitive MAC should capable of adaptively adjusting the bandwidth assigned to the control channel and the data channel based on the real time traffic of a network. However, most of existing MAC protocols for CR or CA networks do not have this capability, which promotes us to design a new MAC for UCAN.

5.2.2.2 Hardware constraints

To solve the multi-channel hidden terminal problem [94] and the rendezvous problem [97] in a cognitive network, people usually assume that each node equips with a secondary transceiver or the time is synchronized across the network [80, 96, 98–100]. According to the survey [82], there are only a few protocols proposed for the non-synchronized, single transceiver cognitive networks.

Actually, neither an additional transceiver nor the time synchronization may be available in UANs. This is because most of communication systems in oceans are resource constrained in terms of bandwidth, size and energy as well as cost. Using the Teledyne Benthos ATM-903 modem [101] as an example, the size and the weight of its transducer are 14 cm $\times$ 10.1 cm (diameter $\times$ height) and 2.27 kg, respectively.

The space limitation makes it hard to carry two or more large size and high weight transducers on a single modem.

In addition, underwater acoustic nodes are usually powered by the battery, which cannot be recharged until they are retrieved. As I analyzed in Section 3.3, if we do the time synchronization in a UAN, the battery will run out after several days. Therefore, it may be impractical to assume that a UAN, which needs to monitor an interesting area several months or even longer, is time synchronization.

The above challenges promote us to propose a new MAC, which can work in the single-transceiver and non-synchronized UCANs reliably and efficiently.

5.2.3 Protocol description

In this section, I first introduce the assumptions that I make in the new cognitive protocol, and then I give an overview of DCC-MAC. After that, I introduce the spectrum sensing and the approach for adaptive bandwidth adjustment. Later on, I discuss the channel structure and the channel selection mechanism in DCC-MAC.

5.2.3.1 Assumptions

In DCC-MAC, I assume that the network is decentralized and non-synchronized. Each node equips with a single half-duplex transducer, which is capable of either transmitting or receiving, but not both at any given time.

Additionally, I assume that a licensed narrowband CCC is available. Nodes can use this channel to transmit some basic control messages. Later on, I will show that how DCC-MAC integrates the in-band channel with this CCC to dynamically adjust the frequency band of its control channel according to the current traffic loads.

Moreover, based upon the principle of reciprocity in the wireless channel [102], I suppose that for any sender-receiver pairs, the channel quality in the forward and

backward links are the same. Therefore, a sender and its intended receiver could send packets to each other with the same transmission rate.

Finally, I assume that a node could hear the entire operating frequency band simultaneously. This assumption is reasonable in underwater communications considering the narrow bandwidth (less than 100 kHz [15]) of an acoustic channel.

5.2.3.2 Protocol Overview

At the beginning of DCC-MAC, a node with a data packet will sense the channel usage of surrounding environment first. Thereafter, the sender initiates a channel negotiation process through transmitting an RTS message on control channel to its intended receiver. The RTS packet involves the ID of each vacant channel explored by the spectrum sensing.

If an RTS packet collides with any other control messages, the receiver broadcasts a control-packet-collision-notification (CPCN) to its neighbors after a random backoff, otherwise it detects whether the oncoming data will collide or not. If not, the receiver senses the channel and selects the one available for both the sender and the receiver. The ID of selected channel is sent out via a CTS packet. How to detect the collision among control packets, and how to choose the proper channel for a data transmission will be introduced in Section 5.2.3.4 and Section 5.2.3.6, respectively.

Once a sender got the CTS, it broadcasts the ID of its following communication channel through a repeat-clear-to-send (RCTS) message on the old control channel. After that, both the sender and its intended receiver turn to the newly selected channel for a data transmission. Finally, if the data is successfully decoded, the receiver sends out an ACK packet to the sender for a reliable transmission.

I introduce details of DCC-MAC in the following sections, but show a glimpse of its flowchart and state machine in Fig. 5.18 and Fig. 5.19, respectively.

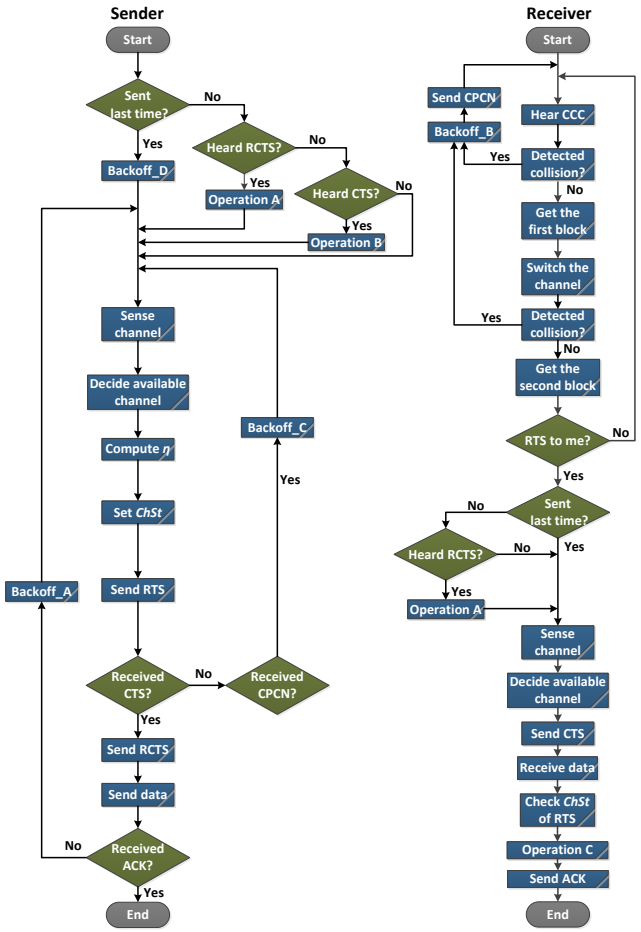

Figure 5.18: The flowchart of DCC-MAC. Operation A: Remove the selected channels involved in `SelCh` of RCTS from the available channels; Operation B: Remove the selected channels involved in `SelCh` of CTS from the available channels; Operation C: Select the channel to increase or decrease the bandwidth of the control channel according to the value if `ChSt` in the corresponding RTS packet.

5.2.3.3 Spectrum sensing in non-synchronized UANs

In a non-synchronized UCAN, when a node is sensing the spectrum, others may be transmitting on the same channel, which may interfere with the sensing process. Nodes in DCC-MAC are thus required to distinguish signals of PUs from that of CA nodes.

To achieve the above goal, we could use the signal feature based spectrum sensing algorithms [103], such as the second-order statistics and the cyclostationary detection methods. These algorithms classify the receiving signals by recognizing the inherent

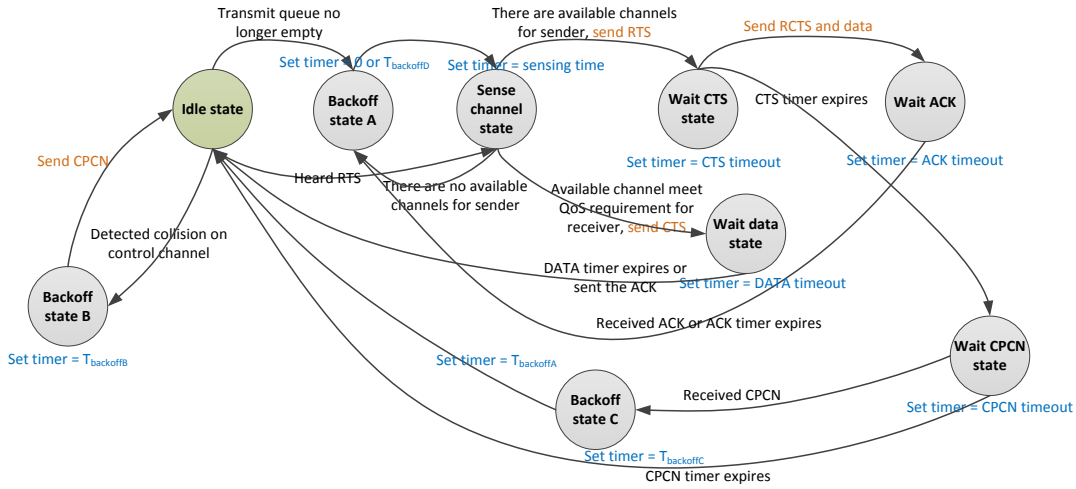

Figure 5.19: The state machine of DCC-MAC.

feature of a secondary signal, like the preamble sequence, the cyclic prefix and the cyclostationary frequency. In addition, the nodes in a cognitive network could embed a digital signature in their data packets to help the signal classification, the details of which could be found in [104].

5.2.3.4 Adaptive bandwidth adjustment

DCC-MAC could smartly adjust the bandwidth of control channel for each sender-receiver pair according to the current traffic loads on the control channel. To achieve this, once a node detected that its control channel is congested, it increases the bandwidth of its control channel by "borrowing" the frequency band from the in-band data channel. Conversely, if the node realizes that the bandwidth assigned to its control channel is excessive, it would "return" some frequencies to the data channel. Next, I introduce the two phases of DCC-MAC.

1) ***Realize the situation of control channel*** : Before adjusting the bandwidth, a node needs to first understand whether its control channel is congesting or not. This could be done by calculating the collision probability of the RTS packets.

More specifically, in DCC-MAC a receiver would miss an incoming RTS packet if (a) it is transmitting either a control message or a data packet, (b) the quality of an acoustic channel is poor, e.g., large noise, sever Doppler spreading and deep fading, or (c) the RTS message collides with a control packet from other nodes.

In the above three cases, the probability of case (a) and case (b) are mainly affected by the traffic generation rate of a network and the underwater environment, respectively, whereas the probability of case (c) is sensitive to the situation of the control channel. Therefore, a node could realize whether its control channel is congested to not by measuring the occurrence frequency of the case (c) in a certain period. To do this, when a receiver is successfully triggered by a specific signal fragment (preamble) on the control channel and enters the receive mode, but cannot decode the received signal correctly[5] , the receiver considers that a collision happen on its control channel.

Once a receiver detected a collision of control packets, it does a random backoff, and then broadcasts a short CPCN packet to report this event. Here the random backoff has two functions. First of all, it can avoid the CPCN packets from different nodes to collide at the sender side. Secondly, it could avoid CTS from the intended receiver to collide with the CPCN packets from other nodes. Now I use Fig. 5.20 as an example to introduce the details of these two functions.

- *Avoid collisions among CPCNs*: If S_1 and S_2 send their RTS messages simultaneously to initiate the handshakes, the two RTS packets will collide at R_c, N_1 and N_2. Each of them (R_c, N_1 and N_2) thus will broadcast a CPCN message to report this collision event. Adding a random backoff before CPCN transmission could avoid the collision of these CPCN messages at S_1 and S_2.
- *Avoid collisions between CPCN and CTS*: Assume the receiver R_c is replying a CTS to the sender S_1; meanwhile, S_3 is sending another control packet to R_3. In this

[5]In this situation, the SNR of the acoustic modem may be high, but the signal-to-interference-plus-noise ratio (SINR) is low, due to the collisions of the packets.

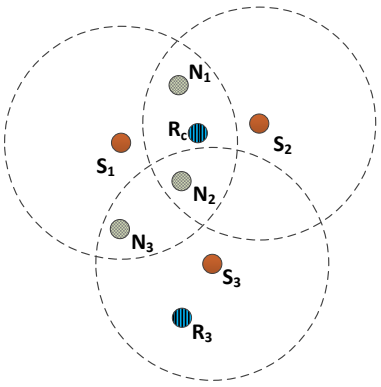

Figure 5.20: Example of the random backoff before transmitting CPCN to avoid the collisions, where R_c is a common receiver of senders S_1 and S_2; S_3 and R_3 is another sender-receiver pair.

case, N_2 and N_3 may detect a collision on the control channel. By doing a backoff before a CPCN transmission, we could guarantee that CTS arrives at S_1 earlier than CPCN packets from N_2 and N_3, which prevents CPCN from interrupting the reception of CTS at S_1.

2) ***Adjust the bandwidth of control channel***: Before transmitting RTS, a sender in DCC-MAC should decide whether the bandwidth of its control channel needs an adjustment through counting the number of CPCN packets it received from its intended receiver during the last several handshakes. Let η be the ratio between the number of RTS packets a sender sent out and that of CPCN packets it received from the intended receiver in the last several periods. According to the definition, η can indicate the situation (idle or congested) of the control channel.

Based upon the measurement of η, a sender sets the status bits of its control channel, which is denoted by `ChSt`, to different values, as shown in (5.22),

$$\texttt{ChSt} = \begin{cases} 00, & \eta \leq \eta_1, \\ 01, & \eta_1 < \eta \leq \eta_2, \\ 11, & \eta > \eta_2, \end{cases} \tag{5.22}$$

where η_1 and η_2 are two predefined thresholds. Here, `ChSt` = 00, 01 and 11 represents that the state of a control channel is congested, normal and idle, respectively. In each handshake, a sender attaches the value of its `ChSt` into the RTS packet, and transmits it to the receiver.

After each successful data reception, a receiver checks `ChSt` from the latest RTS packet it received from the sender. If `ChSt` = 00, the receiver will increase the bandwidth of its control channel by adding a vacant in-band one in the next round of communication. ID of the selected in-band channel is piggybacked on the ACK packet, and sent to the sender on the current control channel. If `ChSt` = 11, the receiver, on another hand, reduces the bandwidth by choosing an in-band channel that is using for the control message transmission, and removes it from control channel in the next round of communication. ID of the selected channel is also transmitted to the sender through ACK.

Let CH_{cur}, CH_{ack} and CH_{sen} be the current control channel, the channel included in ACK that will be either added or removed in the next round of communication and the vacant channel sensed before a new round of communication, respectively. Finally, the new control channel, which is denoted by CH_{new}, should be

$$CH_{new} = CH_{sen} \cap (CH_{cur} \pm CH_{ack}), \tag{5.23}$$

where $\cap$ is the intersection operator. Doing this operation could effectively prevent the transmission of control packets from interfering with a PU, if the PU changes its transmission frequency before the cognitive nodes staring a new round of communication.

It is worth noting that different sender-receiver pairs in DCC-MAC could have different control channels. For instance, assume the control channel between sender S_1 and receiver R_1 is CCC plus an in-band channel C_1, but for the same sender S_1, the control channel between it and another receiver R_2 could be CCC plus an in-band channel C_2. By selecting proper channel, DCC-MAC could improve the channel

utilization while reducing the collision probability among control packets, the details of which will be introduced in the next section.

5.2.3.5 Channel structure

As shown in Fig. 5.21, the acoustic channel in DCC-MAC consists of a single CCC and several in-band channels, where the former devotes to control packets, and the later could be used to send either the control message or the data packet whenever the PU does not occupy it.

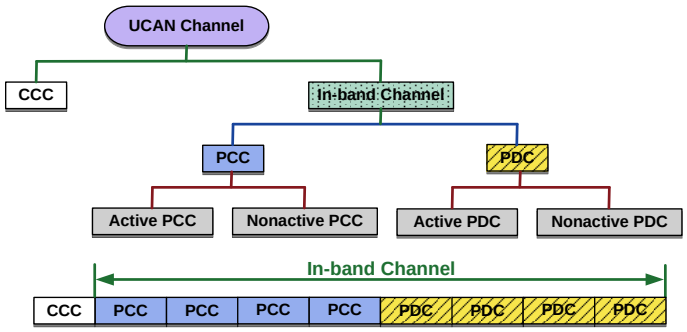

Figure 5.21: The channel structure of DCC-MAC.

Furthermore, the in-band channel is divided into the preassigned control channel (PCC) and the preassigned data channel (PDC). In PCC, a control packet has higher priority than a data packet to use the channel; in PDC, conversely, I reverse the priority of control packet and that of data packet for using the channel.

Finally, I identify each PCC and PDC as an active or a nonactive channel. More specifically, let PC_i represent the number of times the i^{th} PCC is selected to send control packets in the last N period of communications, where $PC_i \leq 0, 1, \ldots, N$. I mark the j^{th} PCC as an active one if $PC_j \geq 0.3 * \max\{PC_i\}$, where $i, j = 0, 1, \ldots, M$, and M is the amount of PCC. The definition of an active PDC is similar to PCC, and I do not repeat it again.

5.2.3.6 Channel selection

In DCC-MAC, a node may choose a in-band channel for a data transmission, increasing or decreasing the bandwidth of its control channel. Next, I introduce how to select a proper in-band channel to achieve these goals.

a) ***Send data***: For a data transmission, the receiver selects a channel from the vacant PDC with the highest average SNR first. If the selected channel cannot meet the requirement of QoS in terms of the transmission rate and outage probability, more channels are chosen from the idle PDC in descending order of SNR. If there is no vacant PDC, or the QoS still cannot reach the requirement after all available PDCs being selected, the receiver chooses additional channels with high SNR from the nonactive PCC. In order to avoid the collisions between data and control packets, a receiver should not choose the active PCC as the data channel, unless there is neither vacant PDC nor nonactive PCC available.

b) ***Extend control channel***: If a sender and its intended receiver plan to increase the bandwidth of their control channel for their next round of communication, the receiver selects a vacant PCC with the highest average SNR as an extension of the current control channel. If none of PCC is available, the node chooses the one from nonactive PCD with the highest average SNR. The receiver should not select an active PDC as the control channel to avoid the collisions between control packets and data packets, unless there is neither idle PCC nor nonactive PDC anymore.

c) ***Remove control channel***: If a sender and its intended receiver are going to release the bandwidth of their control channel, the receiver selects an active PDC with the lowest SNR from its current control channel, and then removes it. If there is no active PDC, the receiver removes the nonactive one with the lowest SNR. If the current control channel has neither active PDC nor nonactive one, the receiver removes a PCC with the lowest SNR.

Here, I highlight several essential points of the above rules for a channel selection. First of all, due to the high dynamic of acoustic channel [105], the instantaneous receiving SNR may not be available at the sender side, thereby, I use the average receiving SNR to select the channel, which is usually stable in a long period. A node can calculate the average receiving SNRs on a channel based on the historical values it measured from receiving or overhearing control packets and data packets[6] from its neighbors.

Secondly, when selecting the channel to send a data or to extend the bandwidth of control channel, a node sort the candidate channels in descending order of the average receiving SNR. Compared to a random selection strategy, this rule helps nodes to use the channel resource more effectively, while reducing the collision probability among data packets. More specifically, due to the spatial diversity [30], the quality of a channel is good on one node may bad on another. Therefore, if a node selects the channel according to its average receiving SNR on each channel, it has a small chance to compete with multiple neighbors for the same channel. Moreover, choosing a channel with the highest SNR first could get a fast improvement on the transmission rate.

Thirdly, when a receiver decreases the bandwidth of its control channel, it selects the one with the worst average receiving SNR first. There are three advantages of this strategy: (a) the receiver could save the bandwidth for other nodes without losing too much transmission rate of its control messages; (b) due to the spatial diversity of the channel, this strategy gives other nodes an opportunity to efficiently use the removed channel if they have higher receiving SNR on this channel than its current owner, and (c) the receiver can avoid to adjust the bandwidth of its control channel frequently. For the point (c), as described in equation (5.22) of Section 5.2.3.4, in order to maintain a stable bandwidth for the control channel, a node should make its `ChSt` stay at `01`. If the node adds an in-band channel with the highest receiving SNR when its control

[6] As a critical parameter in communication systems, the receiving SNR can be measured by most of the commercial acoustic modems directly without any modification on the hardware or the software [35, 101].

channel is congested, and removes a control channel with the lowest receiving SNR when the channel is idle, there is high probability that `ChSt` changes from `11` to `00`, and finally stays at `01`, since removing a channel with low receiving SNR does not effect the transmission rate of control message too much. Conversely, if a node removes a channel with the highest SNR first, the transmission rate of its control packets may decrease sharply. In this case, it is most likely that `ChSt` switches between `11` and `00`, but jumps the stable status `01`.

5.2.4 Control channel rendezvous

As we know, in a handshake based MAC protocol, nodes avoid the hidden terminal and the exposed terminal problem by overhearing the control packets from their neighbors. In DCC-MAC, however, the control packets are sent on multiple different channels. A node may not be able to overhear a control packet correctly if it does not switch to a right channel. This is a unique problem in DCC-MAC, which we call it as the *control channel rendezvous problem*.

Different from the classic data channel rendezvous problem, which could be tackled by exchanging the ID of a selected data channel between a sender and a receiver through the control packets, in DCC-MAC I cannot introduce a new group of control packets to address the rendezvous problem on the current ones. This will make the problem loop infinitely. Next, I introduce a simple solution for this problem, which just needs to reorganize the structure of the control packets without generating any extra overhead traffic into the network.

In DCC-MAC, I divide each control packet (RTS, CTS, CPCN and ACK) into two continuous blocks. The first block is always sent on CCC, which includes only the channel ID of the second block. The second block carries the rest of control information, such as type of the packet, sender ID and receiver ID.

With the above data structure, each node could use the first block for the control channel rendezvous. More preciously, when a node receives or overhears the first block of a control packet, it switches its receive channel to the correct ones based upon the channel ID involved in the first block for a reception of the second block.

There are two advantages of this structure. First of all, a node needs to send only several bytes (channel ID of the second block) on the CCC for control channel rendezvous, which considerably reduces the traffic load on CCC. Moreover, the second block of each control packet could share the preamble sequence with the first block, which is helpful to save the energy and to reduce the transmission time of a control message.

5.2.5 Control packet structure

Here, I introduce the detailed data structure of control packet in DCC-MAC. Assume there are a total number of N_c in-band channels. The first block of all control packets is the channel ID of their second block, which is denoted by `ChID` with N_c status bits (one bit for each channel). The status bit is set to 1 if the second block is transmitted on the corresponding channel, otherwise set to 0.

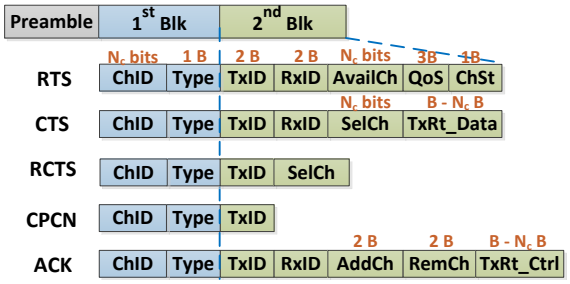

Figure 5.22: Data structure of the control packets, where the red word indicates the size of each section.

As shown Fig. 5.22, the second block of different control packets consists of a subsets of the following sections: (a) sender ID (`TxID`), (b) receiver ID (`RxID`), (c) packet type

(`Type`), (d) vacant channels at the sender side (`AvailCh`) with N_c status bits, which is set to 1 if the corresponding channel is idle, (e) QoS requirements (`QoS`), which includes the required transmission rate and the outage probability of an application, (f) the control channel status `ChSt`, which has been introduced in Section 5.2.3.4, (g) ID of the selected channels for the following data transmission (`SelCh`), which is set to 1 if the corresponding channel is chosen, (h) the transmission rate of data packet on each selected channel (`TxRt_Data`), using 1 byte to indicate the rate on each selected channel, therefore the size of `TxRt_Data` is between 1 and N_c bytes, (i) ID of the selected in-band channel to increase/decrease the bandwidth of control channel (`AddCh`/`RemCh`) for the next round of communication, and (j) the transmission rate of control packet on each selected channel (`TxRt_Ctrl`), using 1 byte to indicate the rate on each selected channel, the size of `TxRt_Ctrl` thus is between 1 and N_c bytes.

5.2.6 Collision avoidance in multi-channel environment

DCC-MAC could reduce collisions caused by the multi-channel hidden terminal problem significantly. It requires neither time synchronization amongst a network nor addition hardwares (secondary transceiver or tune devices) on an acoustic node, which are usually assumed in the most of collision-free cognitive protocols [82]. In addition, compared to the cognitive MAC protocols, which produce many additional control packets for collision detection [106] and multi-channel rendezvous [20], DCC-MAC is a light weight protocol. Next, I introduce the details of the proposed collision avoidance mechanism.

As I discussed at the end of Section. 5.2.3.1, a node in a UCAN could hear its entire operating frequencies (in-band channels plus the CCC). In DCC-MAC, if a node receives the first block of a control packet successfully, based upon the information decoded from this block, it could switch to the correct channel to get the remaining

control messages in the second block, while not stopping the data reception on the current channel. In this way, the node will not miss the control packet from its neighbors when receiving a data packet on other channels.

When designing the strategy to handle the multi-channel hidden terminal problem, I consider a total number of eighteen scenarios carefully. As shown in Fig. 5.23, in each subfigure there are two sender-receiver pairs. I assume that node A is sending data packet to node B on channel C_1. Meanwhile, S_1 and R_1 are handshaking on their control channel, and then reserve channel C_2 for their data transmission. Hence, A and B may miss the control packets from S_1 and R_1, which potentially results in a collision if node A (node B) initiates a new communication with node B (node A), and end up selecting C_2 for their communication.

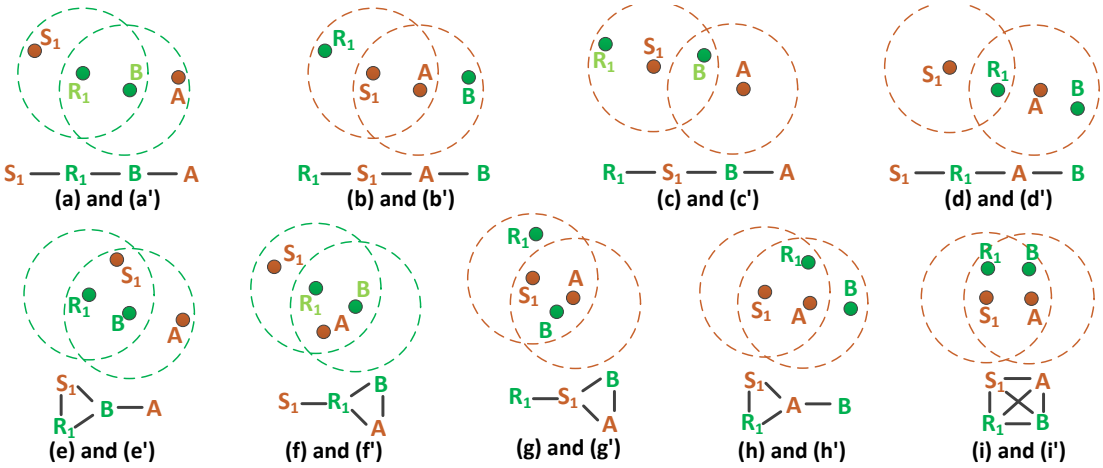

Figure 5.23: Scenarios for collision analysis, where node A and B initiate a new communication in (a) – (i) and (a)′ – (i)′, respectively.

To avoid the collisions among data packets, a node does one of the following four processes depending on what kind of control packet it overheard and what is the role (sender or receiver) it will play in the next round of communication.

- *Process A*: Node B overheard only RTS_1 and RCTS_1 from node S_1 when it was receiving a data packet. No matter B will still work as a receiver (c and g in

Fig. 5.23) or change its role to a sender (c′ and g′ in Fig. 5.23) in the next round of communication, it will not select the channel with `SelCh` = 1 in RCTS_1 for its next round of data reception or transmission.

- *Process B*: Node B overheard only CTS_1 from node R_1 when it was receiving a data packet. If B will still work as a receiver in the next round of communication (a and f in Fig. 5.23), B ignores CTS_1, and the potential collisions between node A and R_1 in the scenario f′ of the Fig. 5.23 could be eliminated via the Process D, which will be introduced later. If B plans to change its role to a sender (a′ and f′ in Fig. 5.23), it will not select the channel with `SelCh` = 1 in CTS_1 for its next round of data transmission.

- *Process C*: Node B overheard RTS_1, RCTS_1 and CTS_1 from node R_1 when it was receiving a data packet. No matter B will still work as a receiver (e and i in Fig. 5.23) or change its role to a sender (e′ and i′ in Fig. 5.23) in the next round of communication, it will not select the channel with `SelCh` = 1 in CTS_1 or RCTS_1 for its next round of data reception or transmission.

- *Process D*: Due to the half-duplex feature of the modem, node A could not overhead the packet when it is transmitting. In the next round of communication, if A will still work as a sender (b, d and h in Fig. 5.23), it will do a backoff after completing the current data transmission. If A is going to change its role to a receiver (b′, d′ and h′ in Fig. 5.23), the collision may happen in the scenarios b′ and h′ of Fig. 5.23, details of which are shown in Fig. 5.24 (a).

With these four processes, except scenarios b′ and h′, there are no collisions among data packets in the other sixteen scenarios of Fig. 5.23.

As described in Process D, a backoff between two continuous data transmissions is required to prevent data packets from colliding in the scenarios d and h of Fig. 5.23. Here, I calculate the length of this backoff in DCC-MAC. Fig. 5.24 (b) shows the worst

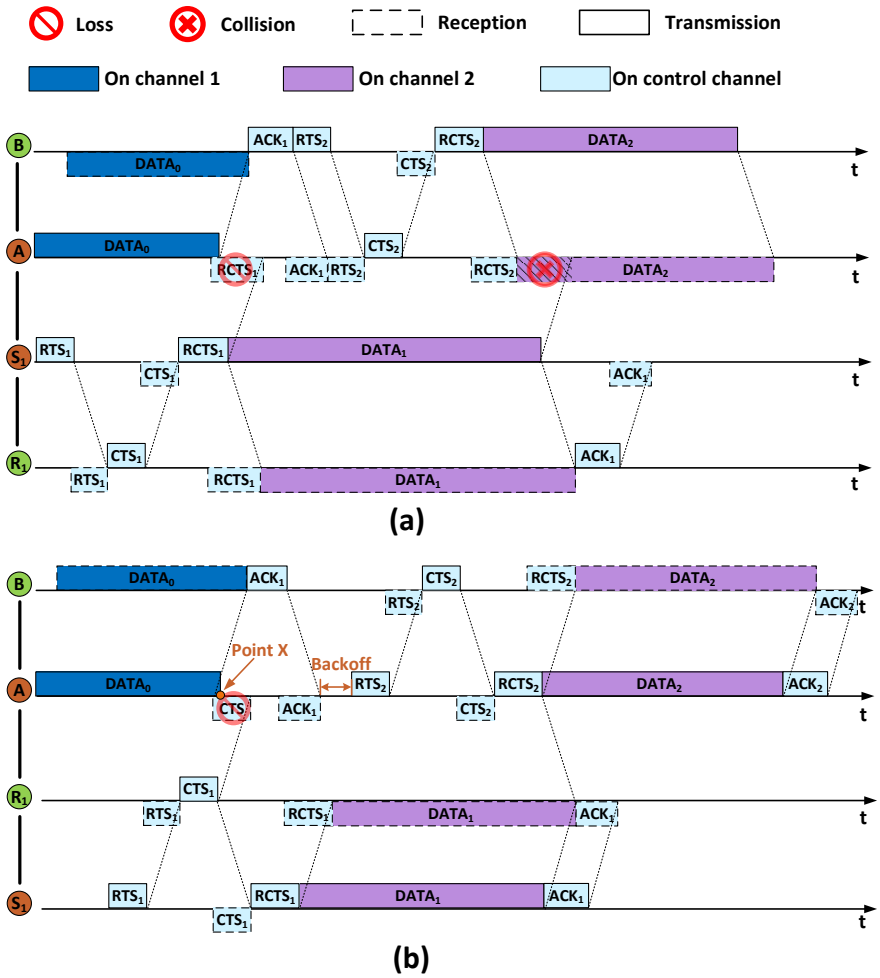

Figure 5.24: (a) Collisions in scenarios b′ of Fig. 5.23, (b) Collision avoidance in scenarios d of Fig. 5.23 with the backoff mechanism.

case, where CTS_1 from R_1 arrives at node A when it is transmitting the last several bits of its data packet DATA_0, and node A misses CTS_1. If A will still work as a sender and finally chooses the same channel with S_1 to send its data DATA_1, in order to avoid the collisions between DATA_1 and DATA_2 at node R_1, A should do a backoff after receiving ACK_1.

Denote the transmission time of RTS, CTS, RCTS, ACK and DATA packets as t_{RTS}, t_{CTS}, t_{RCTS}, t_{ACK} and t_{DATA}, respectively. Let τ_{AB}, τ_{AR} and τ_{RS} be the propagation delays between nodes A and B, A and R_1, and R_1 and S_1, respectively.

Then it is easy to calculate the length of the backoff, which is denoted by t_{BO}, from Fig. 5.24 (b) that

$$t_{BO}=t_{DATA}-t_{RTS}-t_{ACK}+2\tau_{RS}-2\tau_{AR}-4\tau_{AB}. \tag{5.24}$$

Since the distance between nodes B and R_1 in scenarios d and h of Fig. 5.23 is two hops, it must be larger than the one hop distance from S_1 to R_1. Therefore, we have $\tau_{BR} > \tau_{RS}$, where τ_{BR} is the propagation delay between B and R_1. Now, let nodes A, B and R_1 be the three vertexes of a triangle. According to the triangle inequality principle that the sum of the lengths of any two sides of a triangle always exceeds the length of the third side, we have $\tau_{BR}<\tau_{AR}+\tau_{AB}$. Therefore, t_{BO} in (5.24) would be

$$\begin{aligned} t_{BO}&=t_{DATA}-t_{RTS}-t_{ACK}+2\tau_{RS}-2(\tau_{AR}+\tau_{AB})-2\tau_{AB} \\ &<t_{DATA}-t_{RTS}-t_{ACK}-2\tau_{AB}. \end{aligned} \tag{5.25}$$

In the worst case, where $\tau_{AB}\approx 0$, to avoid the collision between DATA_1 and DATA_2 at node R_1, we should set the minimal backoff as

$$t_{BO(\min)} = t_{DATA} - t_{RTS} - t_{ACK}. \tag{5.26}$$

5.2.7 Simulations and analysis

In this section, I conduct simulations on Aqua-Sim to evaluate the performance of DCC-MAC. Simulation results verify the effectiveness of dynamic control bandwidth adjustment on reducing the collision probability among control packets.

To well assess DCC-MAC, I also compare it with two representative cognitive MAC protocols, RISM and MMAC-CR, proposed in recent years. The mechanism of two protocols have been introduced in Section 5.1 and Section 5.1.1

In the simulation, we have 20 underwater sensors deployed as shown in Fig. 5.25. The nodes form two network topologies with different traffic flow. In the Mesh topology, 16 nodes generate and deliver data to a random destination at four corners (N_{10}, N_{11},

N_{13} and N_{18}). The mesh topology network is a general example for underwater ad hoc networks. The tree network represents a data collection system where 20 sub-sea nodes collecting and forwarding data to the sink node, N_0.

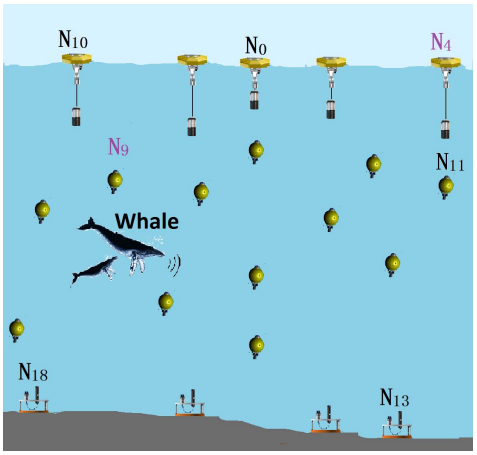

Figure 5.25: Network deployment in simulations. In Mesh topology, 16 underwater sensors select a random destination at four corners (N_{10}, N_{11}, N_{13} and N_{18}) as the final destination. In Tree topology, 20 nodes deliver their data to node N_0.

In the deployment, the average distance among neighboring nodes is 1 km (uniformly distributed between 800 m to 1200 m). I set the maximum transmission range and the maximum transmission power of each node as 1.5 km and 10 W, respectively. The overall communication bandwidth is 16 kHz (from 17 to 33 kHz), which is evenly divided into 32 subchannals. I assign the lowest 500 Hz (17 to 17.5 kHz) to be the CCC in DCC-MAC and assume it is not occupied by any PUs in the area. The remaining 31 subchannels are used as the in-band channel. In the network, I also deploy two PUs. Each of them randomly selects one amongst 31 in-band channels for its communication, and switches its communication channel every 100 secs. In the test, each sender generates data packets of size 250 B following Poisson process. The length of preamble sequence in the acoustic modem is 0.2 secs. The size of each control packet is set as presented in Fig. 5.22.

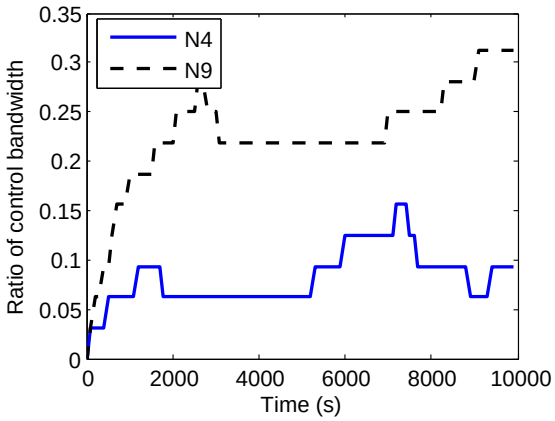

Figure 5.26: A snapshot of dynamic bandwidth adjustment on control channel.

I first evaluate the effectiveness of the dynamic control bandwidth adjustment in DCC-MAC. Fig. 5.26 presents a snapshot of the varying control bandwidth on nodes N_4 and N_9 in the Mesh network. The positions of N_4 and N_9 are marked in Fig. 5.25. Although both nodes have the same data generation rate on the application layer, they get different traffic loads on the MAC layer due to the data forwarding in the multi-hop network. Besides the self-generated data, N_9 also help relaying data for neighbors to the destination, N_{10}. On the contrary, N_4 has few data forwarding request and resulting in light traffic load. As a result of different traffic loads on two nodes, the bandwidth of their control channel is apparently different. When the network was stable, N_4 used about 8 kHz as control channel and N_9 only occupied roughly 3 kHz for control communication. The spatially and temporally varying bandwidth of control channel validates the effectiveness of the control adjustment scheme in DCC-MAC.

As a result of efficient bandwidth adjustment mechanism on control channel, DCC-MAC outperforms RISM and MMAC-CR in terms of high handshake success rate, as shown in Fig. 5.27. The handshake success rate is calculated by the number of transmitted CTS / ORDER / ATIM_ACK dividing the number of RTS / RTR / ATIM sent out, in DCC-MAC, RISM and MMAC-CR. From this figure we observe that (a) the competition success rate of DCC-MAC is much higher than MMAC-CR and RISM

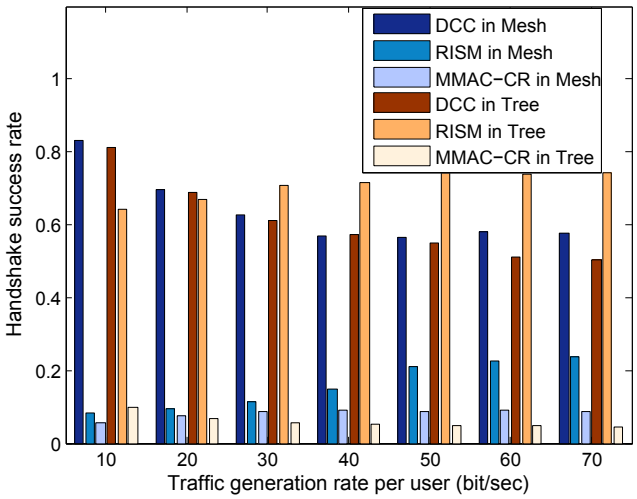

Figure 5.27: Comparison of success rate of negotiation.

in a mesh topology, and (b) the successful competition rate of RISM increases with a growth of traffic generation rate, but it is sensitive to the network topology.

By smartly adjusting the bandwidth when control channel is congested, the collisions among control packet can be reduced significantly. This also explains the comparable performance of DCC-MAC in Mesh and Tree networks, although they have extremely different traffic patterns. The traffic in Mesh topology is scattered across the network, whereas the data packets tend to gather in Tree network. No matter the traffic pattern varies in two networks, the control bandwidth in DCC-MAC can adaptively adjust according to the traffic loads. In contrast, RISM has very low handshake success rate in Mesh network but high success rate in Tree topology. In Mesh networks, the inefficient data polling mechanism is the main cause of failed handshake in the receiver-initiated MAC protocols. In Tree network, however, the gathering traffic flow can considerably increase the polling success rate and, meanwhile, reduce the control overhead in RISM, resulting in high handshake success rate. MMAC-CR has the lowest competition success rate in both topologies due to the heavy congestion on the CCC of 3.4 kHz.

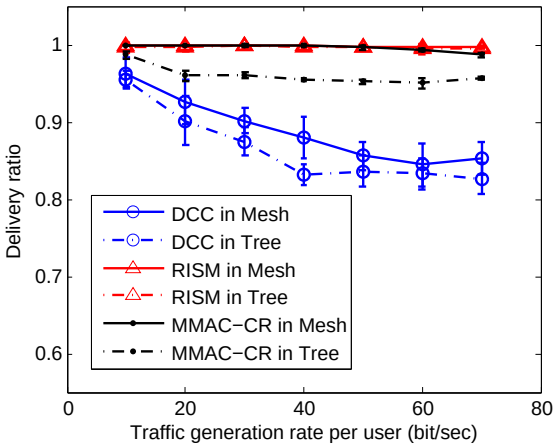

Figure 5.28: Comparison of data delivery ratio.

In Fig. 5.28, I compare the delivery ratio of data packet, which is defined as the ratio of the number of data packets successfully received by receivers. I observer that DCC-MAC has higher data collisions than RISM and MMAC-CR, especially in a Tree network. This is a penalty of dynamic control channel scheme in DCC-MAC. The data collision can not be avoided completely, as I discussed in Section 5.2.6, even though the random backoff mechanism is designed. Note that in a tree topology the data flow is gradually aggregated to the upper nodes in the network. Hence, the traffic load of a node near the destination (node N_0) may be much higher than the traffic generation rate. In this situation, data packets will have higher probability to collide with each other if a MAC protocol is not designed for a collision free data transmission. RISM has the highest delivery ratio as receiver-initiated MAC naturally has better data collision capability than conventional sender-initiated DCC-MAC and MMAC-CR. MMAC-CR has higher delivery ratio than DCC-MAC owing to its two phase design. Only nodes assigned with the same channel compete for channel access in the data phase of MMAC-CR, resulting in lighter collision probability. In Tree topology, however, the data are gathered and network becomes "crowd", which leads to lower delivery ratio for MMAC-CR.

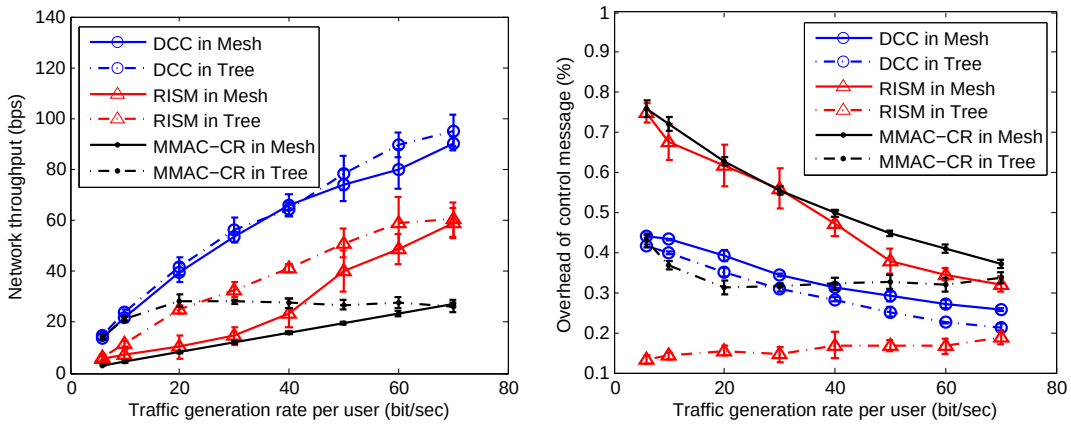

(a) Network throughput (b) Overhead

Figure 5.29: Performance comparison for Poisson traffic in mesh and tree topologies.

Fig. 5.29 demonstrates the network performance of the three protocols in terms throughput and energy efficiency. From this figure we observe that DCC-MAC outperforms the other two protocols in almost all aspects. In addition, compared with RISM and MMAC-CR, the performance of DCC-MAC is resilient to the topology of the network.

More specifically, as shown in Fig. 5.29(a), DCC-MAC achieves the highest throughput benefiting from its smart bandwidth adjustment mechanism on control channel. The dynamic control channel allows DCC-MAC to achieve more efficient spectrum utilization. In addition, by reducing the collision probability of control messages, the congestion on CCC is not the bottleneck of DCC-MAC to achieve high throughput anymore. By contrast, MMAC-CR has the lowest throughput mainly due to the high collisions on the CCC, which is also revealed in Fig. 5.27. Although RISM has comparable or even higher handshake success rate than DCC-MAC in Tree network, the lower spectrum efficiency leads to a lower throughput. In addition, among three protocols, DCC-MAC is the only protocol which has comparable network throughput in Mesh and Tree topologies. As most MAC protocols are sensitive to the network topology

and traffic load, the feature of DCC-MAC on resilient to different network situation make DCC-MAC a practical solution in various underwater applications.

Fig. 5.29(b) compares the overhead, which is defined as the ratio of the energy consumed on transmitting control messages over the total energy consumption (on control plus data packets), of different protocols. This figure reveals that DCC-MAC has the lowest overhead in a Mesh network benefiting from the lowest collision probability on control channel. RISM and MMAC-CR have the highest overhead in Mesh topology for different reasons. Because of the scattering traffic in Mesh network, the receivers fails to poll neighboring senders frequently when there are few data to cumulated. In MMAC-CR, the heavy collisions on CCC is the main cause of the high overhead. This result is consistent with the handshake success rate illustrated in Fig. 5.27. The energy efficiency of DCC-MAC in Tree topology is comparable with in Mesh network, which is a result of adaptive control bandwidth adjustment to the network traffic load. However, RISM and MMAC-CR are sensitive to the topology of a network. The aggregated traffic in Tree network significantly improves the polling success rate in RISM, and leads to the lowest overhead in data gathering network. Although MMAC-CR has higher collisions on control channel in Tree than in Mesh topology, the packet train in data transmission improves the average energy efficiency.

5.2.8 Summary

In this chapter I first introduced a new spectrum management system, RISM, to achieve environment-friendly and spectrum-efficient communications for UCANs. Then, I propose a new MAC, DCC-MAC, to solve the congestion problem on CCC of cognitive networks.

In RISM, the receiver initiates each round of handshake process. This strategy allows receiver in each round of handshake to request packets from multiple senders in

parallel. In addition, in RISM, the three components, i.e., the cooperative spectrum sensing, spectrum sharing and spectrum decision, do not generate control messages separately as independent pieces. Instead, they share control packets with each other without incurring additional control overhead, which significantly improves the negotiation efficiency considering the high latency in UCANs and the long preamble in acoustic modems.

However, there is a unique challenge in receiver-initiated approaches for receivers to decide when to poll without prior knowledge of the data cumulation on senders. This issue is tackled by adopting the traffic predictor. A receiver in RISMs could smartly poll senders adapting to the variation of senders' traffic loads. By employing the smart polling scheme, the receiver could initiate handshakes timely to reduce the packet queuing delay while constraining the energy consumption on transmitting control packets.

Simulation results show that the performance of RISM with smart polling scheme outperforms MMAC-CR, a representative CR based MAC protocol. Specifically, the throughput of RISM is 6× higher than MMAC-CR, while the hop-by-hop delay and overhead of control packet is only 0.25× and 0.3× of MMAC-CR. Moreover, RISM could work better in a tree network than in a mesh network. The throughput in the former scenario is nearly 2× than that in the later one, while maintaining comparable hop-by-hop delay and overhead of control packet.

I believe that RISM is a promising system that enables cognitive technique to work efficiently and environment-friendly in UANs. In next section, I will discuss how to mitigate the congestion problem on the CCC of a distributed cognitive network.

To tackle the congestion problem on CCC of UCANs, I proposed DCC-MAC. One of the most important features of DCC-MAC is that each node could smartly adjust the bandwidth of its control channel by adding frequency band from the in-band channel

when the traffic is heavy, and returning them back when the control channel becomes underutilized. The simulation results demonstrated that DCC-MAC could efficiently eliminate the congestion problem of CCC for a cognitive network. In a high traffic generation rate scenario, DCC-MAC provides a $\times 1.5$ and $\times 4$ higher throughput than RISM and MMAC-CR, respectively, while maintaining a comparable or even lower overhead. In addition, the performance of DCC-MAC is not sensitive to the topology of a network. Therefore, it could work in different underwater applications reliably.

Chapter 6

Underwater COD-COM

The goal of COD-COM is to coordinate the activities (sending and receiving) of each node for the purpose of improving the channel utilization and energy efficiency of underwater uplink communication networks. To achieve this goal, in this chapter I introduce a new protocol, called CT-MAC for underwater uplink networks. The content in this chapter is mainly based on my previous work published in [24][1] .

6.1 Network architecture

Here, we consider an underwater uplink communication network, in which a surface buoy or a sink node works as a common receiver to collect data from a group of underwater static nodes, as shown in Fig. 6.1. Such networks are usually used for the offshore instrument (e.g. wind farm and oil pipeline) health monitoring, underwater data collection and target detection [107]. I assume that each node transmits with the OFDM modulation scheme, which has the ability to cope with severe frequency-selective fading due to multipath in underwater channel [65, 108].

[1] Reprinted from Ad Hoc Networks, Vol. 34, Yu Luo, etc., An efficient MAC protocol for underwater multi-user uplink communication networks, Pages 75 – 91, Copyright (2015), with permission from Elsevier

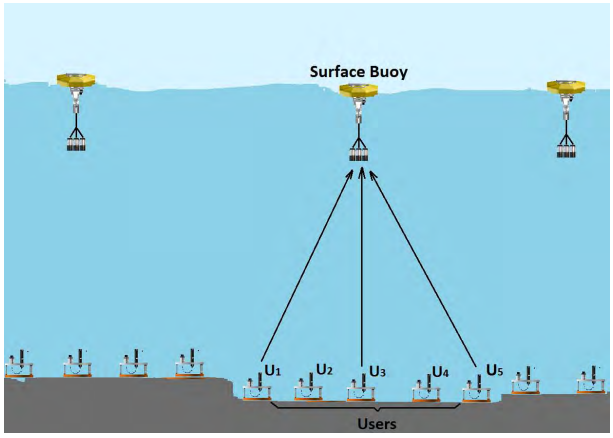

Figure 6.1: An underwater multi-node uplink communication network, where the surface buoy works as the receiver to collect the data from the bottom nodes u_1 to u_5.

Due to the size limitation and the high costs associated with underwater instruments, I suppose that each bottom node in UANs equips with a single transducer. I further assume that the receiver has multiple hydrophones for data reception, since the size of a surface buoy is usually much larger than an underwater node. Now denote the number of hydrophones on the buoy and the amount of underwater nodes in the coverage of the buoy as M_r and L, respectively. Let K represent the maximum number of decodable packets in simultaneous receptions at the receiver, where $K \leq L$.

We start from a general case of multi-node uplink networks first, where each node can have N transducers with $N \geq 1$. Denote the circularly symmetric complex Gaussian noise at hydrophone i of the receiver as $\mathbf{n}_i \in \mathbb{C}^{M_r \times 1}$, where $\mathbf{n}_i \sim N(0, \mathbf{I})$ and let $\mathbf{H}_i^{\dagger} \in \mathbb{C}^{M_r \times N}$ be the channel matrix of node i. By using the successive decoding scheme [109] in the multiple-input and multiple-output (MIMO) uplink communications, the sum-rate capacity of the channel with transmission power constraints $\mathbf{P} = (P_1, \ldots, P_K)$ is given as [110]

$$\mathcal{C}_{uplink}(\mathbf{H}_1, \ldots, \mathbf{H}_K, \mathbf{P}) = \max_{\mathrm{Tr}(\mathbf{Q}_i) \leq P_i, \forall i} \log \left| \mathbf{I} + \sum_{i=1}^{K} \mathbf{H}_i^{\dagger} \mathbf{Q}_i \mathbf{H}_i \right|, \tag{6.1}$$

where each of the matrices $\mathbf{Q}_i$ is an $N \times N$ positive semidefinite covariance matrix. After the derivation, the sum-rate of the successive decoding in (6.1) can be written

as [111]:

$$\mathcal{C}_{uplink}(\mathbf{H}_1,\ldots,\mathbf{H}_K,\mathbf{P}) \leq \min(M_r,K)\,\mathcal{C}_{TDMA}(\mathbf{H}_1,\ldots,\mathbf{H}_K,\mathbf{P}), \tag{6.2}$$

where

$$\mathcal{C}_{TDMA}(\mathbf{H}_1,\ldots,\mathbf{H}_K,\mathbf{P}) \geq \log\left(1+\sum_{i=1}^{K} P_i||\mathbf{H}_i||^2\right), \tag{6.3}$$

is the maximum average rate that can be achieved by time division scheme between single-node transmissions with constant power P_i.

From (6.2) and (6.3) we have that when $N=1$, in order to maximize the sum-rate capacity of an underwater multi-node uplink network, the number of packets simultaneously arrived at the receiver should be equal to the amount of hydrophones, i.e., $K = M_r$. Here I call $K < M_r$ and $K > M_r$ as the *starving reception* and the *supersaturated reception*, respectively, both of which may degrade the throughput and the energy efficiency of a network.

6.2 Motivation

In conventional multi-node uplink MAC protocols, people usually use either the handshake or the feedback mechanism to avoid the starving and the supersaturated receptions [25, 26]. In channel aware Aloha [25], the receiver sends a feedback message after each successful data reception to provide CSI for senders. Only the nodes with good channel qualities are allowed to send their data. By retarding the transmission of nodes with poor channel qualities, this scheme achieves good energy efficiency. In multi-antenna reception MAC [26], the sender and the receiver use two-way handshake to reserve the channel. Once a receiver gets a sending request, it will broadcast a receive capability broadcast (RCBC) packet to inform the surrounding nodes the remaining number of senders it can support to transmit at the same time. Nodes stop sending requests if no more senders can be supported by the receiver.

Although aforementioned MAC protocols work well in terrestrial multi-node uplink networks, they still need an overhaul to operate efficiently in UANs due to the following reasons.

(a) ***Collisions among control packets***: When taking into account the preamble signal, the lengths of control packets in UANs is usually more than half a second [16], three orders of magnitude longer than that in terrestrial networks. Therefore, collisions among control packets in the handshake process become non-negligible. Especially in a high traffic load scenario, the high collision probability among control packets may significantly degrade the network performance in terms of throughput and energy efficiency.

(b) ***Lack of instantaneous CSI***: In multi-node uplink communications, the instantaneous CSI (e.g., the multipath response, channel gain and receiving SNR) is commonly used for adaptive transmission to optimize the communication performance [112, 113]. However, in oceans the instantaneous CSI may not be available due to the long packet transmission time, large propagation delay and high dynamic of acoustic channel [**?**, 114]. With these three features, there could be a large divergence between the estimated channel state at the transmitter side and the actual one when a packet arrives at the receiver.

(c) ***Unexpected reception***: In a terrestrial multi-node uplink network, packets sent in the same slot can arrive at the receiver simultaneously in light of the ignorable propagation delays. However, in underwater networks due to the low propagation speed of the acoustic signal, packets sent by different nodes simultaneously may arriver at the receiver at different time, and vice versa. Thus the number of packets received by the receiver may be different from the number of active senders. An example is shown in Fig. 6.2. Assume the surface buoy can decode at most three overlapped packets. The distances from the surface buoy to sender u_1, u_2, u_4 and u_5 are 1500, 1500, 750 and

750 m, respectively. The duration of each data packet is 0.5 secs. If the senders u_2 and u_4 are arranged to send data after the transmission of u_1 and u_5, there are only two active senders at each time slot. In radio networks with negligible propagation delays, there are only two packets received by the receiver in each time slot. However, since senders u_1 and u_5 to the surface buoy have 0.5 secs longer propagation delay than u_2 and u_4 in water, all packets from the four nodes arrive at the receiver at the same time, causing a supersaturated reception. I call it as the unexpected reception problem, which potentially degrades the throughput and the energy efficiency of underwater networks.

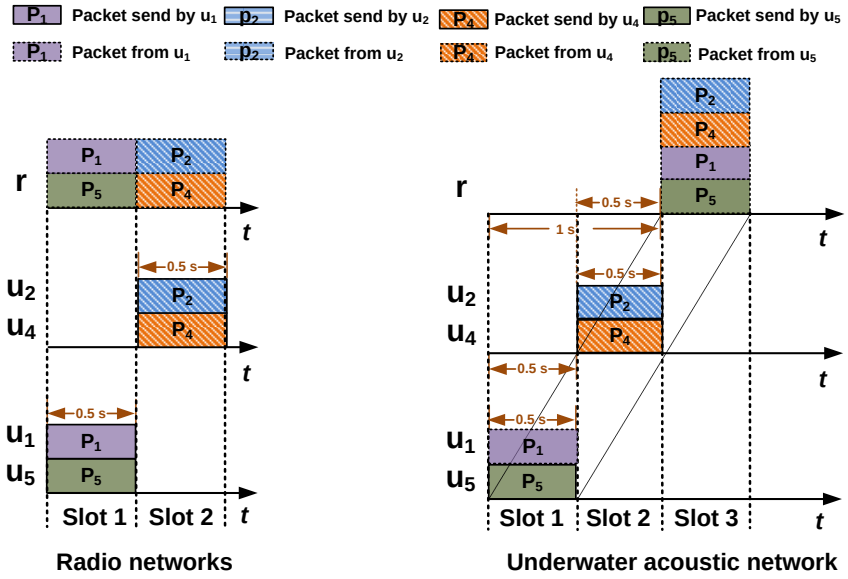

Figure 6.2: Unexpected reception problem in underwater multi-node uplink communication networks, where r is the surface buoy and u_i is the node i in Fig. 6.1.

(d) ***Low propagation speed***: The sound speed in water is only about 1500 m/sec, five orders of magnitude lower than the electromagnetic wave in air. The low acoustic speed may cause the following problems to conventional multi-node uplink MAC protocols.

- *Low channel utilization:* In a handshake or feedback based multi-node uplink MAC, the time spend on waiting for the control packets is considerable because of the low

propagation speed of acoustic signal. This greatly reduces the channel utilization of these protocols.

- *Fairness issue:* In an underwater multi-node uplink network, the difference of propagation delays between the receiver and different senders cannot be ignored anymore. If we use protocols proposed for the terrestrial network, like [25] and [26] in oceans, a node further from the receiver needs to wait a longer time to get a response (handshake or feedback message) than the closer one. In this case, the transmission opportunities for different nodes are heterogeneous, which leads to a fairness problem.

The aforementioned problems motivate us to propose a new MAC protocol for underwater multi-node uplink networks with fair data transmissions, high channel utilization, small end-to-end delay and low energy consumption.

6.3 CT-MAC protocol

In CT-MAC, I suppose that the network is time synchronized[2] , which can be done by using the approach proposed in [71] at the initial stage of a network. In this section, I first introduce how CT-MAC works in one-dimensional uplink networks. Then I extend the protocol to the two-dimensional scenario.

6.3.1 One-dimensional uplink networks

A typical one-dimensional network is a string topology network, where acoustic nodes are deployed in a line, as shown in Fig. 6.1. This topology is widely envisioned in the oil pipeline monitoring and coastline protection systems.

[2]The overhead of time synchronization in UANs is much higher than that in radio networks. However, the collision free data transmission and the high channel utilization of CT-MAC could compensate for the additional overhead on running a time synchronization protocol.

In CT-MAC, the time is divided into slots with equal length. Each time slot consists of a competition cycle and a data transmission cycle.

6.3.1.1 Competition cycle

In the competition cycle, each node performs the following three tasks:

(a) Generate a random value[3] as a priority level (PL) to compete for a sending opportunity. If a node does not have any packet to send, it sets its PL as zero.

(b) Deliver the PLs to its direct neighbors instead of broadcasting to the whole network to reduce the energy consumption.

(c) If a node has received PLs from its neighbors in previous competition cycles, it works as a helper to relay these PLs in the current competition cycle.

In a certain competition cycle, if all nodes know the PLs of all others, they can decide to send their data or not independently in the following data transmission cycle by comparing the value of corresponding PLs. It is easy to have that with the multihop transmission, a PL requires at most $L-1$ time slots to propagate to the whole network, where L is the number of nodes in a string network.

In conventional MAC protocols, the competition is processed in a serial fashion, where a new round of competition will not start until the old one is completed. A typical example is the handshake based MAC, in which a node sends an RTS packet to its intended receiver and waits for the response, e.g. a CTS packet. During the waiting time, even if this node generates a new data packet to the same receiver, it could not initiate a new round of competition until the previous handshake process is ended.

If we use the serial competition scheme in CT-MAC, the channel utilization will be very low, since each competition needs $L-1$ time slots for PLs propagating to the whole network. Therefore, I propose a *parallel competition scheme* for my protocol.

[3]More advanced competition schemes for fair transmissions will be introduced in Section 6.4.

In this scheme, the competition is continuous. Even if the PLs produced by a node in previous time slots have not yet reached the whole network, new PLs will still be generated and sent in each competition cycle.

More specifically, let CC_i and TC_i denote the competition cycle and the data transmission cycle of the i^{th} time slot, respectively. $PL_{i,j}$ represents the PL generated by node j in CC_i. In Fig. 6.3, I use three nodes as an example to show the details of PL propagation in my parallel competitions. In CC_1, the PL produced by each node in the first time slot is only known by the most direct neighbors. Starting from CC_2, nodes in the network not only generate and transmit new PLs in the current competition cycle, but also help relay old PLs which they received in the previous competition cycle to their neighbors. It is easy to observe that in CC_2, all PLs produced in CC_1 are available to all nodes.

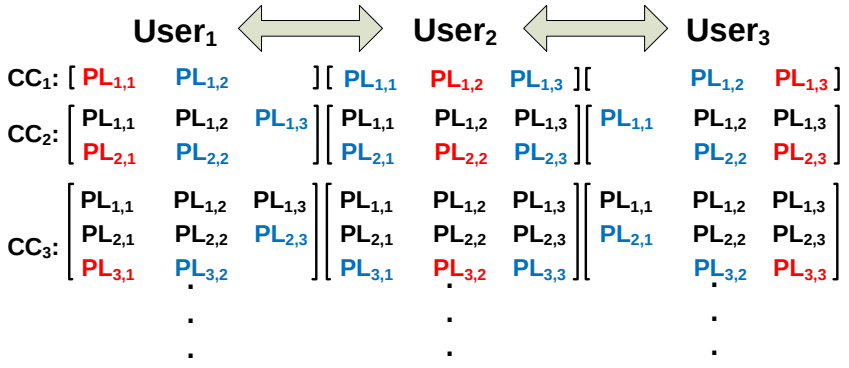

Figure 6.3: The PL transmission scheme in CT-MAC, where the red, blue and black colors represent the newly generated PLs, the overheard PLs from direct neighbors and the historical PLs, respectively.

In general, if there are L nodes in a one-dimensional uplink network, PLs generated at CC_i can be received by all nodes at CC_{i+L-2}. This implies that in the first $L-2$ time slots of CT-MAC, no node can transmit without a common view on PL competitions. I call these $L-2$ time slots as the *delaying slots*.

Since nodes in CT-MAC need to help relay the PLs from others, a node may push out multiple PLs in one competition cycle. Here I assume in CC_i, node j puts all PLs it needs to send in the current competition cycle into the competition packet (CP), $CP_{i,j}$. In order to avoid collisions among CPs, each node does a random backoff before sending the CP.

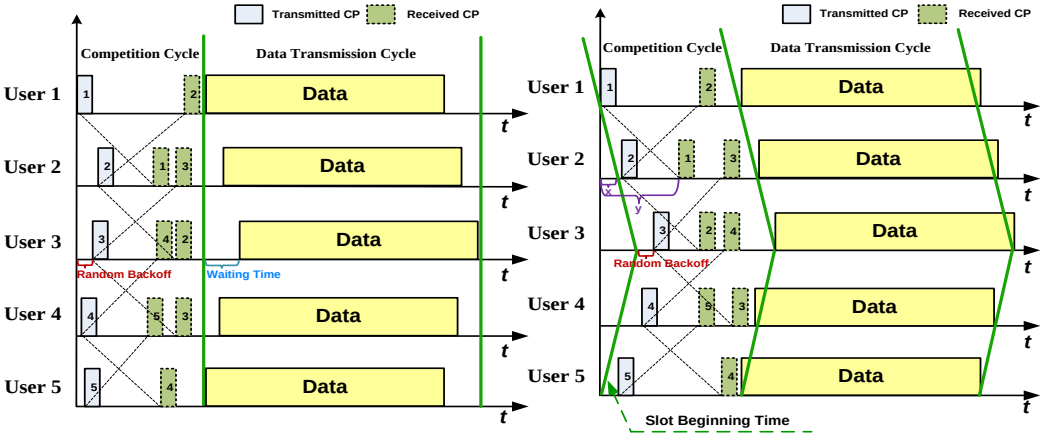

(a) TS 1 (b) TS 2

Figure 6.4: Comparison between two transmission schemes.

6.3.1.2 Transmission cycle

To avoid the supersaturated reception, only K out of L nodes with the highest $PL_{i-L+2,j}$ are allowed to send their data in TC_i, where $i = L-1, L, L+1, \ldots$ and $j = 1, 2, \ldots, L$. The symbols I used in this chapter are described as follows:

- c as the sound speed in water,
- d_i as the distance between the receiver and sender i ,
- t_{cc} as the length of a competition cycle,
- t_{tc} as the length of a data transmission cycle,
- T_s as the length of a time slot (sum of t_{cc} and t_{tc}),
- t_{cp} as the transmission time of a CP,
- t_{bo} as the maximum time of a random backoff,

- t_{dp} as the transmission time of a data packet,
- $l_{i,j}$ as the distance between sender i and sender j,
- l_{max} as the maximum distance between any two neighboring nodes,
- Δd_{max} as the maximum difference between distances from the receiver to any two neighboring nodes.

Here d_i, $l_{i,j}$ can be measured at the initial stage of a network by using a classic two-way handshake method, which is generally used in sender–receiver based time synchronization protocols [71]. Similar distance measurement approach has been successfully tested in the sea experiment [72]. l_{max} and Δd_{max} are available at the receiver based on the measurements of d_i and $l_{i,j}$, respectively. It is worth noting that CT-MAC cannot work in the highly mobile networks. In a mobile network, the distance among nodes changes with time, indicating the length of competition cycle in CT-MAC needs to be updated frequently. However, CT-MAC measures the distance at the initial stage of a network. Once the protocol starts, the length of competition cycle will remain unchanged. In addition, to eliminate the impact of the error in distance measurements, a guard time is necessary between any two neighboring time slots.

In CT-MAC, I want to make packets from different nodes arrive at the receiver simultaneously[4] . In this way, the unexpected reception described in Section 6.2 could be avoided. To achieve this goal, I design two transmission schemes for my protocol.

- *Transmission Scheme 1* (TS_1): All nodes in TS_1 start their time slots concurrently. To make packets from different senders reach the receiver at the same time, the node with a shorter d_i should wait for the one with a larger d_i before its data transmission, as shown in Fig. 6.4(a). Using five nodes in Fig. 6.1 as an example, the distance between u_3 and the receiver is the shortest among the five nodes. The waiting time of u_3 before its data transmission should be $\max\{d_i - d_j\}/c$, where $i \neq j$

[4]If packets from different nodes arrive at the receiver not exactly at the same time, the packets are still decodable, but with degraded decoding performance. The research on the misalignment symbol timing of OFDM based multiuser uplink communications can be found in [21] and [23].

and $i, j = 1, 2, \ldots, L$. Hence, the minimum t_{tc} and t_{cc} are $\max\{d_i - d_j\}/c + t_{dp}$ and $l_{max}/c + t_{cp} + t_{bo}$, receptively. Finally, we have

$$T_{s1} = t_{cc} + t_{tc} = \frac{\max\{d_i - d_j\} + l_{max}}{c} + t_{dp} + t_{cp} + t_{bo}. \tag{6.4}$$

• *Transmission Scheme 2* (TS_2): Different from TS_1, I allow nodes in TS_2 to start their time slots at different time for more efficient data transmissions. As shown in Fig. 4(b), a node with a larger d_i starts its time slot ahead of a node with a smaller d_i. For node i, the advanced time of its time slot, which is denoted by x_i, is $x_i = (d_i - \min\{d_j\})/c$, where $j = 1, 2, \ldots, L$. With this scheme, we have $t_{tc} = t_{dp}$. The minimum t_{cc} should be $t_{cc} = (\Delta d_{max} + l_{max})/c + t_{cp} + t_{bo}$ to guarantee that the competition cycle is long enough for all CPs reception. Finally, we have

$$T_{s2} = t_{cc} + t_{tc} = \frac{(\Delta d_{max} + l_{max})}{c} + t_{dp} + t_{cp} + t_{bo}. \tag{6.5}$$

In TS_2, since nodes do not start their time slot at the same time, the competition cycle of a node may overlap with part of the data transmission cycle of its neighbors. Therefore we should ensure that there are no sending–receiving collisions between data packets and CPs. Using u_1 and u_2 in Fig. 6.4(b) as an example, if a CP from u_1 arrives at u_2 earlier than the slot beginning time of u_2, i.e., $y < x$, the reception of this CP may conflict with u_2's data transmission. Next, I prove that this collision does not happen in CT-MAC.

Proof: $y \times c = l_{1,2}$, and $x \times c = d_1 - d_2$. Let nodes u_1, u_2 and the receiver be the three vertexes of a triangle, then $l_{1,2}$, d_1 and d_2 are three sides of this triangle. According to the *triangle inequality principle* that the sum of the lengths of any two sides of a triangle always exceeds the length of the third side, we have $l_{1,2} + d_2 > d_1$. Hence, we have $l_{1,2} > d_1 - d_2$, i.e., $y > x$. ■

Compared with TS_1, the length of each time slot in TS_2 is reduced by $\max\{d_i - d_j\} - \Delta d_{max}$, which improves the channel utilization of the protocol. Finally, the channel

utilization of CT-MAC with TS_2, which is denoted by U, is

$$U = \frac{Kt_{tc}}{T_s} = \frac{Kct_{dp}}{\Delta d_{max} + l_{max} + c\,(t_{dp} + t_{cp} + t_{bo})}. \tag{6.6}$$

It is worth noting that in the conventional single-input and single-output (SISO) network, the channel utilization is less than one. However, in multi-node network, this value may be larger than one, since the network supports multiple nodes to send their data at the same time without any collision.

6.3.2 Two-dimensional uplink networks

CT-MAC can be easily extended to two-dimensional uplink networks. Its competition mechanism in a two-dimensional network is the same as it in one-dimensional networks. By using the parallel competition scheme, K out of L nodes with the highest PLs are allowed to send their data in each data transmission cycle. However, in order to transmit CPs efficiently while avoiding the supersaturated reception in a two-dimensional network, the transmission scheme TS_2, which is originally designed for one-dimensional networks, needs a slight modification.

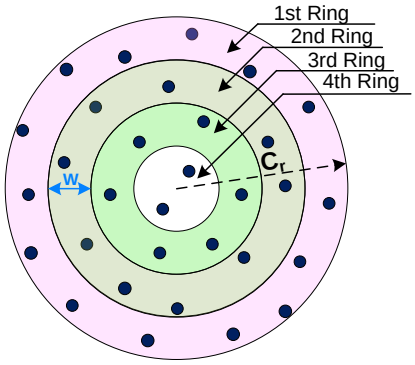

Figure 6.5: A general two-dimensional uplink network, where the coverage of the receiver is a cycle with the radius C_r.

In a two-dimensional network, I divide the coverage area of a receiver into several concentric rings, as shown in Fig. 6.5. The width of each rings is equal, which is denoted

by W. Now, I set $W = d_{avg}$, where d_{avg} is the average distance between neighboring nodes in the two-dimensional network. Let r_i and d'_i represent the i^{th} ring and the average distance from the receiver to nodes in the i^{th} ring, respectively.

Since the distances between the receiver and nodes in the same ring are close, all nodes in the same ring start their time slot at the same time. Moreover, nodes in an outer ring start their time slots earlier than the ones in an inner ring with an advanced time depending on the distance difference to the receiver. Referring to TS_2 in Section 6.3.1.2, the advanced time of nodes in the ring r_i, which is represented as x'_i, is $x'_i = (d'_i - \min\{d'_i\})/c$.

Similar to TS_2 in a one-dimensional network, a random backoff before each transmission of CP is also required in the two-dimensional network to avoid collisions among CPs. Therefore, in each competition cycle, a node can successfully receive CPs from its neighbors not only in the same ring but also in the neighboring rings. If there are no isolated nodes, PL produced by each node can propagate to the whole network within several delaying slots, the number of which is less than or equal to $L - 2$.

Let $\Delta d'_{max}$ be the maximal distance difference between the receiver and any two nodes in different neighboring rings, which can be calculated by the receiver at the initial stage of the network with a two-way handshake approach. Referring to (6.5) we have that the minimal length of the time slot in a two-dimensional uplink network is

$$T_s = \frac{(d'_{max} + l_{max})}{c} + t_{dp} + t_{cp} + t_{bo}. \tag{6.7}$$

Replacing parameter Δd_{max} in (6.6) with $\Delta d'_{max}$, we can get the channel utilization of CT-MAC in the two-dimensional uplink networks.

6.4 Competition schemes for fair transmissions

To make the flow of CT-MAC easy to understand, in the previous section, a node just compete for sending opportunities with a random PL. However, the network may

have the fairness issue with this simple strategy. In this section, I propose two specific competition schemes for CT-MAC, aiming to improve both the short-term and the long-term fairness of the network.

6.4.1 Homogeneous traffic generation

I start from a common scenario that nodes in a network have homogeneous traffic generation rates. In this network, the number of packets generated by different nodes are almost the same in a long time period. In a short time, however, the differences may still exist due to the randomness of the traffic generation at each node.

Here, I have two goals for the fair transmission: (a) In a network, the more packets a node accumulated in its sending queue, the higher the transmission opportunity it has to achieve the short-term fairness, (b) The total number of packets sent by nodes are close in a long period to achieve the long-term fairness. In the following two sections I introduce how to design a competition scheme to achieve these two goals.

6.4.1.1 Short-term fairness

If each node use a random value as the PL to compete for the sending opportunities in the data transmission cycle as what I did in Section 6.3, transmissions in a short time may be unfair, since the PL of each node is independent with the number of packets it accumulated. Therefore, we need to revise the basic competition scheme to improve its short-term fairness in a homogeneous traffic generation scenario.

I assume that each node generates its data packets at the beginning of a time slot. Let $g_{i,j}$ and $g'_{i,j}$ be the total number of packets accumulated by node j at the end of i^{th} time slot and the number of new packets generated by node j in the i^{th} time slot, respectively. Here, $g'_{i,j}$ is supposed to follow the Poisson distribution with the mean value λ_j. For a homogeneous traffic generation rates network, we have $\lambda_j \equiv \lambda$, for

$j=1,2,\ldots,L$. Therefore, the number of packets accumulated by node j in the i^{th} time slot, which is denoted by $A_{i,j}$, is $A_{i,j} = g_{i-1,j} + g'_{i,j}$. Now, I define two events:

- *Successful Competition Event:* If node j wins the competition for transmission in the i^{th} time slot, I call it as a successful competition to node j, which is denoted by $H^1_{i,j}$.
- *Failed Competition Event:* If node j loses the competition for transmission the i^{th} time slot, I call it as a failed competition to node j, which is denoted by $H^0_{i,j}$.

In order to achieve the short-term fairness, the goal of a competition scheme is to make the conditional transmission probability of $H^1_{i,j}$ meet

$$\mathrm{P}(H^1_{i,m}|A_{i,m}=x_1) > \mathrm{P}(H^1_{i,n}|A_{i,n}=x_2), \text{ if } x_1 > x_2. \tag{6.8}$$

To make (6.8) hold, in each competition cycle of CT-MAC, node j includes not only the PL, but also the number of accumulated packets, i.e., $A_{i,j}$, into $\mathrm{CP}_{i,j}$. In the data transmission cycle, K out of L nodes with the largest $A_{i,j}$ are allowed to send their data. If several nodes have the same number of accumulated packets, then they compare the corresponding PLs as described in Section 6.3 to determine the final data transmission. I call this competition scheme as CS.1.

6.4.1.2 Long-term fairness

For a network with homogeneous traffic generation rates, the long-term fairness can be measured by the Jain's fairness index F_J [115].

$$F_J = \frac{(\sum_{j=1}^{L}\gamma_j)^2}{L\sum_{j=1}^{L}\gamma_j^2}, \tag{6.9}$$

where γ_j is the channel occupancy rate of node j. The transmissions of a network are fair if F_J is close to one; otherwise, it loses the long-term fairness. In Section 6.8.1, I will show that CT-MAC has a good long-term fairness with the competition scheme CS.1 in a homogeneous traffic generation rates network.

6.4.2 Heterogeneous traffic generation

In a network with heterogeneous traffic generation rates, I assume that the traffic generation rate of node j, namely $g'_{i,j}$, follows the Poisson distribution, but $\lambda_i \neq \lambda_j$, if $i \neq j$.

According to (6.8), if we still use CS.1 in CT-MAC, a node with a large λ_j may always have larger $A_{i,j}$ in each time slot than a node with a small λ_j. In this case, nodes with small λ_j may lose all competitions and have no chance to send their data, which will be shown in Section 6.8.1. Therefore, CS.1 is no longer appropriate for the fair transmission in a heterogeneous traffic generation rates network. For this reason, a new competition scheme is required.

6.4.2.1 Short-term fairness

To achieve the short-term fairness in a heterogeneous traffic generation rates network, the goal of a competition scheme is to make the conditional transmission probability of $H^1_{i,j}$ meet

$$\mathrm{P}(H^1_{i,j}|A_{i,j}=x_1) > \mathrm{P}(H^1_{k,j}|A_{k,j}=x_2), \text{ if } x_1 > x_2. \tag{6.10}$$

Different from (6.8), which is the comparison of accumulated packets among different nodes in the same time slot, (6.10) is the comparison of accumulated packets for the same node in different time slots. Therefore, (6.10) guarantees that nodes with slow increment on accumulated packets (small λ) still have small but not zero transmission opportunity to send their data. In this situation, all nodes will have a chance to transmit.

6.4.2.2 Long-term fairness

To achieve the long-term fairness in a network with heterogeneous traffic generation, I expect that the average channel occupancy rate of each node is proportional to its traffic generate rate,[5] i.e.,

$$E(\gamma_j) = \frac{K\lambda_j}{\sum_{j=1}^{L}\lambda_j}. \tag{6.11}$$

From (6.11) we have that the total channel occupancy rate $\sum_{j=1}^{L} E(\gamma_j)$ equals to K, which is the maximum number of packets a receiver can received at the same time. If I design a competition scheme based on (6.11), all nodes will have a chance to send their data.

Now, I start from $E(\gamma_j)$, where

$$E(\gamma_j) = \lim_{m\to\infty}\frac{1}{m}\sum_{i=1}^{m}\mathrm{P}(H_{i,j}^{1}) = \lim_{m\to\infty}\frac{1}{m}\sum_{i=1}^{m}\sum_{x=0}^{\infty}\mathrm{P}(H_{i,j}^{1}|A_{i,j}=x)\mathrm{P}(A_{i,j}=x). \tag{6.12}$$

Several kinds of functions can be selected as $\mathrm{P}(H_{i,j}^{1})$ to make (6.10) hold, e.g. exponential function, step function and liner function. Here I use the step function as an example to design my competition scheme. We make

$$\mathrm{P}(H_{i,j}^{1}|A_{i,j}=x) = \begin{cases} 1, & x > u_{i,j} \\ \alpha_{i,j}, & x = u_{i,j} \\ 0, & \text{otherwise,} \end{cases} \tag{6.13}$$

where $\alpha_{i,j}$ and $u_{i,j}$ can be calculated by substituting (6.13) into (6.12), i.e.,

$$\mathrm{P}(A_{i,j} > u_{i,j}) + \alpha_{i,j}\mathrm{P}(A_{i,j} = u_{i,j}) = \frac{K\lambda_j}{\sum_{j=1}^{L}\lambda_j}. \tag{6.14}$$

In the competition cycle, each node includes both its PL and the value of $\mathrm{P}(H_{i,j}^{1}|A_{i,j})$ into its CP. In the data transmission cycle, K out of L nodes with the largest $\mathrm{P}(H_{i,j}^{1}|A_{i,j})$ are allowed to send the data. If there are multiple nodes have the same $\mathrm{P}(H_{i,j}^{1}|A_{i,j})$,

[5] Although here I make $E(\gamma_j) \propto \lambda_j$, CT-MAC can support arbitrary channel occupancy pattern by modifying $K\lambda_j/\sum_{j=1}^{L}\lambda_j$ in (6.11) and (6.14) to $K\upsilon_j$, where $\sum_{j=1}^{L}\upsilon_j = 1$ and υ_j is the target channel occupancy rate of node j.

then these nodes compare their PLs for the final decision. I denote this competition scheme as CS.2. The long-term fairness of CS.2 will be evaluated in Section 6.8.1.

The competition scheme CS.2 requires nodes in each time slot to calculate their conditional transmission probabilities $\mathrm{P}(H^1_{i,j}|A_{i,j})$ based on the number of accumulated packets in the sending queue. Next, I introduce an iterative algorithm to calculate this parameter.

Algorithm 1

Initialization: Let $A_{1,j} = g'_{1,j}$. According to the Poisson distribution of $g'_{1,j}$ with mean value λ_j, we have

$$\mathrm{P}(A_{1,j}=x) = \frac{(\lambda_j)^x e^{-\lambda_j}}{x!}. \tag{6.15}$$

Substitute (6.15) into (6.13) and (6.14) to calculate $\mathrm{P}(H^1_{1,j}|A_{1,j})$.

Step 1: $\mathrm{P}(g_{i,j})$ can be calculated through

$$\begin{aligned}\mathrm{P}(g_{i,j}=x) = {} & \mathrm{P}(H^1_{i,j}|A_{1,j}=x+1)\mathrm{P}(A_{i,j}=x+1) \\ & + [1-\mathrm{P}(H^1_{1,j}|A_{i,j}=x)]\mathrm{P}(A_{i,j}=x).\end{aligned} \tag{6.16}$$

Step 2: By using $A_{i+1,j} = g_{i,j} + g'_{i+1,j}$, where $g_{i,j}$ and $g'_{i+1,j}$ are independent, we can calculate $\mathrm{P}(A_{i+1,j})$ through

$$\mathrm{P}(A_{i+1,j}) = \mathrm{P}(g_{i,j}) * \mathrm{P}(g'_{i+1,j}), \tag{6.17}$$

where $*$ is the convolution operator, and $g'_{i+1,j} \sim \mathrm{Pois}(\lambda_j)$.

Step 3: Substitute $\mathrm{P}(A_{i+1,j})$ into (6.14) to calculate $u_{i+1,j}$ and $\alpha_{i+1,j}$.

Step 4: Substitute $u_{i+1,j}$ and $\alpha_{i+1,j}$ into (6.13) to compute $\mathrm{P}(H^1_{i+1,j}|A_{i+1,j})$.

By repeating **Step 1** to **Step 4**, nodes can calculate their $\mathrm{P}(H^1_{i,j}|A_{i,j})$ in each time

slot iteratively.

6.5 Power allocation

The power allocation strategy in a multi-node network aims to decide the appropriate transmission power to maximize the channel capacity. There have been intensive research in this area to optimize the transmission power in both terrestrial and underwater multi-node uplink networks. Since the power allocation is not the focus of this section, I just give a brief introduction on power allocation in CT-MAC.

As I discussed in Section 6.2, the instantaneous CSI may not be available in underwater communications, due to the large propagation delay, long packet transmission time and high dynamic of acoustic channel. However, the statistical information of underwater channel can be utilized for power allocation, since it is relatively stable in a relative long time period.

In CT-MAC, we can measure the statistical information, such as the average receiving SNR and the distribution of channel gain, at the initial stage of the network, and then consider it as a priori knowledge. In this way, existing algorithms, such as [113] and [116], can be employed by CT-MAC to decide the optimum transmission power on active senders.

It is worth noting that the aforementioned power allocation algorithms usually require the MAC layer to provide the information about which node will transmit. This information is available in CT-MAC with its parallel competition scheme, since nodes completely know who wins the competition for the data sending in each time slot. This is one superior of CT-MAC when compared with some conventional MAC protocols [25, 117].

6.6 Bad request issue

In this section, I introduce a specific issue in CT-MAC, which may degrade the channel utilization of the protocol.

To improve the channel utilization, I designed a parallel competition scheme for CT-MAC. Essentially, nodes in this scheme utilize their current statuses, namely $A_{i,j}$, PL and $\mathrm{P}(H^1_{i,j}|A_{i,j})$ to compete for the transmission opportunities in the future time slots. If their statuses are changed during the propagation of CP, these transmission opportunities may be wasted. I call this problem as the *bad request issue*.

Using a string topology network with 20 nodes as an example, suppose the traffic generation rates of the network are homogeneous, and the competition scheme CS.1 is employed. Denote the time slot i as S_i. I assume that in S_1, node u_1 has a data to send. According to CS.1, it sends $A_{1,1}=1$ to its neighbors. However, in the following seventeen slots, even if u_1 does not generate any new data, it still produces $A_{i,1}=1$, $i=2,\ldots,18$ to compete for the transmission opportunities in the slots from S_2 to S_{18}. This is because the competition results in S_1 are not known immediately but be delayed by 18 slots as described in Section 6.3. Therefore, u_1 continually competes the sending opportunity for the single data packet it generated in S_1.

After delaying slots, at S_{19}, I suppose that u_1 wins the competition and sends out the only packet it accumulated in the queue. However, u_1 has attended all the competitions between S_2 and S_{18}. In this case, u_1 wastes the sending opportunities if it wins one or more competitions in these slots, since it currently has no data to send.

I will evaluate the impact of the bad request issue on channel utilization of CT-MAC in Section 6.8.1.

6.7 The CP loss problem

In CT-MAC, CP carries the competition information for each node. The successful transmission of CPs is thus important. Although I have used the backoff mechanism to prevent collisions among CPs, the reception of CP may still fail due to the poor channel quality caused by the high noise level, long multipath or wide Doppler spread [118]. In this section, I first evaluate the effect of the CP loss in one-dimensional networks, and then propose two feasible solutions to handle the lost CPs.

6.7.1 Effect of CP loss

In a string network, the quality of acoustic channels between different neighbors may have some differences. Therefore, I assume that the successful transmission probability (delivery ratio) of CPs also varies on different links.

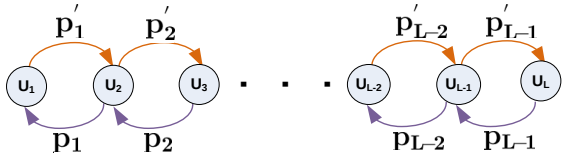

Figure 6.6: The delivery ratio of CP in a string network.

Let p_j and p'_j be the delivery ratio of the CP from node $(j+1)$ to node j, and from node j to node $(j+1)$, respectively, as shown in Fig. 6.6. The delivery ratio of a CP from node i to node j is represented as $\mathcal{P}_{ij}$, where

$$\mathcal{P}_{ij}=\begin{cases}\prod_{k=i-1}^{j} p_k, & i>j,\\ 1, & i=j,\\ \prod_{k=i}^{j-1} p'_k, & i<j.\end{cases} \tag{6.18}$$

If a node misses $\mathrm{CP}_{i,j}$, the corresponding competition information, such as $\mathrm{PL}_{i,j}$, $A_{i,j}$ and $\mathrm{P}(H^1_{i,j}|A_{i,j})$, which is carried by this CP, is also lost. Using $\mathrm{PL}_{i,j}$ as an example, let w_j be the number of lost PLs on node j in a specific cycle. Denote the

probability density of w_j as $\mathrm{P}(w_j)$. It is easy to have that the probability that node j successfully receive all PLs, which are generated in a same competition cycle, is

$$\mathrm{P}(w_j=0)=\prod_{i=1}^{L}\mathcal{P}_{ij}. \tag{6.19}$$

The probability that node j misses one of these PLs is

$$\begin{aligned}\mathrm{P}(w_j=1) =&\sum_{i=1}^{L}(1-\mathcal{P}_{ij})\prod_{\substack{k=1\\k\neq i}}^{L}\mathcal{P}_{kj}\\ =&\sum_{i=1}^{L}\frac{1-\mathcal{P}_{ij}}{\mathcal{P}_{ij}}\prod_{k=1}^{L}\mathcal{P}_{kj}\\ =&\sum_{i=1}^{L}\left(\frac{1}{\mathcal{P}_{ij}}-1\right)\mathrm{P}(w_j=0).\end{aligned} \tag{6.20}$$

Then the probability that node j misses two of these PLs is

$$\begin{aligned}\mathrm{P}(w_j=2) =&\frac{1}{2!}\sum_{i=1}^{L}(1-\mathcal{P}_{ij})\sum_{\substack{k=1\\k\neq i}}^{L}(1-\mathcal{P}_{kj})\prod_{\substack{m=1\\m\neq i,k}}^{L}\mathcal{P}_{mj}\\ =&\frac{1}{2}\left[\sum_{i=1}^{L}\left(\frac{1}{\mathcal{P}_{ij}}-1\right)\mathrm{P}(w_j=1)-\sum_{k=1}^{L}\left(\frac{1}{\mathcal{P}_{kj}}-1\right)^2\mathrm{P}(w_j=0)\right].\end{aligned} \tag{6.21}$$

Finally, we can calculate $\mathrm{P}(w_j)$ iteratively with the following expression:

$$\mathrm{P}(w_j=x)=\frac{1}{x}\sum_{i=1}^{x}(-1)^{i-1}\psi_j(i)\mathrm{P}(w_j=x-1), \tag{6.22}$$

where $x=1,\ldots,L$ and

$$\psi_j(i)=\sum_{k=1}^{L}(\frac{1}{\mathcal{P}_{kj}}-1)^i. \tag{6.23}$$

The mean value of w_j is

$$E(w_j)=\sum_{x=1}^{L}x\mathrm{P}(w_j=x). \tag{6.24}$$

The analytical expression of the average number of lost PLs in (6.24) could help us evaluate the performance of CT-MAC in real network easily.

If a node misses the competition information from others in a competition cycle, it is unable to accurately decide if it should send data or not in the following data transmission cycle. In the next section, I introduce how to handle this problem.

6.7.2 Handling the CP loss problem

In CT-MAC, we can use two simple strategies, namely, the *underestimation* and the *overestimation*, to handle the lost CPs.

In the underestimation strategy, if a node loses any other nodes' competition information, e.g., $\mathrm{PL}_{i,j}$, $\mathrm{P}(H^1_{i,j}|A_{i,j})$ and $A_{i,j}$, it assumes that these nodes have the lowest priority in this round of competition. It is easy to understand that with the this strategy, the number of active nodes in each data transmission cycle is possibly larger than the maximum number of senders that a network can support, which causes a supersaturated reception.

In the overestimation strategy, a node assumes that the nodes, the competition information of which are lost, have the highest priority for the data transmission. With this strategy, the channel resource may be wasted, since the number of active nodes is possibly less than the maximum number of active senders that a network can support if the lost priority information is overestimated, which causes a starving reception.

Although the channel utilization is not optimal when the starving reception happens, all packets could be decoded by the receiver successfully as long as the channel is good. By contrast, if supersaturated reception happens, the data packets will collide at the receiver, which is the worst case and should be avoided in underwater communications. For this reason, in CT-MAC I consider the overestimation as a wiser option than the underestimation strategy to handle the lost CPs.

Now, I derive the channel utilization of CT-MAC in a homogeneous traffic rates network with the overestimation strategy. In an ideal situation, where there is no lost CP, the average transmission probability of each node in the data transmission cycle is K/L. When taking into account the lost CPs, this probability is reduced to $(K - w_j)/(L - w_j)$ for node j. Denote the average number of active nodes as K', we

have

$$K' = \sum_{i=1}^{L} \sum_{x=1}^{K} \frac{K-x}{L-x} \mathcal{P}(w_j = x), \tag{6.25}$$

which is less than or equal to K.

Finally, replacing K in (6.6) with K', we will get the channel utilization of CT-MAC in a network with homogeneous traffic generation rates and under CP loss effect.

6.8 Simulations and analysis

In this section, I evaluate the performance of CT-MAC in a string network. The depth of nodes and the distance between neighboring nodes are 500 m and 200 m, respectively. In the simulation, I use two different sizes of network, $L = 10$ and $L = 20$, as examples for performance evaluation. The number of hydrophones on the receiver is $M_r = 4$. I first evaluate the fairness of different competition schemes, and show the impact of the CP loss problem and bad request issue on CT-MAC in Section. 6.8.1. Then, I compare CT-MAC with two representative multi-node MAC protocols in terms of the channel utilization, energy efficiency and end-to-end delay in Section 6.8.2.

6.8.1 Performance evaluation

Firstly, I evaluate the long-term fairness of competition scheme CS.1 in a string network with homogeneous traffic generation rates. For comparison purpose, two different competition schemes, which are denoted by CS.3 and CS.4, are also investigated. In CS.3, K out of L nodes with the lowest $A_{i,j}$ are allowed to send their data, which is completely opposite to CS.1. In CS.4, $K/2$ out of L nodes with the highest $A_{i,j}$, and another $K/2$ nodes with the lowest $A_{i,j}$ are arranged to send their data in each data transmission cycle. This competition scheme can be considered as a mixture of CS.1 and CS.3.

In Fig. 6.7, I set the traffic generation rate $\lambda_j = 1$ for $j = 1, 2, \ldots, 20$, in a network with 20 senders and plot the Jain's fairness index F_J for all three competition schemes. From this figure, we observe that F_J of CS.1 is gradually close to one with the running of the protocol. This proves that CT-MAC with CS.1 achieves a good long-term fairness in the network with homogeneous traffic generation rates. By contrast, F_J of CS.3 and CS.4 are very low, close to 0.2 and 0.4, respectively. This implies that CT-MAC loses its long-term fairness with these two competition schemes.

In addition, we observe that F_J of all three competition schemes in Fig. 6.7 starts from 0.2. This is because no matter which competition scheme I used, after the first data transmission, if node j sends the data, γ_j in (6.9) always equal to one; otherwise, $\gamma_j = 0$. In each data transmission cycle, there are K nodes are allowed to transmit. Therefore, F_J of all competition schemes starts from K/L, which is 0.2.

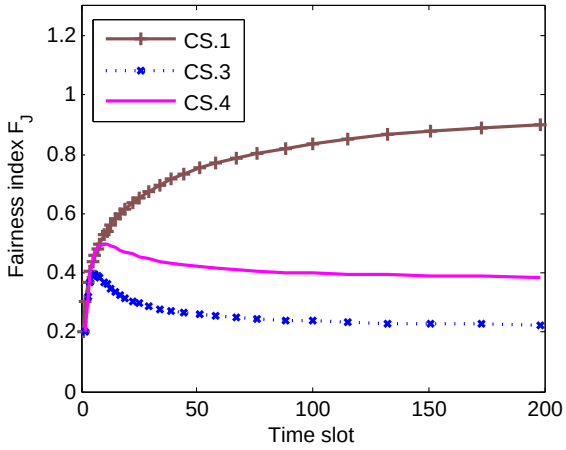

Figure 6.7: Comparison of the long-term fairness in a network with homogeneous traffic generation rates.

To give us an insight into Fig. 6.7, I plot the distribution of the number of accumulated packets, i.e., $\mathrm{P}(A_{i,j})$, after the protocol ran $10,000$ time slots, as shown in Fig. 6.8. If none of nodes in the network send data, then the average number of $A_{i,j}$ should equal to the number of time slots, which is $10,000$, because $\lambda_j = 1$, $j = 1, 2 \ldots, L$. In this figure, when using CS.1, we observe that $A_{i,j}$ is distributed around 8000. More

specifically, since the data transmission in CS.1 is fair in a long-term period, the packet transmission opportunity of all nodes are almost equal, which is $K/L = 0.2$. Therefore, after $10,000$ time slot the average number of $A_{i,j}$ is $(1 - 0.2) \times 10,000 = 8000$, which proves the long-term fairness of CS.1 again.

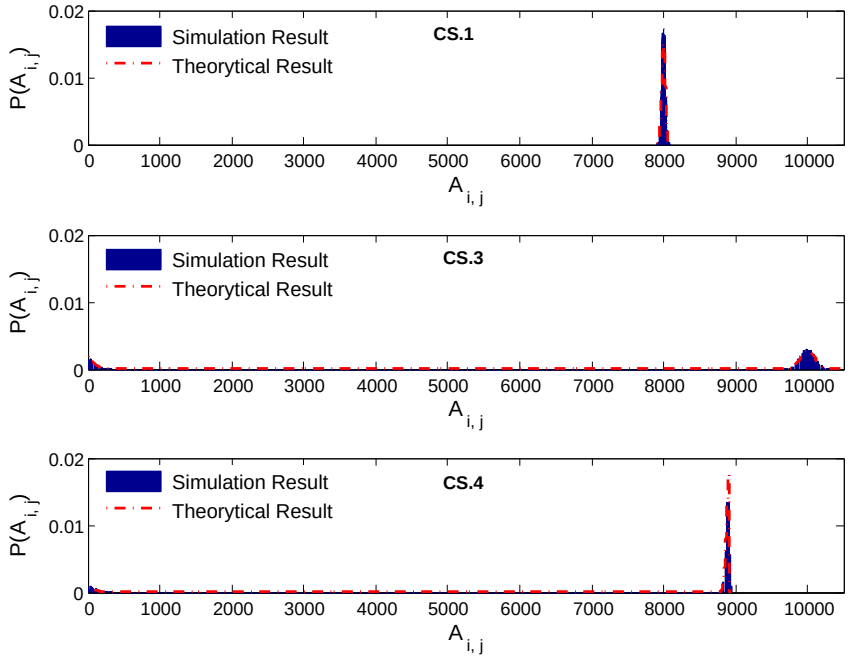

Figure 6.8: The distribution of $A_{i,j}$ in CT-MAC with different competition schemes.

For comparison, when I use CS.3 in CT-MAC, a node with a larger $A_{i,j}$ is more likely to fail the transmission competition than a node with a smaller $A_{i,j}$. This finally leads to an extremely differentiated $A_{i,j}$. Part of nodes, who win first, easily get the chance to send their data later on ($A_{i,j}$ goes down to zero), and others that failed the competition at the beginning keep losing the sending opportunities in the future competitions ($A_{i,j}$ goes up to 10,000). The fairness problem also occurs in CS.4, but less severe than that in CS.3. This is because each node in CS.4 has a chance to send its data in each time slot, although the sending opportunities are not equal for all nodes. More specifically, both nodes with the largest and smallest $A_{i,j}$ in CS.4 have transmission opportunities. That is why the left peak of $\mathrm{P}(A_{i,j})$ in CS.4 of Fig. 6.8 is

round 9000 rather than $10,000$, and the area of the right part in CS.4 is smaller than that in CS.3.

In addition, to test the accuracy of Algorithm 1, I also compare the theoretical analysis of $\mathrm{P}(A_{i,j})$ with the simulation results. From the comparisons in Fig. 6.8 we have that the theoretical computations of $\mathrm{P}(A_{i,j})$ match the simulation results very well in all three competition schemes.

In a network with heterogeneous traffics, I make λ_j of different nodes uniformly distributed between 0.1 and 2 to evaluate the long-term fairness of CS.2. As shown in Fig. 6.9, the channel occupation rate of λ_j conforms to (6.11), which is proportional to the traffic generation rates. By contrast, if we still use CS.1 in the heterogeneous traffic generation rates network, the transmission opportunity of nodes with small λ_j may be "plundered" by nodes with larger λ_j. This can be found in Fig. 6.9, where the channel occupancies of the eleven nodes with lower traffic loads (λ_j between 0.1 and 1) are almost zero.

In Fig. 6.10, I use a 10 senders network as an example to show the average number of lost PLs at each node with respect to the delivery ratio of CPs, i.e., p_j and p'_j. From this figure we observe that p_j affects $E(w_j)$ significantly. When $p_j = 0.99$, two edge nodes, u_1 and u_{10}, lose 0.5 PLs in average, which is only 5% out of the total. However, when p_j reduces to 0.9, the average number of lost PLs at u_1 and u_{10} grows to 3.5, six times higher than that in the case with $p_j = 0.99$. Moreover, the position of a node in the network also affects its $E(w_j)$. Compared with nodes on the edge of network, nodes in the central of network have much smaller $E(w_j)$ owing to the less number of hops for CP forwarding. In addition, Fig. 6.10 also shows the consistence between the simulation results of lost CPs and the theoretical analysis derived from (6.22) to (6.24).

Fig. 6.11 demonstrates the impact of lost CPs on CT-MAC, where the overestimation strategy is employed. we observe an improvement on the channel utilization

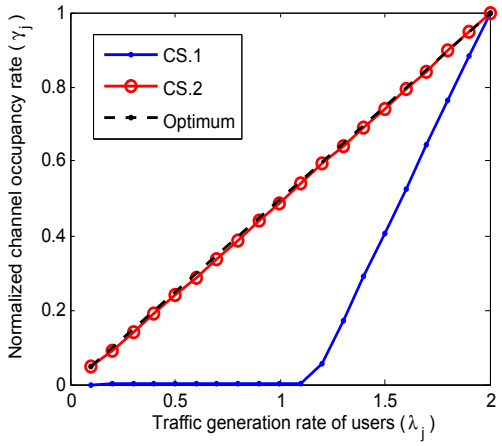

Figure 6.9: The long-term fairness.

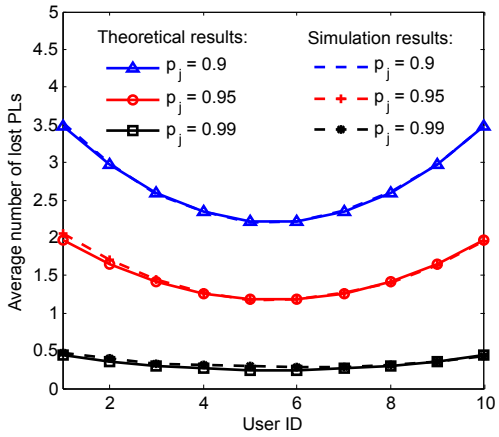

Figure 6.10: Lost PLs.

as the size of the network reduces and the delivery ratio of CPs increases. This figure reveals that the multi-node uplink network with a larger number of nodes is much more sensitive to the CP loss than a network with smaller size. When reducing p from 1 to 0.9, the throughput degrades by 60% for the network with 10 nodes, compared with 99% reduction for the network with 20 nodes. Therefore, a larger size of a network requires a higher reliability on CP transmission in CT-MAC.

Again, the validity of the theoretical analysis on the channel utilization of CT-MAC under the effect of CP loss is confirmed by comparing with simulation results. As shown in Fig. 6.11, the theoretical results derived from (6.6) and (6.25) match the simulation results very well.

In Fig. 6.12, I evaluate the effect of the bad request issue on CT-MAC. In the ideal situation, I suppose that nodes in the simulation get aware of all $A_{i,j}$ information immediately. To compare with this ideal case, I plot the channel utilization of CT-MAC in the real scenario, where $L-2$ delaying slots exist in the protocol. From Fig. 6.12 we observe that the bad request problem slightly degrades the channel utilization especially in a large network, where the PL information need more time slots to propagate to the whole network, and the number of packets accumulated by each node has high

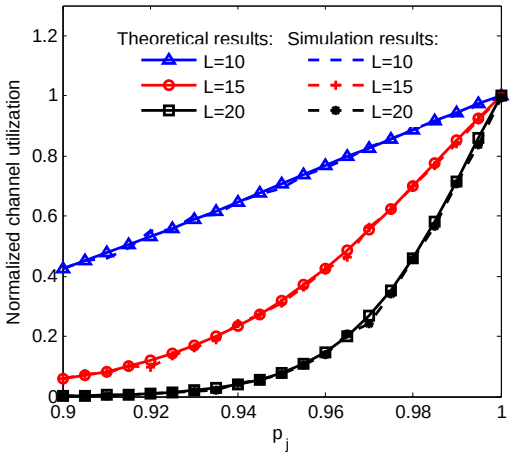

Figure 6.11: Channel utilization with p_j.

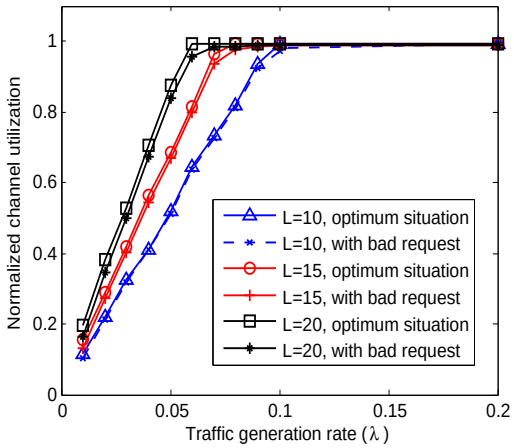

Figure 6.12: Bad request effect.

probability to change during the propagation of PLs. If nodes have competed more transmission opportunities than they need, the bad request incurs and degrades the network throughput. In addition, with the increment of traffic generation rates, the negative effect of bad request issue becomes negligible. This is because in a high traffic network, the amount of accumulated packets on each node has small chance to be zero, thus reducing the probability to waste transmission opportunities.

6.8.2 Performance comparison

To verify the advantages of CT-MAC on channel utilization, energy efficiency and end-to-end delay, I compare CT-MAC with two representative multi-node MAC protocols, namely, channel aware Aloha [25] and multi-antenna reception MAC [26], both of which were briefly introduced in Section. 6.2. Here, the channel utilization is defined as the ratio of the channel resource utilized for successful data transmissions,[6] which can be a value larger than one in multi-node uplink networks. The energy efficiency is measured as the average power consumption on both control and data transmissions

[6]The network throughput can be represented as the channel utilization times data transmission rate.

per each successful data delivery. The end-to-end delay measures the average delay for a data packet to be delivered to the surface receiver.

The default network size I used in the following simulations is $L=10$. The duration of a preamble signal in each packet is 0.5 s, which is the same as the real acoustic modem [16]. The lengths of data and CP are 400 B and 40 B, respectively. The transmission rate of acoustic modems is 3 kbps. I use Rayleigh fading [7] to model the acoustic channel with mean value β_j [57], where β_j is proportional to the square of communication range, d_j^2. The default successful transmission rate of CPs is set as $p_j = p'_j \triangleq 0.98$ [8] for $j = 1, 2, \ldots, L-1$. The performance of CT-MAC with different p_j is also evaluated. Since the receiver in my simulations can support a maximum of 4 simultaneous transmissions, the upper-bound of the channel utilization is 400%.

From Fig. 6.13(a) we observe that the channel utilizations of all three MAC protocols are close in low traffic scenarios ($0 \leq \lambda_j \leq 0.02$). This is because with a small λ_j, nodes in all protocols have enough time to send out the generated packets. The channel utilization in this case is constrained by the traffic generation rate. However, with the growth of traffic rate, CT-MAC demonstrates remarkably higher channel utilization than the two representative MAC protocols, because the parallel competition mechanism of CT-MAC can avoid starving and supersaturated receptions with very low latency. By contrast, the poor collision avoidance ability of channel aware Aloha and the high latency of the handshake process in multi-antenna reception MAC lead to low channel utilization. I suggest that CT-MAC outperforms the random access based channel aware Aloha and handshake based multi-antenna reception MAC in terms of channel utilization.

[7] There have been extensive studies on modeling underwater horizontal channel [**?**,57,119]. However, the models of underwater vertical channel are still rare. The impact of different channel models on performance of the protocols will be discussed at the end of this section.

[8] According to the long term experimental results we collected at the Long Island Sound, the average delivery ratio of short packets can achieve at least 95% for the middle range (556 m) shallow water OFDM communications [120]. Higher delivery ratio can be expected for CP transmissions due to the shorter distance (200 m) and deeper water communication environments.

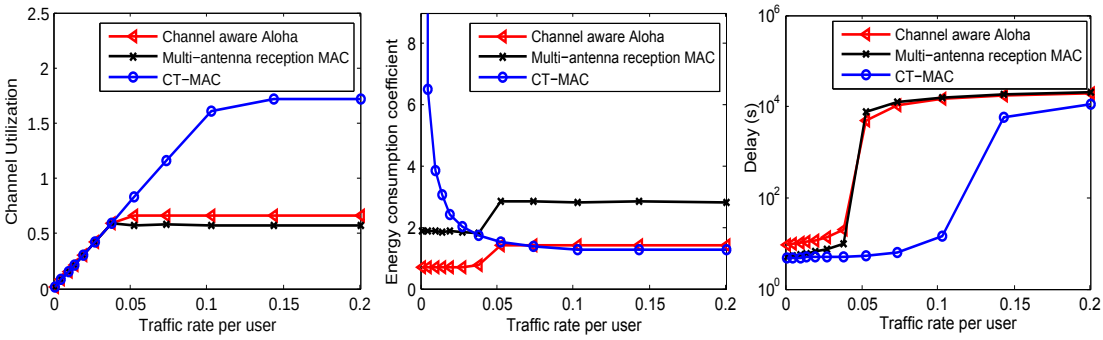

(a) Channel utilization (b) Energy efficiency (c) Delay

Figure 6.13: Performance comparisons among the three protocols with $p_j = 0.98$.

In Fig. 6.13(b), I use the energy consumption coefficient to evaluate the energy efficiency of the protocols. The energy consumption coefficient is calculated as the energy consumption on sending a single data packet dividing the total energy consumed on each successful data delivery, which takes the collision and control packet overhead into account. A high energy consumption coefficient stands for a low energy efficiency of a protocol.

As revealed in Fig. 6.13(b), the energy efficiency of CT-MAC is considerably lower than the other two protocols if the traffic rate is lower than 0.038 packets per second. In the low traffic rate situation, even if a node does not have any data to send, it still needs to transmit and forward PL information in each time slot. Therefore, the large overhead on CP transmissions results in a high energy consumption coefficient for CT-MAC at low traffic rates. However, with the growth of traffic rate, CT-MAC achieves comparable or even better energy efficiency than channel aware Aloha. The channel aware Aloha has low energy consumption because it only allows nodes with the best channels to send their data, which significantly improves the energy efficiency. However, the fairness issue will be a problem, as a node with bad channel (e.g., the node at the edge of a network) has less chance to send its data than a node with a good channel

quality. The multi-antenna reception MAC has the highest energy consumption among the three protocols due to the heavy overhead on broadcasting and retransmitting the control packets through long distance links.

Fig. 6.13(c) illustrates the end-to-end delays of the three protocols. When the traffic rate is lower than 0.038 packets per secs, the end-to-end delays of both CT-MAC and muti-antenna reception MAC are around 4.9 s, whereas channel aware Aloha has 9.5 s by contrast. In CT-MAC and muti-antenna reception MAC, the end-to-end delay at low traffic loads consists of the transmission time of control and data packets, and the propagation delay. Channel aware Aloha has extra delays waiting for the channel going good, since only nodes with the good channels are allowed to transmit. This explains why there are large delays in the channel aware Aloha with low traffic loads. When the traffic load goes heavy, the end-to-end delays of all protocols shapely increase as the channel starts to saturate. However, for different MAC protocols, the saturated traffic rates are different. Owing to the high channel utilization, CT-MAC can afford a much higher traffic rate than the other two protocols without overwhelming the acoustic channel, which results in the lowest end-to-end delay.

It is worth noting that the channel model I used in Fig. 6.13 is Rayleigh fading channel. This model is appropriate for the channels between the surface buoy and its furthest nodes, which are horizontal channels. For nodes underneath the buoy, the vertical channel has much less multipath, and the channel model, such as Rice [59] and Gaussian fading [57], may be more appropriate than the Rayleigh model. When the channel model used in simulations does not fit the channel in the real environment, the channel utilization of channel aware Aloha may be different from what I illustrated in Fig. 6.13, since the transmission strategy of this protocol is optimized based on the Rayleigh model. In addition, although the design of CT-MAC and muti-antenna

reception MAC is independent with the channel model I am using, it still affects the performance of these two protocols by affecting their packet (data or CP) loss ratio.

Table 6.1: Performance of CT-MAC with respect to the delivery ratio of CP (p_j).

	$L = 10$				$L = 20$			
	Max channel utilization		Min energy consumption		Max channel utilization		Min energy consumption	
p_j	Value	Percentage	Value	Percentage	Value	Percentage	Value	Percentage
1	1.94	100	7.02	100	1.84	100	6.84	100
0.98	1.73	89.18	7.18	102.24	1.15	62.19	7.35	107.42
0.95	1.39	71.37	7.55	107.49	0.18	9.53	14.33	209.40
0.93	1.15	59.15	7.89	112.27	0.08	4.24	23.80	347.94
0.9	0.83	42.67	8.73	124.24	0.04	2.33	40.09	585.98

The significant effect of CP loss on the performance of CT-MAC has been illustrated in Fig. 6.11. In order to give an insight into this problem, I compare the maximum channel utilization and the minimum energy consumption coefficient of CT-MAC with respect to different CP delivery ratios, and list the results in Table 6.1. The percentage values are relative to the situation with no CP loss ($p_j = 1$). On the one hand, the channel utilization of CT-MAC is remarkably affected by p_j. When p_j decreases from 1 to 0.95 for $L = 10$, the channel utilization reduces by about 30%. It is acceptable as the performance of CT-MAC in this case is still better than the channel aware Aloha and multi-antenna reception MAC. However, when p_j continuously decreases to 0.9 for $L = 10$, the degradation on channel utilization will be too high to work efficiently, due to the significant CP loss. On the other hand, the energy efficiency is less affected by p_j. Compared with the scenario of no CP loss, only 20% additional energy is consumed when $p_j = 0.9$. This is because the lost CPs do not increase the collision of data packet with overestimation scheme. From Table 6.1 we also observe that CT-MAC cannot work well in a large size network with low CP delivery ratio. For $L = 20$, CT-MAC cannot work efficiently when p_j is lower 0.98. When $p_j = 0.9$, most of PLs are lost by nodes and no data could be sent, which results in the channel utilization reducing by 97% and the energy consumption increasing by 486%.

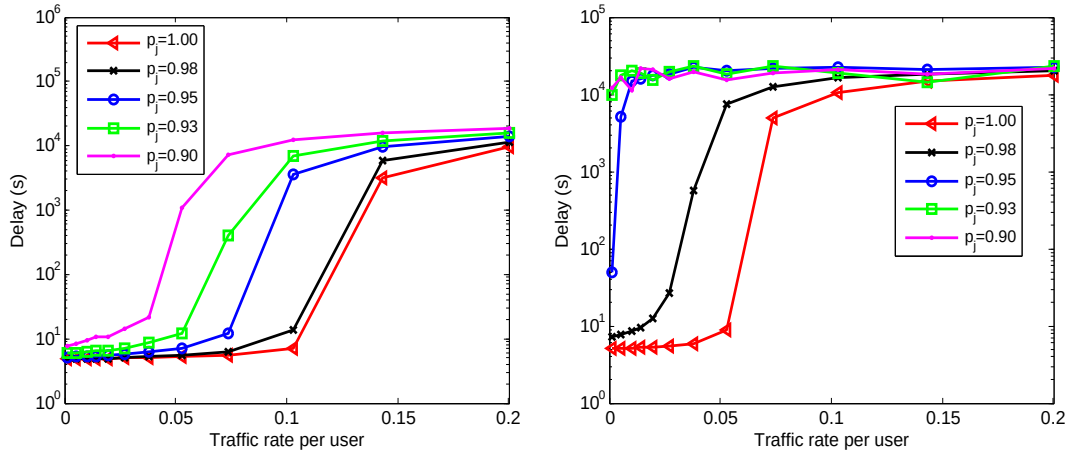

(a) L=10 (b) L=20

Figure 6.14: Delay of CT-MAC with respect to the delivery ratio of CP and traffic generation rate.

In Fig. 6.14, I show the end-to-end delays of CT-MAC with respect to the delivery ratio of CP and traffic generation rate. It is easy to observe that the delays have sharp increase when the traffic load reaches to a certain threshold. In another word, when the traffic generation rate exceeds the throughput a network, tremendous packets will be accumulated and cause considerable end-to-end delays. The increase of CP loss ratio reduces the channel utilization of CT-MAC, which results in a lower threshold, as shown in Fig. 6.14. For example, when $L=10$ and $p_j=1$, the end-to-end delay increases significantly if traffic rate higher than 0.12. This threshold is reduced to 0.038 when $p_j = 0.9$. Moreover, when considering the lost CPs, a large size network ($L = 20$) has incredibly long delays at low traffic rates. It can be observed by comparing the traffic rate thresholds in Fig. 6.14(a) with that in Fig. 6.14(b). This is because a larger network has more PL losses in average than a smaller network, causing considerable waste of data transmission opportunities in overestimation scheme. The degraded channel utilization of CT-MAC makes the packet cannot be sent out timely and leads to long end-to-end delays.

The results in Table 6.1 and Fig. 6.14 reveal the fact that the reliable transmission of CP is crucially important to CT-MAC, especially in a large size network. In order to guarantee the efficiency of this protocol, the feasible solutions include (a) increasing the reliability of CP delivery, especially in a large size network, and (b) dividing the large network into small ones, and let each subnetwork runs CT-MAC in parallel.

6.9 Summary

In this chapter, I presented CT-MAC for underwater multi-node uplink communication networks. In CT-MAC, the unique features of underwater acoustic systems, such as the long propagation delay, low transmission rate and long preamble of acoustic modem are considered carefully. To improve the channel utilization, the energy efficiency and end-to-end delay, nodes in CT-MAC use a parallel competition scheme to compete for the data transmission opportunities. With this scheme, data generated by nodes in different time slots can join the transmission competitions in parallel, and the control packets from each node only need to reach its direct neighbors instead of the whole network.

Additionally, two competition schemes are proposed for the fair transmission in networks with both homogeneous and heterogeneous traffic generation rates. Moreover, two specific problems, namely, the bad request issue and the lost CP problem in CT-MAC are studied. The solutions to address these problems are also proposed in this chapter.

Finally, I evaluate the performance of CT-MAC through theoretical analysis and simulations. Compared to the channel aware Aloha and the multi-antenna reception MAC, CT-MAC has higher channel utilization under a wide range of traffic generation rates. Especially in a high traffic scenario, the channel utilization of CT-MAC is about 3.15 and 3.4 times higher than the channel aware Aloha and the multi-antenna

reception MAC, respectively. Moreover, the energy consumption per each successful data transmission of CT-MAC at the high traffic rates also outperforms the other two protocols. Finally, CT-MAC has remarkably lower end-to-end delay than the channel aware Aloha and the multi-antenna reception MAC, as the high channel utilization allows CT-MAC to send packets in a much faster way without overwhelming the acoustic channel. However, the performance of CT-MAC considerably relays on the reliable transmission of CP. Once the delivery ratio of CP is low, the performance of CT-MAC will degrade significantly, which should be avoided in the real applications.

Chapter 7

Conclusions

UAN is a key enabling technique to explore the oceans. Today, both the acoustic communication technology and the sensor technology are mature enough to motivate the idea of UAN. To turn this idea into reality, however, one must face some real challenges prosed by the unique features of UANs.

In this dissertation, I introduced several critical features of acoustic communications, such as the long propagation delay of acoustic signal and narrow communication bandwidth of acoustic system, that have attracted people's attention in both academia and industry. Other unique problems, like the heavily shared acoustic channel and long preamble sequence of acoustic that are still overlooked by the research community were also studied.

According the analysis I found that compared with terrestrial radio network, the unique features of UANs might significantly reduce the utilization of acoustic channel, increase the time and energy consumption on transmissions of control messages and challenge the ability of coexistence among acoustic systems. Existing acoustic networks may not be able to handle these problems very well. With this in mind, I proposed new communications techniques, namely COP-COM, COG-COM and COD-COM for UANs.

COP-COM essentially is a cooperative multiple transmitter technique for improving the channel capacity. It exploits the diversity of channel by combining signals from the source and the relay at the detonation. In the dissertation, I presented two works for COM-COM:

• *COBRA*: It is a new best relay selection criterion that I proposed for underwater cooperative networks. Different from existing criteria, which mainly consider the channel quality, and choose the relay to maximize the transmission rate of the source node, COBRA takes the long propagation delay of acoustic signal into account, and selects the relay to minimize the OPT time. Simulation results demonstrated that the throughput and the end-to-end delay of a cooperative network with COBRA is about 20% higher and 4% than it with the channel quality based criterion, respectively.

• *MNAC*: It is a novel cooperative scheme for UANs. Different from existing cooperative schemes, which utilize the spatial diversity of wireless channel to improve the receiving SNR at the destination, MNAC improves the network performance by allowing multiple data streams to transmit in parallel without causing any collisions. I achieved this through selecting a mirror node for each specific source node, and made signals from the source and the detonation add destructively at a protected receiver. Therefore, the data from an intended receiver to the protected receiver would not be disrupted by the mirror assisted source node, several independent data stream thus could travel in the same channel without interfering each other. Simulation results illustrated that compared with non-mirror node assisted situation, the performance of a network in terms of throughput and the delay was dramatically improved with MNAC. However, from my analysis I also observed that MNAC is sensitive to the error of distance measurement and the bandwidth of a signal, a small error and a wide frequency band could significantly degrade the performance of MNAC. Through using the pre-filter to line up the phase of sub frequencies before the transmission of a mirror

signal, the problem caused by the wideband signal on MNAC was solved. How to increase the resilience of MNAC on error of distance measurement, however, is still an open issue.

In addition to COP-COM, I proposed COG-COM to handle the coexistence problem between UANs and marine mammals. According to analysis, existing MAC protocol proposed for CR, may work inefficient in underwater environment due to the long propagation delay and high cost of control overhead. To make the cognitive technique reliable in underwater environment, in this dissertation I developed a new system and designed a new MAC protocol for UCANs:

• *RISM system*: One important feature of RISM is that it considers the spectrum sensing, the spectrum sharing and the spectrum decision as a whole rather than three independent components that assumed in CR network. With this feature, different components could attach their information on the same control message without generating too much overhead traffic. In addition, RISM starts a handshake process at the receiver side to instead of the sender-initiated one. Therefore, a receiver in RISM could work as a small control center to collect the information from neighboring senders or allocate the transmission power and channel to its neighbors efficiently. According to simulation results I observed that the throughput and of RISM is 6 times higher and than MMAC-CR, a IEEE 802.11 based cognitive MAC. Meanwhile, its hop-by-hop delay in only one-fourth of MMAC-CR. Moreover, RISM could work better in a tree network than in a mesh network. The throughput in the former scenario is nearly twice than that in the later one, while maintaining comparable hop-by-hop delay and energy consumption.

• *DCC-MAC*: Many MAC protocols for cognitive network transmit control messages on CCC. However, the CCC may congest in some situations, thereby limiting the performance of a network. To handle this problem, I proposed DCC-MAC in this

dissertation. One of the most important feature of DCC-MAC is that each node in this protocol could smartly adjust the bandwidth of control channel by "borrowing" frequency band from the in-band data channel when the traffic is heavy, and "returning" them back when the traffic becomes light. Our simulation results demonstrated that DCC-MAC could efficiently eliminate the congestion problem of CCC, and improve the network performance significantly in terms of throughput and end-to-end delay.

COD-COM was the last thread of this dissertation. It aimed to coordinated the sending and receiving activities among acoustic nodes for performance improvement of UANs. In this thread, I focused on improving the performance of underwater multi-node uplink communication network. The goal was to maximize sum-rate capacity of the uplink network. To achieve this goal, a dedicated MAC protocol was proposed:

• *CT-MAC*: In CT-MAC, each node uses only a small transmission power to broadcast the control message to its neighbors instead of the whole network. Compared with conventional handshake based MAC protocols, this strategy is very helpful to reduce the energy consumption, propagation relay and the collision probability of control packets. At the same time, I designed a parallel competition scheme for CT-MAC to allow nodes with new data to quickly participate in a new round of competition mechanism before the results of the old one is announced. In this way, a node could join in multiple rounds of competitions in parallel, which significantly improves the competition efficiency of the protocol. In order to have a fair transmission in different network conditions, I also proposed two specific competition schemes for CT-MAC. The theoretical analysis and simulation results illustrated that CT-MAC could achieve both the short-term and the long-term fairness in different network scenarios. Additionally, compared to the channel aware Aloha and the multi-antenna reception MAC, CT-MAC has higher channel utilization and much lower end-to-end delay, while maintaining comparable energy efficiency. Especially in the high traffic generation rate scenario, the channel

utilization of CT-MAC is about 3.15 and 3.4 times higher than the two representative MAC protocols, respectively. From both the theoretical analysis and the simulation I also observed that CT-MAC is susceptible to lose of control packet. Therefore, to make CT-MAC reliable in real UANs, a high delivery ratio of control packets is required.

In general, the work presented in this dissertation could be considered as a cross-layer design between the physical layer and the MAC layer. All three techniques studied here aimed to increase the channel efficiency of existing UANs. I hope my work could give people an insight into the features and challenges of a UAN, and inspirit people to propose feasible solutions for more efficient, more reliable and more environment-friendly UANs in the future.

Bibliography

[1] National Oceanic and Atmospheric Administration. Oceans. noaa.gov. [Online]. Available: http://www.noaa.gov/ocean.html. [Accessed: December, 2015].

[2] European Wind Energy Association. The european offshore wind industry: Key trends and statistics 2012. ewea.org. [Online]. Available: http://www.ewea.org/fileadmin/files/library/publications/statistics/European_offshore_statistics_2012.pdf, 2012. [Accessed: December, 2015].

[3] The Bureau of Ocean Energy Management. Offshore stats and facts. boem.gov. [Online]. Available: http://www.boem.gov/uploadedFiles/BOEM/Newsroom/Offshore_Stats_and_Facts/Gulf_of_Mexico_Region/OCSPlatformActivity.pdf, 2010. [Accessed: January, 2010].

[4] Center for International Earth Science Information Network. Percentage of total population living in coastal areas. sedac.ciesin.columbia.edu. [Online]. Available: http://sedac.ciesin.columbia.edu/es/papers/Coastal_Zone_Pop_Method.pdf, 2008. [Accessed: December, 2015].

[5] Australian Bureau of Statistics. Mineral and petroleum exploration. abs.gov.au. [Online]. Available: `http://www.abs.gov.au/ausstats/abs@.nsf/mf/8412.0/`, 2012. [Accessed: December, 2015].

[6] John Heidemann, Milica Stojanovic, and Michele Zorzi. Underwater sensor networks: Applications, advances and challenges. *Philosophical Transactions of the Royal Society A: Mathematical, Physical and Engineering Sciences*, 370(1958):158–175, 2012.

[7] John Heidemann, Wei Ye, Jack Wills, Affan Syed, and Yuan Li. Research challenges and applications for underwater sensor networking. In *Proceedings of Wireless Communications and Networking Conference (WCNC)*, volume 1, pages 228–235. IEEE, 2006.

[8] Zheng Peng, Son Le, Michael Zuba, Haining Mo, Yibo Zhu, Lina Pu, Jun Liu, and Jun-Hong Cui. Aqua-TUNE: A testbed for underwater networks. In *Proceedings of OCEANS*, pages 1–9, Santander, Spain, 2011. IEEE.

[9] Yao-Win Hong, Wan-Jen Huang, Fu-Hsuan Chiu, and C-CJ Kuo. Cooperative communications in resource-constrained wireless networks. *IEEE Signal Processing Magazine*, 24(3):47–57, 2007.

[10] J Nicholas Laneman, David NC Tse, and Gregory W Wornell. Cooperative diversity in wireless networks: Efficient protocols and outage behavior. *IEEE Transactions on Information Theory*, 50(12):3062–3080, 2004.

[11] Mohammad Janani, Ahmadreza Hedayat, Todd E Hunter, and Aria Nosratinia. Coded cooperation in wireless communications: Space-time transmission and iterative decoding. *IEEE Transactions on Signal Processing*, 52(2):362–371, 2004.

[12] Gerhard Kramer, Michael Gastpar, and Piyush Gupta. Cooperative strategies and capacity theorems for relay networks. *IEEE Transactions on Information Theory*, 51(9):3037–3063, 2005.

[13] Yu Luo, Lina Pu, Zheng Peng, Zhong Zhou, Jun-Hong Cui, and Zhaoyang Zhang. Effective relay selection for underwater cooperative acoustic networks. In *Proceedings of the International Conference on Mobile Ad-Hoc and Sensor Systems (MASS)*, pages 104–112. IEEE, 2013.

[14] Yu Luo, Lina Pu, Michael Zuba, Zheng Peng, and Jun-Hong Cui. Cognitive acoustics: Making underwater communications environment-friendly. In *Proceedings of the International Conference on Underwater Networks & Systems (WUWNet)*, pages 48–49. ACM, 2014.

[15] Yu Luo, Lina Pu, Michael Zuba, Zheng Peng, and Jun-Hong Cui. Challenges and opportunities of underwater cognitive acoustic networks. *IEEE Transactions on Emerging Topics in Computing*, 2(2):198–211, 2014.

[16] Lina Pu, Yu Luo, Yibo Zhu, Zheng Peng, Jun-Hong Cui, Shruti Khare, Lei Wang, and Benyuan Liu. Impact of real modem characteristics on practical underwater MAC design. In *Proceedings of OCEANS*, pages 1–6, Yeosu, Korea, 2012. IEEE.

[17] Yu Luo, Lina Pu, Zheng Peng, Yibo Zhu, and Jun-Hong Cui. RISM: An efficient spectrum management system for underwater cognitive acoustic networks. In *Proceedings of the International Conference on Sensing, Communication, and Networking (SECON)*, pages 414–422. IEEE, 2014.

[18] Qing Zhao, Lang Tong, Ananthram Swami, and Yunxia Chen. Decentralized cognitive MAC for opportunistic spectrum access in ad hoc networks: A POMDP

framework. *IEEE Journal on Selected Areas in Communications*, 25(3):589–600, 2007.

[19] Juncheng Jia, Qian Zhang, and Xuemin Shen. HC-MAC: A hardware-constrained cognitive MAC for efficient spectrum management. *IEEE Journal on Selected Areas in Communications*, 26(1):106–117, 2008.

[20] Michael Timmers, Sofie Pollin, Antoine Dejonghe, Liesbet Van der Perre, and Francky Catthoor. A distributed multichannel MAC protocol for multihop cognitive radio networks. *IEEE Transactions on Vehicular Technology*, 59(1):446–459, 2010.

[21] Myonghee Park, Kyunbyoung Ko, Hwasun Yoo, and Daesik Hong. Performance analysis of OFDMA uplink systems with symbol timing misalignment. *IEEE Communications Letters*, 7(8):376–378, 2003.

[22] Andrew LC Hui and Khaled Letaief. Successive interference cancellation for multiuser asynchronous DS/CDMA detectors in multipath fading links. *IEEE Transactions on Communications*, 46(3):384–391, 1998.

[23] Zhaohui Wang, Shengli Zhou, Josko Catipovic, and Peter Willett. Asynchronous multiuser reception for OFDM in underwater acoustic communications. In *Proceedings of OCEANS*, pages 1–6, Yeosu, Korea, 2012. IEEE.

[24] Yu Luo, Lina Pu, Zheng Peng, Zhong Zhou, and Jun-Hong Cui. An efficient MAC protocol for underwater multi-user uplink communication networks. *Ad Hoc Networks*, 34:75–91, 2015.

[25] Xiangping Qin and Randall Berry. Exploiting multiuser diversity for medium access control in wireless networks. In *Proceedings of the International Conference*

on Computer Communications (INFOCOM), volume 2, pages 1084–1094. IEEE, 2003.

[26] Norihiko Sato and Takeo Fujii. A MAC protocol for multi-packet ad-hoc wireless network utilizing multi-antenna. In *Proceedings of Consumer Communications and Networking Conference (CCNC)*, pages 1–5. IEEE, 2009.

[27] Zheng Peng Yu Luo, Lina Pu and Jun-Hong Cui. Dynamic control channel MAC for underwater cognitive acoustic networks. In *Proceedings of the International Conference on Computer Communications (INFOCOM)*. IEEE, 2016. (Accepted).

[28] Moray Rumney. Imt-advanced: 4g wireless takes shape in an olympic year. *Agilent Measurement Journal*, 1:1–10, 2008.

[29] Eldad Perahia and Robert Stacey. *Next generation wireless LANs: 802.11 n and 802.11 ac*. Cambridge university press, 2013.

[30] Xavier Lurton. *An introduction to underwater acoustics: Principles and applications*. Springer Science & Business Media, 2002.

[31] RE Francois and GR Garrison. Sound absorption based on ocean measurements: Part I: Pure water and magnesium sulfate contributions. *The Journal of the Acoustical Society of America*, 72(3):896–907, 1982.

[32] RE Francois and GR Garrison. Sound absorption based on ocean measurements. Part II: Boric acid contribution and equation for total absorption. *The Journal of the Acoustical Society of America*, 72(6):1879–1890, 1982.

[33] Teledyne Benthos Incorporation. Benthos modem. teledynebenthos.com [Online]. Available: `http://teledynebenthos.com/product`. [Accessed: May, 2015].

[34] Evologics GmbH Incorporation. Evologics modem. evologics.de [Online]. Available: `http://www.evologics.de/en/products/acoustics/index.html`. [Accessed: May, 2015].

[35] Aquasent Company. AM-OFDM-S1 acoustic modem. aquasent.com. [Online]. Available: `http://www.aquasent.com/acoustic-modems/`. [Accessed: December, 2014].

[36] M.M. Wang, A. Agrawal, A. Khandekar, and S. Aedudodla. Preamble design, system acquisition, and determination in modern OFDMA cellular communications: An overview. *IEEE Communications Magazine*, 49(7):164–175, 2011.

[37] C. Stevenson, G. Chouinard, Z. Lei, W. Hu, S. Shellhammer, and W. Caldwell. IEEE 802.22: The first cognitive radio wireless regional area network standard. *IEEE Communications Magazine*, 47(1):130–138, 2009.

[38] W.J. Richardson and D.H. Thomson. *Marine mammals and noise*. Academic Press, 1998.

[39] Chane L Fullmer and JJ Garcia-Luna-Aceves. Floor acquisition multiple access (FAMA) for packet-radio networks. In *Proceedings of the Conference on Applications, Technologies, Architectures, and Protocols for Computer Communication (SIGCOMM)*, pages 262–273. ACM, 1995.

[40] Chane L Fullmer and JJ Garcia-Luna-Aceves. FAMA-PJ: A channel access protocol for wireless LANs. In *Proceedings of the International Conference on Mobile Computing and Networking (MobiCom)*, pages 76–85. ACM, 1995.

[41] Zheng Peng, Yibo Zhu, Zhong Zhou, Zheng Guo, and Jun-Hong Cui. COPE-MAC: A contention-based medium access control protocol with parallel reservation for underwater acoustic networks. In *Proceedings of OCEANS*, pages 1–10,

Sydney, Australia, 2010. IEEE.

[42] Nitthita Chirdchoo, Wee-Seng Soh, and Kee Chaing Chua. MACA-MN: A MACA-based MAC protocol for underwater acoustic networks with packet train for multiple neighbors. In *Proceedings of Vehicular Technology Conference (VTC)*, pages 46–50. IEEE, 2008.

[43] Son Le, Jun Liu, Zheng Peng, Jiaxing Che, Yu Luo, and Jun-Hong Cui. Seamark-assisted inertial navigation for autonomous underwater vehicles. In *Proceedings of the International Conference on Underwater Networks & Systems (WUWNet)*, pages 1–8. ACM, 2014.

[44] Saurabh Ganeriwal, Ram Kumar, and Mani B Srivastava. Timing-sync protocol for sensor networks. In *Proceedings of the International Conference on Embedded Networked Sensor Systems (SenSys)*, pages 138–149. ACM, 2003.

[45] Lina Pu, Yu Luo, and Jun-Hong Cui. Exploring underwater synchronization protocols in real systems. Technical Report Technical Report: UbiNet-TR15-01, UCONN CSE, 2014.

[46] Rohit U Nabar, Helmut Bolcskei, and Felix W Kneubuhler. Fading relay channels: Performance limits and space-time signal design. *IEEE Journal on Selected Areas in Communications*, 22(6):1099–1109, 2004.

[47] J Nicholas Laneman and Gregory W Wornell. Distributed space-time-coded protocols for exploiting cooperative diversity in wireless networks. *IEEE Transactions on Information Theory*, 49(10):2415–2425, 2003.

[48] Madhavan Vajapeyam, Satish Vedantam, Urbashi Mitra, James C Preisig, and Milica Stojanovic. Distributed space-time cooperative schemes for underwater

acoustic communications. *IEEE Journal of Oceanic Engineering*, 33(4):489–501, 2008.

[49] Zhu Han, Yan Lindsay Sun, and Hongyuan Shi. Cooperative transmission for underwater acoustic communications. In *Proceedings of International Conference on Communications (ICC)*, pages 2028–2032. IEEE, 2008.

[50] Cecilia Carbonelli and Urbashi Mitra. Cooperative multihop communication for underwater acoustic networks. In *Proceedings of the International Conference on Underwater Networks & Systems (WUWNet)*, pages 97–100. ACM, 2006.

[51] Shuguang Cui, Andrea J Goldsmith, and Ahmad Bahai. Energy-efficiency of MIMO and cooperative MIMO techniques in sensor networks. *IEEE Journal onSelected Areas in Communications*, 22(6):1089–1098, 2004.

[52] Zhong Zhou, Shengli Zhou, Jun-Hong Cui, and Shuguang Cui. Energy-efficient cooperative communication based on power control and selective single-relay in wireless sensor networks. *IEEE Transactions on Wireless Communications*, 7(8):3066–3078, 2008.

[53] Kanchan Vardhe, Daryl Reynolds, and Brian D Woerner. Joint power allocation and relay selection for multiuser cooperative communication. *IEEE Transactions on Wireless Communications*, 9(4):1255–1260, 2010.

[54] Aggelos Bletsas, Ashish Khisti, David P Reed, and Andrew Lippman. A simple cooperative diversity method based on network path selection. *IEEE Journal on Selected Areas in Communications*, 24(3):659–672, 2006.

[55] Hangguan Shan, Weihua Zhuang, and Zongxin Wang. Distributed cooperative MAC for multihop wireless networks. *IEEE Communications Magazine*, 47(2):126–133, 2009.

[56] R. J. Urick. *Sound propagation in the sea*. Peninsula Publishing, Los Altos, CA, 1982.

[57] Mandar Chitre, John Potter, and Ong Sim Heng. Underwater acoustic channel characterisation for medium-range shallow water communications. In *Proceedings of OCEANS*, pages 40–45, Kobe, Japan, 2004. IEEE.

[58] W.B. Yang and TC Yang. Characterization and modeling of underwater acoustic communications channels for frequency-shift-keying signals. In *Proceedings of OCEANS*, pages 1–6, Boston, USA, 2006.

[59] Fernando Ruiz-Vega, M Carmen Clemente, Pablo Otero, and José F Paris. Ricean shadowed statistical characterization of shallow water acoustic channels for wireless communications. In *Proceedings of Underwater Communications & Networking (UComms)*, pages 1–3. IEEE, 2012.

[60] M. Balazs. Sum of independent exponentials. maths.bris.ac.uk. [Online]. Available: `http://www.maths.bris.ac.uk/~mb13434/sumexp.pdf`. [Accessed: December, 2015].

[61] James Preisig. Acoustic propagation considerations for underwater acoustic communications network development. *SIGMOBILE Mobile Computing and Communications Review*, 11(4):2–10, 2007.

[62] Max Born and Emil Wolf. *Principles of optics: Electromagnetic theory of propagation, interference and diffraction of light*. Cambridge university press, 1999.

[63] Marvin K Simon and Mohamed-Slim Alouini. *Digital communication over fading channels*, volume 95. John Wiley & Sons, 2005.

[64] Leonid Maksimovich Brekhovskikh and Y. Pavlovich Lysanov. *Fundamentals of ocean acoustics*. Springer Science & Business Media, 2003.

[65] Baosheng Li, Shengli Zhou, Milica Stojanovic, Lee Freitag, and Peter Willett. Multicarrier communication over underwater acoustic channels with nonuniform Doppler shifts. *IEEE Journal of Oceanic Engineering*, 33(2):198–209, 2008.

[66] Lei Wan, Hao Zhou, Xiaoka Xu, Yi Huang, Sengli Zhou, Zhijie Shi, and Jun-Hong Cui. Adaptive modulation and coding for underwater acoustic OFDM. *IEEE Journal of Oceanic Engineering*, 40(2):327–336, 2015.

[67] Dinesh Bharadia and Sachin Katti. FastForward: Fast and constructive full duplex relays. In *Proceedings of the Conference on Applications, Technologies, Architectures, and Protocols for Computer Communication (SIGCOMM)*, pages 199–210. ACM, 2014.

[68] Kyle Jamieson, Hari Balakrishnan, and YC Tay. Sift: A MAC protocol for event-driven wireless sensor networks. In *Proceedings of the European Workshop on Wireless Sensor Networks (EWSN)*, pages 260–275. ETH Zurich, 2006.

[69] Milosav Andelic, Stevan Berber, and Akshya Swain. Collaborative event driven energy efficient protocol (CEDEEP). *IEEE Wireless Communications Letters*, 2(2):231–234, 2013.

[70] Lucas DP Mendes and Joel JPC Rodrigues. A survey on cross-layer solutions for wireless sensor networks. *Journal of Network and Computer Applications*, 34(2):523–534, 2011.

[71] Affan A Syed and John S Heidemann. Time synchronization for high latency acoustic networks. In *Proceedings of the International Conference on Computer Communications (INFOCOM)*, pages 1–12. IEEE, 2006.

[72] Son N Le, Yibo Zhu, Jun-Hong Cui, and Zaihan Jiang. Pipelined transmission MAC for string underwater acoustic networks. In *Proceedings of the International*

Conference on Underwater Networks & Systems (WUWNet), pages 1–9. ACM, 2013.

[73] Li Wei, Z Peng, Hao Zhou, Jun-Hong Cui, Shengli Zhou, Zhijie Shi, and James O'Donnell. Long island sound testbed and experiments. In *Proceedings of OCEANS*, pages 23–26, San Diego, USA.

[74] Xiaoxing Guo, Michael R Frater, and Michael J Ryan. Design of a propagation-delay-tolerant mac protocol for underwater acoustic sensor networks. *IEEE Journal of Oceanic Engineering*, 34(2):170–180, 2009.

[75] Yu Luo, Lina Pu, Zheng Peng, Zhong Zhou, and Jun-Hong Cui. CT-MAC: A MAC protocol for underwater MIMO based network uplink communications. In *Proceedings of the International Conference on Underwater Networks & Systems (WUWNet)*, pages 1–8. ACM, 2012.

[76] Nicola Baldo, Paolo Casari, and Michele Zorzi. Cognitive spectrum access for underwater acoustic communications. In *Proceedings of the International Conference on Communications (ICC)*, pages 518–523. IEEE, 2008.

[77] Wang Yonggang, Tang Jiansheng, Pan Yue, and Huangfu Li. Underwater communication goes cognitive. In *Proceedings of OCEANS*, Quebec City, Canada, 2008. IEEE.

[78] Wendong Hu, Daniel Willkomm, Murad Abusubaih, James Gross, George Vlantis, Mario Gerla, and Adam Wolisz. Cognitive radios for dynamic spectrum access-dynamic frequency hopping communities for efficient IEEE 802.22 operation. *IEEE Communications Magazine*, 45(5):80–87, 2007.

[79] Hyoil Kim and Kang G Shin. Efficient discovery of spectrum opportunities with MAC-layer sensing in cognitive radio networks. *IEEE Transactions on Mobile Computing*, 7(5):533–545, 2008.

[80] Carlos Cordeiro and Kiran Challapali. C-MAC: A cognitive MAC protocol for multi-channel wireless networks. In *Proceedings of the International Symposium on New Frontiers in Dynamic Spectrum Access Networks (DySPAN)*, pages 147–157. IEEE, 2007.

[81] Qian Chen, Ying-Chang Liang, Mehul Motani, and Wai-Choong Wong. A two-level MAC protocol strategy for opportunistic spectrum access in cognitive radio networks. *IEEE Transactions on Vehicular Technology*, 60(5):2164–2180, 2011.

[82] Antonio De Domenico, Emilio Calvanese Strinati, and M-G Di Benedetto. A survey on MAC strategies for cognitive radio networks. *IEEE Communications Surveys & Tutorials*, 14(1):21–44, 2012.

[83] Kyouwoong Kim, IA Akbar, KK Bae, Jung-sun Urn, CM Spooner, and JH Reed. Cyclostationary approaches to signal detection and classification in cognitive radio. In *Proceedings of the International Symposium on New Frontiers in Dynamic Spectrum Access Networks (DySPAN)*, pages 212–215, 2007.

[84] Brian M. Sadler and Amod V. Dandawate. Nonparametric estimation of the cyclic cross spectrum. *IEEE Transactions on Information Theory*, 44(1):351–358, 1998.

[85] Jarmo Lundén, Visa Koivunen, Anu Huttunen, and H Vincent Poor. Collaborative cyclostationary spectrum sensing for cognitive radio systems. *IEEE Transactions on Signal Processing*, 57(11):4182–4195, 2009.

[86] E. T. Ar and I. E. Telatar. Capacity of Multi-antenna Gaussian Channels. *European Transactions on Telecommunications*, 10:585–595, 1999.

[87] Cheong Yui Wong, Roger S Cheng, K Ben Lataief, and Ross D Murch. Multiuser OFDM with adaptive subcarrier, bit, and power allocation. *IEEE Journal on Selected Areas in Communications*, 17(10):1747–1758, 1999.

[88] Fadel F Digham. Joint power and channel allocation for cognitive radios. In *Proceedings of Wireless Communications and Networking Conference (WCNC)*, pages 882–887. IEEE, 2008.

[89] Lina Pu, Yu Luo, Zheng Peng, Haining Mo, and Jun-Hong Cui. Traffic estimation based receiver initiated MAC for underwater acoustic networks. In *Proceedings of the International Conference on Underwater Networks & Systems (WUWNet)*, pages 1–9. ACM, 2013.

[90] Simon S Haykin. *Adaptive filter theory*. Pearson Education India, 2008.

[91] B Yegnanarayana. *Artificial neural networks*. Prentice Hall of India Private Limited, 2009.

[92] Eric A Wan. *Finite impulse response neural networks with applications in time series prediction*. PhD thesis, Department of Electrical Engineering, Stanford University, California, USA, 1993.

[93] Peng Xie, Zhong Zhou, Zheng Peng, Hai Yan, Tiansi Hu, Jun-Hong Cui, Zhijie Shi, Yunsi Fei, and Shengli Zhou. Aqua-Sim: An NS-2 based simulator for underwater sensor networks. In *Proceedings of OCEANS*, pages 1–7, Biloxi, Mexico, 2009.

[94] Jungmin So and Nitin H Vaidya. Multi-channel MAC for ad hoc networks: Handling multi-channel hidden terminals using a single transceiver. In *Proceedings*

of the International Symposium On Mobile Ad Hoc Networking and Computing (MobiHoc), pages 222–233. ACM, 2004.

[95] Liangping Ma, Chien-Chung Shen, and Bo Ryu. Single-radio adaptive channel algorithm for spectrum agile wireless ad hoc networks. In *Proceedings of the International Symposium on New Frontiers in Dynamic Spectrum Access Networks (DySPAN)*, pages 547–558. IEEE, 2007.

[96] Yogesh Reddy Kondareddy and Prathima Agrawal. Synchronized MAC protocol for multi-hop cognitive radio networks. In *Proceedings of the International Conference on Communications (ICC)*, pages 3198–3202. IEEE, 2008.

[97] Nick C Theis, Ryan W Thomas, and Luiz A DaSilva. Rendezvous for cognitive radios. *IEEE Transactions on Mobile Computing*, 10(2):216–227, 2011.

[98] Carlos Cordeiro, Kiran Challapali, Dagnachew Birru, and Nov Sai Shankar. IEEE 802.22: The first worldwide wireless standard based on cognitive radios. In *Proceedings of the International Symposium on New Frontiers in Dynamic Spectrum Access Networks (DySPAN)*, pages 328–337. IEEE, 2005.

[99] Hang Su and Xi Zhang. Cross-layer based opportunistic MAC protocols for QoS provisionings over cognitive radio wireless networks. *IEEE Journal on Selected Areas in Communications*, 26(1):118–129, 2008.

[100] Jun Zhao, Haitao Zheng, and Guang-Hua Yang. Distributed coordination in dynamic spectrum allocation networks. In *Proceedings of the International Symposium on New Frontiers in Dynamic Spectrum Access Networks (DySPAN)*, pages 259–268. IEEE, 2005.

[101] Teledyne Benthos Incorporation. ATM-903 acoustic modem. teledynebenthos.com [Online]. Available: `http://teledynebenthos.com/product/acoustic_modems/903-series-atm-903`. [Accessed: December, 2015].

[102] Maxime Guillaud, Dirk TM Slock, and Raymond Knopp. A practical method for wireless channel reciprocity exploitation through relative calibration. In *Proceedings of the International Symposium on Signal Processing and Its Applications (ISSAP)*, pages 403–406. IEEE, 2005.

[103] Erik Axell, Geert Leus, Erik G Larsson, and H Vincent Poor. Spectrum sensing for cognitive radio: State-of-the-art and recent advances. *IEEE Signal Processing Magazine*, 29(3):101–116, 2012.

[104] Paul D Sutton, Keith E Nolan, and Linda E Doyle. Cyclostationary signatures in practical cognitive radio applications. *IEEE Journal on Selected Areas in Communications*, 26(1):13–24, 2008.

[105] Milica Stojanovic and James Preisig. Underwater acoustic communication channels: Propagation models and statistical characterization. *IEEE Communications Magazine*, 47(1):84–89, 2009.

[106] Zhong Zhou, Zheng Peng, Jun-Hong Cui, and Zaihan Jiang. Handling triple hidden terminal problems for multichannel MAC in long-delay underwater sensor networks. *IEEE Transactions on Mobile Computing*, 11(1):139–154, 2012.

[107] Nader Mohamed, Imad Jawhar, Jameela Al-Jaroodi, and Liren Zhang. Sensor network architectures for monitoring underwater pipelines. *Sensors*, 11(11):10738–10764, 2011.

[108] Yi Huang, Lei Wan, Shengli Zhou, Zhaohui Wang, and Jianzhong Huang. Comparison of sparse recovery algorithms for channel estimation in underwater acoustic OFDM with data-driven sparsity learning. *Elsevier Journal on Physical Communication*, 13:156–167, 2014.

[109] Thomas M Cover and Joy A Thomas. *Elements of information theory*. John Wiley & Sons, 2012.

[110] Andrea Goldsmith, Syed Ali Jafar, Nihar Jindal, and Sriram Vishwanath. Capacity limits of MIMO channels. *IEEE Journal on Selected Areas in Communications*, 21(5):684–702, 2003.

[111] Nihar Jindal and Andrea Goldsmith. Dirty-paper coding versus TDMA for MIMO broadcast channels. *IEEE Transactions on Information Theory*, 51(5):1783–1794, 2005.

[112] Wei Yu, Wonjong Rhee, and John M Cioffi. Optimal power control in multiple access fading channels with multiple antennas. In *Proceedings of the International Conference on Communications (ICC)*, volume 2, pages 575–579. IEEE, 2001.

[113] Alkan Soysal and Sennur Ulukus. Optimum power allocation for single-user MIMO and multi-user MIMO-MAC with partial CSI. *IEEE Journal on Selected Areas in Communications*, 25(7):1402–1412, 2007.

[114] Lina Pu, Yu Luo, Haining Mo, Son Le, Zheng Peng, Jun-Hong Cui, and Zaihan Jiang. Comparing underwater MAC protocols in real sea experiments. *Computer Communications*, 56:47–59, 2015.

[115] Raj Jain. *The art of computer systems performance analysis*. John Wiley & Sons, 1991.

[116] Wonjong Rhee and John M Cioffi. Ergodic capacity of multi-antenna Gaussian multiple-access channels. In *Proceedings of the Asilomar Conference on Signals, Systems and Computers*, volume 1, pages 507–512. IEEE, 2001.

[117] Lin X Cai, Hangguan Shan, Weihua Zhuang, Xuemin Shen, Jon W Mark, and Zongxin Wang. A distributed multi-user MIMO MAC protocol for wireless local area networks. In *Proceedings of GLOBECOM*, pages 1–5. IEEE, 2008.

[118] Qin Lu, Yi Huang, and and Zhou Shengli Wang, Zhaohui. Characterization and receiver design for underwater acoustic communications over channels with large Doppler spread. In *Proceedings of OCEANS*, pages 23–27, Washington, DC, USA, 2015.

[119] Wen-Bin Yang and TC Yang. Characterization and modeling of underwater acoustic communications channels for frequency-shift-keying signals. In *Proceedings of OCEANS*, pages 1–6, Boston, USA, 2006. IEEE.

[120] Yu Luo, Lina Pu, Zheng Peng, Zhijie Shi, and Jun-Hong Cui. RSS-based secret key generation in underwater acoustic networks: Advantages, challenges and performance improvements. Technical Report Technical Report: UbiNet-TR14-01, UCONN CSE, 2014.